HYPERFINE FIELD FLUCTUATIONS IN THE MOSSBAUER SPECTRUM OF MAGNETIC MATERIALS: APPLICATION TO SMALL PARTICLES AND TO THE BULK ANTIFERROMAGNET FE(2–X)CR(X)AS

Denis Gabriel Rancourt

1984

HYPERFINE FIELD FLUCTUATIONS IN THE MOSSBAUER SPECTRUM OF MAGNETIC MATERIALS: APPLICATION TO SMALL PARTICLES AND TO THE BULK ANTIFERROMAGNET FE(2-X)CR(X)AS

by

Denis Gabriel Rancourt

A Thesis submitted in conformity with the requirements
for the Degree of Doctor of Philosophy in the
University of Toronto

à ma mère,

Fleurette Rancourt

A B S T R A C T

We describe the new phenomenon of "superferromagnetism" and show that it is an essential ingredient in understanding the Mossbauer behaviour of very small (d < 40 Å) alpha-Fe2O3 particles at temperatures below the blocking temperature. A technique of size determination, whereby the volume of these particles can be deduced from their high temperature behaviour, is presented. Also, we demonstrate the important role of microcrystal defects and characterize the anisotropy in the superparamagnetic relaxation by the "anisotropy factor", h.

The magnetic material Fe(2-X)Cr(X)As (with $0 \leq X \leq 1$) is studied and particular attention is given to Fe2As. Neutron diffraction* shows two seperate crystal phases that coexist over a large range in the composition and have quite different magnetic properties. The iron-rich phase is antiferromagnetic with a Néel temperature which decreases with chromium content. Also, the spin relaxation can be seen in the Fe-57 Mossbauer spectrum of this phase and the corresponding relaxation time is found to increase with chromium content. The chromium rich phase (X > ~.8) is paramagnetic but exhibits isotropic spin relaxation in its Mossbauer spectrum at T = 4K.

A detailed look at Fe2As showed an electric field

*The data was collected by Dr. D. Khatamian, see page 3.

gradient asymmetry, η, in the c-plane, which is induced by the sublattice magnetization in that plane. Previous Mossbauer results for Fe2As disagree with the spin structure deduced from neutron diffraction. To solve this we introduce the "equisurface" which is a surface in a space of n dependent Mossbauer parameters. Points on this surface correspond to the best fit given constraints in the redundant variables and an assumed lineshape. These points are, most often, indistinguishable on the basis of the Mossbauer measurement alone. We find that the previous Mossbauer studies of Fe2As have restricted themselves to the equisurface slice with $\eta = 0$. Our Mossbauer results are in agreement with neutron diffraction and find site-II spins in the Fe2As tetragonal structure which are exactly confined to the c-plane. This is also in agreement with the observed XY-type critical behaviour.

ACKNOWLEDGEMENTS

Support, guidance, and encouragement ... I wish to thank my supervisor Dr. J. M. Daniels. It has been a pleasure to work in the enviroment of trust and confidence which he creates for all his students. Special thanks to my fellow graduate student and friend Stephen Julian with whom I have had many important discussions.

Thank you to my non-physics friends in Toronto: Pam, Jeff, Sandy, Yvonne, Laslo, Greg, Jen, Jocelyn, Gisella, Rob, ... for understanding. Merci a ceux qui sont toujours la: Mich, Louise, Raymond, Cecile, Maman, Marielle, et puis ma grande amie Louise Latremouille - pour un amour soutenu et bien recu.

In preparing the manuscript Andrew Rutenberg typed much of the text and Laslo Najmanyi helped to prepare many of the figures and tables - thank you.

I am very greatful to Dr. D. Khatamian for performing all the neutron diffraction measurements of Fe(2-X)Cr(X)As at McMaster University, to Dr. F. D. Manchester who agreed to let one of his He cryostats be "adapted" to our Mossbauer spectrometer for some of the He-temperature measurements, to H.-Y. Lam for making many of the Fe-Cr-As samples and running preliminary tests on them, to L. F. Nazar and her

supervisor Dr. G. A. Ozin from the Chemistry Department for synthesizing all of the small-particle preparations, and to Rose Mora and her supervisor Dr. R. L. Armstrong for fitting the room temperature Fe2As neutron diffraction data at Chalk River.

The financial support of the N.S.E.R.C. of Canada is gratefully acknowledged.

SYMBOLS AND ABBREVIATIONS

a	(= Eb/kT) ratio of barier energy to kT; dimensionless
Å	angstrom; 10^{-10} meters
a2, a1	the areas of the high and low energy lines in a Voigt quadrupole-doublet; arbitrary absorption units
A, B	constants which appear in superparamagnetic frequency formulaes; Hz
b	(= e $\hbar$/2m; 5.0505×10^{-27} J-m^2/Wb) one nuclear magneton
C	cubic crystal field term; J
C.S.	center shift; mm/s
d	equivalent spherical particle diameter; angstroms
δ	[= (w2 - w1)]; mm/s
Δ	[= $\pi(90^\circ - \theta) / 180^\circ$] spin canting out of c-plane in Fe2As; radians
D	tetragonal crystal field term; J
e	electronic charge; 1.60×10^{-19} Coul.
e.f.g.	electric field gradient
ϵ	= (hν1 - hν2) / (hν1 + hν2)
Eb	barrier energy; erg.
η	[= (Vxx -Vyy)/q , such that q > Vxx > Vyy] asymmetry parameter; dimensionless
f	(1/t) characteristic frequency; Hz
f+, f-	hyperfine field fluctuation frequencies in uniaxial case; Hz
fm	(= 1/tm) measurement frequency; Hz
F+, F-, F	superparamagnetic relaxation frequencies; Hz
g	nuclear g-factor for ground state of Fe-57, magnetic moment of ground state is gb; dimensionless

g* nuclear g-factor for first excited state of Fe-57, magnetic moment of excited state is g*b; dimensionless

G gyromagnetic ratio; between e/mc and e/2mc Hz/gauss

G(argument) Gaussian lineshape

G-K Goldanskii-Karyagin (effect)

Γ natural linewidth; mm/s

h (= M v Heff / 2 Eb = M Heff / 2 K) anisotropy factor; dimensionless

$\hbar$ Plank's constant; 1.055×10^{-34} J-sec.

$\mathcal{H}$ spin hamiltonian acting on ion; J

h.f. hyperfine field

hv Voigt height; arbitrary absorbtion units

hv2,hv1 Voigt heights for high and low energy lines in a quadrupole-doublet.

H hyperfine field; kOe

Ho true value of H

He effective hyperfine field determined by one or more fast relaxation processes; kOe

Heff effective external field applied along particle's uniaxial direction; gauss.

HFD high frequency domain

I nuclear spin; dimensionless

k Boltzmann's constant; 1.38×10^{-23} J/K

K degrees Kelvin; K - or - uniaxial magnetic anisotropy constant; erg/cm^3

Ks surface anisotropy constant; erg/cm^2

K(x,y) dimensionless Voigt integral

l Lorentzian line height; arbitrary absorption units

λ spin-orbit coupling; J

L Lorentzian full width at half maximum; mm/s

L,Lx,Ly,Lz orbital angular momentum quantum numbers

L(argument) Lorentzian lineshape

mp magnetic moment of particle; erg/gauss

M magnetization; erg-gauss/cm^3

MHS measured hyperfine splitting, obtained from the separation of lines 1 and 6 in the Mossbauer spectrum [for Z << g*bHe, and when no relaxation processes with f ~ fm are present, MHS ~ (4.75)g*bHe]; mm/s

no Voigt and Gaussian line centers; mm/s

π 3.1415926...

q electronic electric field gradient at nucleus in principal axis direction; N/Coul.-m

Q nuclear electric quadrupole moment; m^2/Coul.

Q.S. [= $Z\ (1 + (1/3)\eta^2)^{1/2}$] quadrupole splitting; mm/s

r (= a2/a1) area ratio for a quadrupole-doublet

R ratio of quadrupole-doublet contribution to total spectral area in a SP system

s Gaussian width , where half-width is given by $s[(2\ \ln 2)^{1/2}]$; mm/s

Sv Gaussian half width at half maximum for a volume distribution

S spin quantum number

SOD second order doppler (effect or shift)

SP superparamagnetic

t (=1/f) characteristic time between fluctuations; sec.

tm (=1/fm) measurement time; sec.

Tb (= Eb/k) blocking temperature; K

Tm Mossbauer measurement temperature, temperature at which (f+ + f-)/2 ~ fm; K

TM Morin temperature in alpha-Fe2O3; K

TN Néel temperature; K

TTS — transitional type spectra; these occur when 10fm < f+,f- < 1000fm

θ, ϕ — polar angles between hyperfine field and electric field gradient principal axis system.

u, $\bar{u}$ — Fe2As lattice parameters; dimensionless - fraction of c-axis in angstroms

μ — Bohr magneton; 0.93X10 erg/gauss

v — particle volume; cm^3

vM — particle volume at which the SP transition occurs for a given temperature; cm^3

Vm — molecular volume of alpha-Fe2O3 (two Fe atoms, three O atoms); 50 +- 2 $\AA^3$

Vxx — electric field gradient along x-direction in principal axis system; N/Coul.-m

Vyy — electric field gradient along y-direction in principal axis system; N/Coul.-m

V(argument) — Voigt lineshape

w2,w1 — Lorentzian half-width at half maximum for the higher and lower energy lines in a quadrupole -doublet; mm/s

W — [= (Weiss field)(local moment)] Weiss field magnetic interaction; J

X — stoicheometric parameter, as in Fe(2-X)Cr(X)As; dimensionless

y — [= $w / s\sqrt{2}$] Voigt profile dimensionless width parameter

Z — [= $(e^2)qQ/2$] quadrupole parameter; mm/s

Zo — true value of Z

note: in the above list "mm/s" is used as a unit of energy for the Mossbauer parameters; 1 mm/s = 4.808 X 10^{-8} eV

LIST OF FIGURES

LIST OF TABLES

TABLE OF CONTENTS

1. INTRODUCTION

1.1 Organization and justification

As a probe of the solid state, the Mossbauer effect has been used most extensively on the simpler systems. That is, systems in which the characteristic time of interaction between the electronic enviroment and the Mossbauer nucleus is either so short, compared to the measurement time, that there is an averaging of the interaction, or so long that the interaction can be considered to be truly static. This thesis is concerned with two cases where the characteristic time of the hyperfine interaction, between the nuclear magnetic moment and the electronic magnetic moment at the nucleus, is comparable to the measurement time. The electronic magnetic field at the nucleus undergoes fluctuations in both magnitude and direction. There are various mechanisms for these fluctuations and each has its own characteristic time t - examples are as follows: (1) the fast quantum fluctuations which correspond to the electron hopping in itinerant electron systems, $t \sim 10^{-15}$ sec, (2) spin-waves in a ferromagnet typically have a frequency of $1/t \sim 10^{12}$ Hz, (3) thermal fluctuations of highly localized magnetic moments in paramagnetic and magnetically ordered systems are known, from ferro and paramagnetic resonance studies, to have $t \sim 10^{-6} - 10^{-12}$ sec., and also (4) the fluctuations in magnetization

known as collective magnetic excitations, t ~ 10^{-12} sec, and superparamagnetism, t ~ 10^{-4} - 10^{-12} sec, which occur in small particles of magnetic material below the magnetic transition temperature. The measurement time, tm, is $\hbar/\Gamma$ where Γ is the natural linewidth of the Mossbauer transition - with Fe-57 $\Gamma = 4.651 \times 10^{-9}$ eV which corresponds to tm ~ 10^{-8} sec. This time marks the region where the fluctuations have a large effect on the Mossbauer lineshape and where the spectrum is most sensitive to the ratio t/tm. With Fe-57 the region spans frequencies from about 10^{7} Hz to as high as 10^{12} Hz and is the region of interest in the present work. The thesis is divided into three major parts which are contained in sections 2, 3, and 4.

Section 2 deals with small particle magnetism. We introduce the idea of unequal magnetization direction probabilities (ref.79) and demonstrate its usefullness in the first Mossbauer characterization of d < 40 Å alpha-Fe2O3 particles (ref.80). The small particle preparations have many interesting features apart from the novel relaxation processes wich they exhibit. For example, we have found that the superparamagnetism is very sensitive to the microcrystal defects, to the particle's size and shape, and to the interaction with its medium. These, and other intricacies, are described in terms of how they affect the Mossbauer spectrum. We also introduce a simple and reliable method for obtaining

the average equivalent spherical particle diameter for a sample of ultra-fine antiferromagnetic particles and apply it to alpha-Fe2O3.

Section 3 is a thorough study of the bulk antiferromagnet Fe2As. The hyperfine fluctuations in this material are treated by the same formalism that makes the small-particle Mossbauer analysis possible, although the underlying mechanism is quite different. Fe2As has been controversial in that the previous Mossbauer studies have disagreed with the spin structure deduced from neutron diffraction experiments. We solve this controversy (ref.81) by showing that two previously ignored effects have an influence on the Mossbauer spectrum but do not affect the neutron diffraction result. These are (1) hyperfine fluctuations near and below the Néel temperature of Fe2As and, (2) an asymmetry in the electronic electric field gradient at the nucleus which is induced by the magnetism in the ordered state. The second of these represents a new mechanism which may explain many of the observed electric field gradient "jumps" near second order magnetic phase transitions.

Section 4 is a "first look" at the intermetallic compund Fe(2-X)Cr(X)As with $0.1 \leq X \leq 1.0$. We present an overview of some crystallographic and magnetic properties. Much to our surprise, this material has two distinct crystallographic phases which coexist over a large range in X - one phase is paramagnetic down to 4K

and the other is antiferromagnetic with a Néel temperature which decreases with increasing chromium content. The Mossbauer spectra of both phases show hyperfine fluctuations and offer the possibility of studying the relaxation as a function of X - that is, as a function of the coupling strength between spins.

Spin fluctuations in magnetically ordered materials have traditionally been studied by ferromagnetic resonance. That technique has serious shortcomings. The resonance linewidth, which would ideally determine the relaxation frequency, has many spurious contributions from such factors as: nonuniformity of the sample, nonuniformity of the internal magnetizing field, the condition of the surface of the sample, and variations in the magnetic anisotropy of polycrysalline samples. These effects can increase the linewidth by a factor of one hundred and make the intrinsic relaxation process difficult to observe.

By comparison, Mossbauer spectroscpy is a local technique which looks directly at nuclei with penetrating gamma-rays and is therefore relatively insensitive to sample conditions. It can give the configuration and symmetry of the local prefered spin directions and the frequencies for transitions between those directions.

In magnetic materials the relaxation is anisotropic because the spins spend more time along the

magnetization direction. This anisotropy is not detected by other relaxation sensitive techniques and its presence is most often not recognized by Mossbauer spectroscopists themselves (ref.101). Anisotropic relaxation is a pervasive theme in this thesis - we demonstrate its usefulness in understanding both bulk and microcrystalline materials and show how its effect on the Mossbauer spectrum has been repeatadly mistaken for various other causes - some truly unbelievable and others indistinguishable from relaxation effects.

1.2 Static Mossbauer parameters for Fe-57

In this section we review the terminology and describe the static Mossbauer parameters which, in the absence of relaxation and under ideal experimental conditions, completely determine the Mossbauer spectrum for nuclei in identical electronic enviroments. We are concerned with the 14.4 keV gamma-ray transition between the ground state (I = 1/2) and the first excited state (I = 3/2) of the Fe-57 nucleus. The interactions between the nucleus and the surrounding electrons are parameterized as follows. $Z = (e^2)qQ/2$ represents the energy of interaction between the nuclear quadrupole moment, Q, (which is zero in the ground state) and the electronic electric field gradient (e.f.g), q, at the nucleus. When the e.f.g. is not axially symmetric there is a non-zero asymmetry parameter, η, which by

definition (η = (Vxx-Vyy)/q, q > Vxx > Vyy) is dimensionless and has a value between zero and one. The effective electronic magnetic field, H, at the nucleus is called the hyperfine field (h.f.) and causes a Zeeman type splitting which is g*bH for the excited state and gbH for the ground state where g*b and gb are the corresponding magnetic moments in nuclear magnetons. The two polar angles θ and ϕ between the h.f. and the e.f.g. principal axis system also affect the Mossbauer spectrum. The electric monopole interaction between the nuclear charge and the total s-electron density at the nucleaus will cause a compound to compound variation in the unsplit nuclear level separation and this, in combination with the second order Doppler (SOD) effect will cause the center shift (C.S.) in the observed spectrum.

In the static case then, the absorption line positions are completely determined by the C.S., Z, η, θ, ϕ, and g*bH, given that g/g* = -.1806/+.103 = -1.751 +- .002 . Under ideal experimental conditions these lines are Lorentzian and have a full width at half maximum L ~ 2Γ (note that there is a contribution of approximately one Γ from the source whose single Lorentzian emission line is convoluted with the absorber's pattern to yield the observed spectrum). The line intensities are given by the Golden Rule and depend only on Z, η, θ, ϕ, g*bH and g/g* for randomly

oriented samples and unpolarized gamma-rays.

The main contribution to the h.f. in iron compounds arises as a result of the exchange interaction between the 3d-electrons and the s-electrons of the ionic core, which makes the densities at the nucleus of s-electrons of opposite spin orientation unequal. This is equivalent to a field which is parallel to the net 3d spin. Given thermal averaging, the effective field is, most often, zero for a paramagnet and closely proportional to the magnetization for a magnetically ordered substance.

When H = Z = 0 the Mossbauer spectrum consists of a single Lorentzian line whose position is given by the C.S. . When H = 0 and Z is non-zero the Mossbauer spectrum consists of two Lorentzian lines (called a quadrupole-doublet) with equal intensities and separated by an amount $Z[1+(1/3)\eta^2]^{1/2}$, referred to as the quadrupole splitting (Q.S.). When H is non-zero and Z = 0 (or Z << g*bH) the Mossbauer spectrum is said to be a hyperfine-pattern and is composed of six absorption lines. These typical Mossbauer spectra and their corresponding nuclear level diagrams are shown in Figure 1-1.

FIGURE 1-1

Typical Mossbauer spectra and their associated level diagrams. The level diagram is that of Fe-57 in different electronic enviroments. The relaxation times are assumed to be very long compared to the lifetime of the excited state and, under ideal experimental conditions, the resulting lineshape is Lorentzian. The lines in the hyperfine pattern are labelled 1,2,...,6 in the conventional way and we refer to them in the text as "line-1", etc. The absorber is assumed to be a random powder and to have an isotropic Debye-Waller factor. These assumptions lead to a symmetric quadrupole-doublet with equal areas for the two Lorentzian components and to a line area ratio, in the hyperfine pattern, which is 3:2:1:1:2:3.

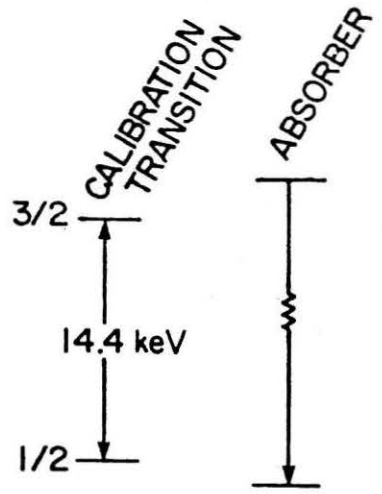
CALIBRATION TRANSITION
ABSORBER
3/2
14.4 keV
1/2

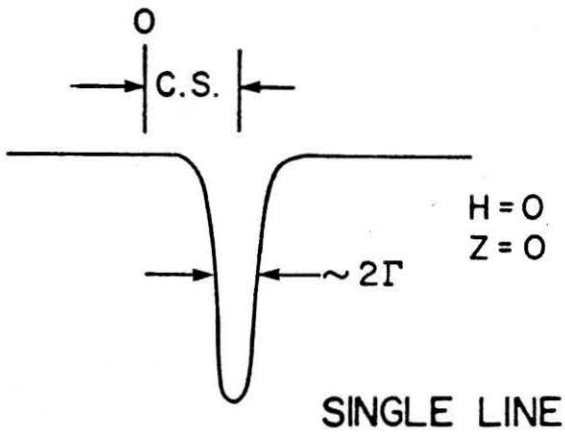
0
C.S.
H=0
Z=0
~2Γ
SINGLE LINE

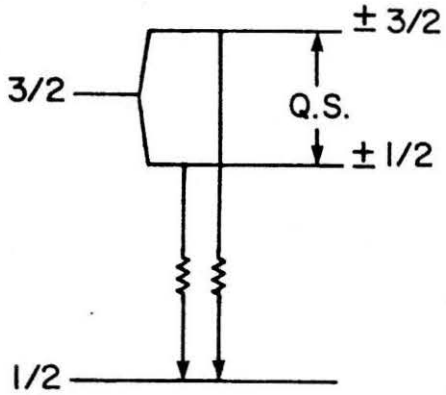
±3/2
3/2
Q.S.
±1/2
1/2

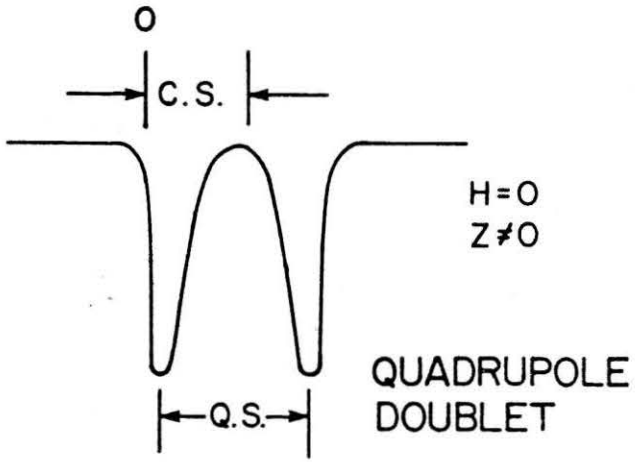
0
C.S.
H=0
Z≠0
QUADRUPOLE DOUBLET
Q.S.

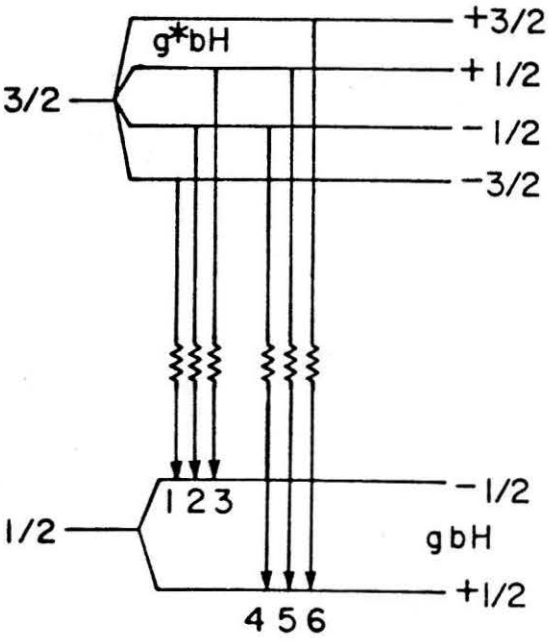
+3/2
g*bH
+1/2
3/2
-1/2
-3/2
1 2 3
-1/2
1/2
gbH
+1/2
4 5 6

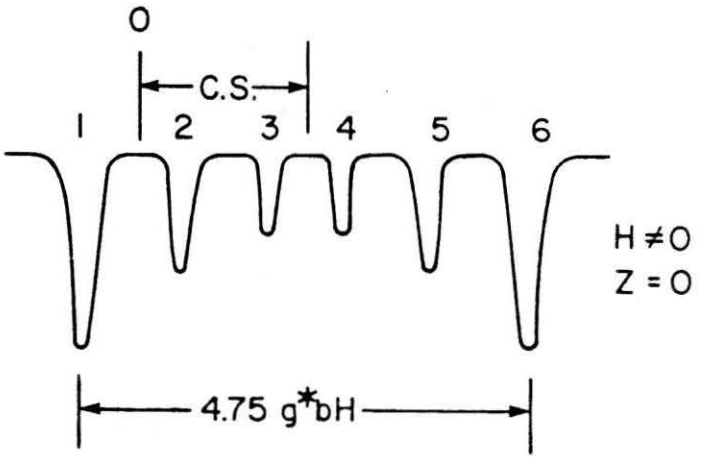
0
C.S.
1
2
3
4
5
6
H≠0
Z=0
4.75 g*bH
HYPERFINE PATTERN

FIGURE 1-2

Effect of hyperfine field fluctuations on the Fe-57 Mossbauer spectrum. The relaxation lineshape of Blume and Tjon (ref.9) was used to simulate these spectra. The relaxation symmetry is taken to be uniaxial with the e.f.g. principal axis parallel to the hyperfine field and the relaxation frequencies, f+/f-, are given in units of fm (~ 10^8 Hz). The velocity range is from -10 mm/s to +10 mm/s. The static Mossbauer parameters of bulk hematite (alpha-Fe2O3) at room temperature were used except the C.S. is taken to be zero. The parameters are: L = 0.36 mm/s, Z = -.569 mm/s, g*bH = 3.512 mm/s, and η = 0. Note that, in real hematite at room temperature, we are above the Morin point (TM ~ 248K) and the e.f.g. is perpendicular to the h.f..

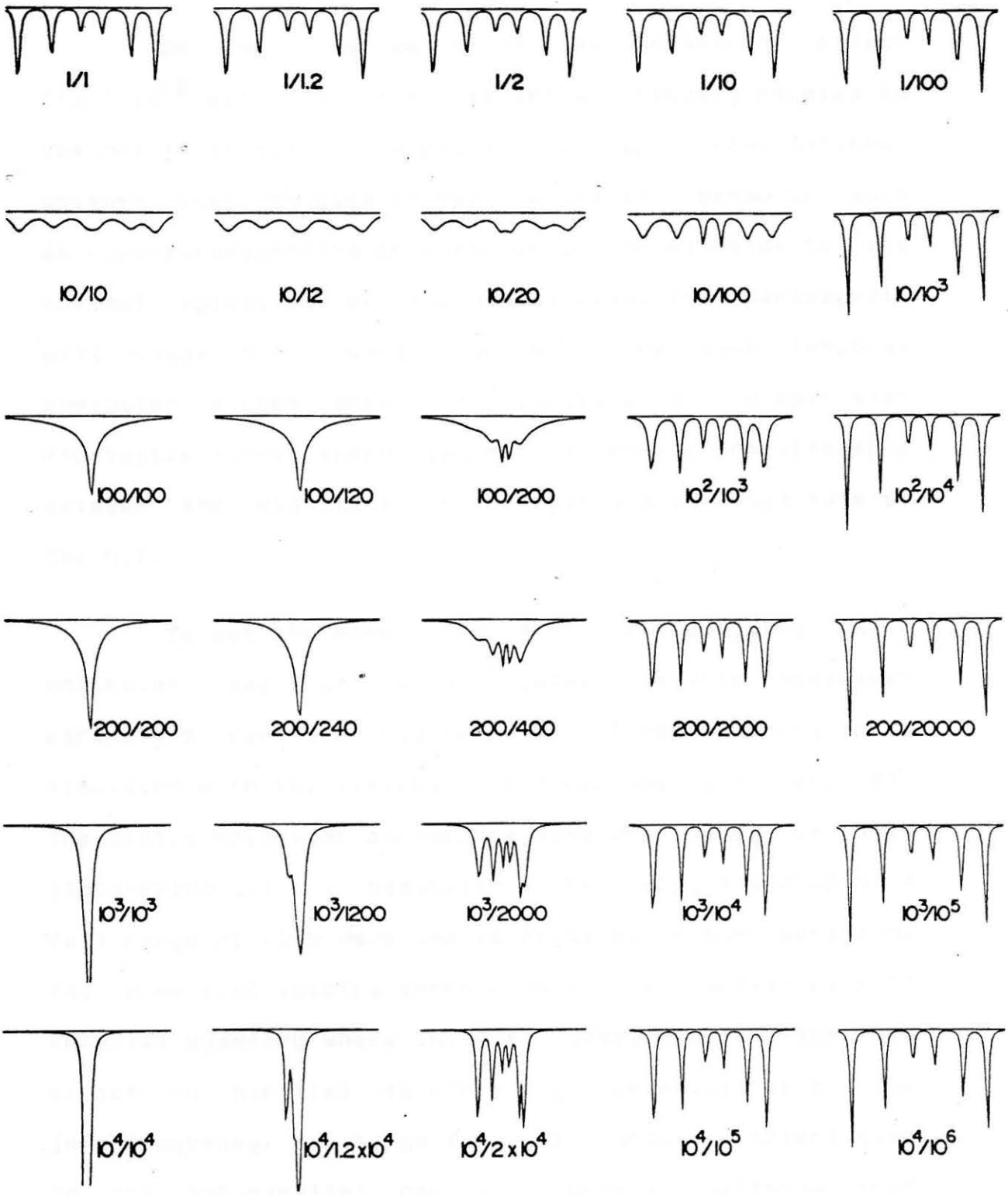
1/1
1/1.2
1/2
1/10
1/100
10/10
10/12
10/20
10/100
10/10^3
100/100
100/120
100/200
10^2/10^3
10^2/10^4
200/200
200/240
200/400
200/2000
200/20000
10^3/10^3
10^3/1200
10^3/2000
10^3/10^4
10^3/10^5
10^4/10^4
10^4/1.2x10^4
10^4/2x10^4
10^4/10^5
10^4/10^6

1.3 The effect of hyperfine field fluctuations on the Mossbauer spectrum

On the time scale of the Mossbauer effect ($\tau_m \sim 10^{-8}$ sec.) the h.f. is instantaneously coupled to the net local spin. Therefore, all spin fluctuations, whether they originate from a collective behaviour such as superparamagnetism or correspond, for example, to the thermal agitation of individual spins in a paramagnet, will cause h.f. variations with the same temporal evolution except when the magnitude of the spin also fluctuates since there is not a simple relationship between the magnitude of the spin and the magnitude of the h.f. .

To see the effect of h.f. fluctuations on a Mossbauer spectrum with typical static Mossbauer parameters consider Figure 1-2. These spectra were simulated with the lineshape of Blume and Tjon (ref. 9). The static Mossbauer parameters used are those of bulk alpha-Fe2O3 (i.e., hematite). The energy scale spans a full range of 20.0 mm/s and is centered on the spectrum. The simulated spectra correspond to the simplest case of uniaxial symmetry where the h.f. jumps between the two directions parallel to the e.f.g. principal axis. The jump frequency, f+, to go from the parallel orientation to the antiparallel one is, in general, different from the jump frequency, f-, to go in the opposite direction and these frequencies are given below each spectrum in

units of the Mossbauer measurement frequency, fm (= 1/tm).

The important features to be noticed in Figure 1-2 are as follows. In the high frequency limit (bottom row) relaxation line broadening is negligible and the effective h.f., He, is given by $He = H(f+ - f-)/(f+ + f-)$. In hematite the spin relaxation is very fast and the sublattice magnetization is proportional to He so that moving from right to left on the bottom row reproduces the observed spectra as we approach the Néel temperature from the low temperature side.

The paramagnetic case corresponds to $f+ = f- = f$ and is shown in the left hand column. When f is small the h.f. is effectively frozen along one of the uniaxial directions during the measurement time and, since in this case identical Mossbauer spectra result from the two orientations of H, we get a single hyperfine pattern with a line broadening that goes to zero as f goes to zero and with He = H. As f is increases to ~ 10 fm we obtain progressively more important line broadening and the line positions are preserved to first order but there is a redistribution of the line intensities from the outer lines to the middle lines. When f ~ 100 fm there is complete collapse to a single highly asymmetric line which, as f is increased still further, becomes a single Lorentzian line when the e.f.g. is zero or a

quadrupole-doublet when, as in hematite, there is a non-zero e.f.g. at the Mossbauer nucleus.

When both f+ and f- are small (top row) or when one of the frequencies is much larger than the other (right hand column) the Mossbauer spectrum is insensitive to the ratio f+/f-, has negligible line broadening, and is entirely determined by the static Mossbauer parameters.

The spectrum with f+/f- = 10/100 is worthy of special mention since it could easily be mistaken for a distribution of hyperfine patterns (to account for the broad outer lines) on to which is superimposed a quadrupole-doublet (to account for the strong and sharp central lines). Another point of special interest is the following. As we go from 200/2000 to 200/20000, from $10^3/10^4$ to $10^3/10^5$, and from $10^4/10^5$ to $10^4/10^6$, the spectra are very similar except that there is a slight increase in He and that the line-1 to line-2 area ratios go from being approximately 1:1 to 3:2. The later point is important because the degree of sample non-randomness also affects the ratio so that partial magnetization of the absorber could mistakenly be invoked where a more natural explanation from relaxation would apply.

In most instances the spin fluctuations are caused by two or more seperate relaxation processes. If one process is very fast and the other has a rate

comparable to fm then the fast process will cause a true averaging of H to some effective value He = <H>fast and this effective value replaces the static value of H which would be used to calculate the lineshape in the presence of only the slower relaxation process. The middle part of Figure 1-2 shows the spectra whose lineshapes are most strongly effected by the spin fluctuations and these occur when one of the relaxation processes has a rate between ~ fm and ~ 10^3 fm and a ratio, f+/f-, between 1 and ~ 0.1.

1.4 Experimental setup and remarks

For all of the Mossbauer experiments reported in this thesis the standard Mossbauer absorption geometry was used with the transducer in the constant acceleration mode. A 5 to 20 mCi Rh-matrix/Co-57 source was used and all the center shifts are given with respect to metallic iron at 22 degrees Celsius. All the absorbers are fine powders of randomly oriented grains. The spectrometer and its associated peripheral equipment is described in detail elsewhere (ref.102).

A measured Mossbauer spectrum consists of 256 channels which are equally spaced in energy and typically contain 5 million counts or so. The transducer goes through the velocity range twice before it returns to the same point on its position-velocity curve so that two

sets of data can be collected simultaneously and then folded in order to achieve a flat background. The Mossbauer signal typically represents an absorption of 5 to at most 30 per cent and the noise to signal ratio is usually ~ 0.02 . The duration of an experiment is typically between 15 hrs. and 2 weeks depending on the strength of the signal and of the source. The transducer is quite stable and the zero velocity channel does not change by more than ~ .02 channels in the time of an experiment.

2. SMALL PARTICLES OF MAGNETIC MATERIAL

2.1 Mossbauer spectroscopy and small particles

2.1.1 Superparamagnetism and superferromagnetism

With particles of ferromagnetic material at temperatures below the Curie point, the direction of magnetization can fluctuate between stable orientations at a rate which can become very rapid as the size of the particles becomes very small. This is known as superparamagnetism and can be explained in the following way. The stable orientations are the easy directions of magnetization which, in larger particles, are predominantly set up by the spin-orbit coupling to the

lattice. The resulting anisotropy (or barrier) energy, Eb, represents the work which must be done to turn the particle's magnetic moment, mp, from an easy direction to a hard direction. In smaller particles, the anisotropy energy can have important self-magnetostatic, particle-particle, and magnetostrictive strain contributions in addition to the above mentioned magnetocrystalline contribution. The resulting free energy as a function of the two polar angles for the magnetization directions has various minima (whose number and positions are determined by the symmetry of the contributing anisotropies) and various barrier heights between minima. The barrier heights can become comparable to kT (for temperatures below the Curie point) only for small enough particles because the magnetocrystalline anisotropy energy is roughly proportional to the volume, v, of the particle. The small volume behaviour is paramagnetic-like to the extent that transitions between the free energy minima can be such that the long-time average of the magnetization is zero but the free energy is not a flat surface like it is for a classical paramagnet.

Similar phenomena occur with particles of antiferro and ferrimagnetic materials. We refer to the case where the transitions are such that the long-time average of the magnetization (or sublattice magnetization) is not zero as "superferromagnetism".

The transition frequencies were first calculated by Néel (ref.75), who considered the case of a uniaxial particle whose magnetization jumps between two parallel directions, Brown (ref.13) derived a formula which is similar to Néel's result and has shown that this formula must break down as the ratio T/v (the absolute temperature to the volume of the particle) increases. He also obtained another formula which is valid at large T/v and developed (ref.14) an extrapolation method for the range with intermediate values of T/v. Both authors also considered the case where there is an external magnetic field Heff applied along the uniaxial direction. This causes the two stable positions to have different energies. The relaxation is governed by these two energies and the barrier energy Eb, and unequal values of the energies can arise, not only from an external magnetic field, but also from many other causes (e.g., an interaction between particles, microcrystal defects, a chemical interaction with the support, a physical interaction such as magnetorestrictive strain, a competition between magnetocrystalline anisotropy and shape anisotropy, etc. (ref.84,29)) For convenience, we represent all these effects by an effective external field, Heff, which is expressed in the dimensionless form $h = mp\ Heff / 2Eb$ where we shall refer to h as the "anisotropy factor". If we assume a uniform magnetization, M, for the particle and that the barrier energy is predominantly given by the uniaxial anisotropy

constant K, then h can also be expressed as $h = M\,Heff / 2K$.

Let $a = Eb / kT$; then Brown's formulae are

$$F\pm = A\, a^{1/2}\, (1-h^2)\, (1\pm h)\, \exp[-a(1\pm h)^2] \qquad (1)$$

and

$$F+ = F- = B\,(1/a)\,[1 - (2/5)\,a + (48/875)\,a^2 + (2/5)\,h^2 a^2 + \ldots] \qquad (2)$$

which are valid, respectively, for low and high values of T/v. A and B are constants which depend only on certain properties of the particle; one approximation (ref.29) gives A equal to $KG/M\pi$ where G is the gyromagnetic ratio and, in this approximation, B is related to A by $B = A / 2\sqrt{\pi}$.

The blocking temperature, Tb, is defined as $Eb = kTb$; it characterizes the region close to which there is the greatest variation in F+- with T, and, according to Brown (ref.13) marks the region of crossover between equations (1) and (2). Aharoni (ref.2) has made a more complete study of the range of validity of equation (1), and the subject has been discussed thoroughly by Dormann (ref.29).

When the two stable directions of magnetization

have the same energy, the superparamagnetic (SP) relaxation frequencies, F+ and F-, for transitions between these two directions, are equal. A non-zero value of h will cause the magnetization to spend more time along one stable direction and the relaxation frequencies will not be equal. The effect of these unequal relaxation frequencies on the Mossbauer spectra of small particles had not, until recently (see Rancourt and Daniels, ref.79), been discussed in the literature. We proceed to these considerations and also describe when this effect can be distinctly recognized (and therefore must be considered) and when it cannot be distinguished from the other factors which determine the spectra of SP particles. We use the Blume and Tjon (ref.9) Mossbauer lineshape for uniaxial hyperfine field fluctuations. It has been applied to various relaxation phenomena, including superparamagnetism, and has thus been shown to be essentially correct. In our application we must assume (1) that the hyperfine field direction is locked into alignment with the particle's magnetization, (2) that the nuclear relaxation can be ignored, and (3) that the hyperfine Hamiltonian is diagonal with respect to the electronic states (ref.17).

The measurement frequency, fm, represents the SP frequency at which the Mossbauer spectrum will undergo dramatic changes in appearance and structure. Many authors have confused the temperature at which this

occurs (that is, the measurement temperature Tm, determined by the condition fm ~ F+-) with the blocking temperature. Equation (1) and its logarithm are plotted in Figure 2-1 and it can be seen from this figure that, depending on the value of A, Tm can be quite a small fraction of Tb - notably, for A = 10^{12} Hz, Tm ~ Tb / 10.

In any sample of small particles there is always a distribution of particle volumes and its associated distribution of blocking temperatures. At a given temperature, particles in the sample for which F+- << fm will exhibit the usual bulk type 6-line Fe-57 Mossbauer pattern except that the hyperfine splitting obtained from the separation of the lines (i.e., the measured hyperfine splitting; MHS) can be slightly but measurably reduced from its true bulk value at the same temperature. This reduction has been explained in terms of collective magnetic excitations (ref.70,71) when a dependence of the Curie (or Néel) point on particle size can be ruled out and when reduced surface hyperfine fields (ref.59) contribute negligibly (see section 2.2 for further discussion of these points).

Particles in the sample for which F+- >> fm will often have a paramagnetic-type spectrum (He = 0), but it is possible, in this frequency range, to see a hyperfine structure if the ratio F+/F- is sufficiently different from 1. Finally, the particles for which F+- is comparable to fm will exhibit transitional type spectra

(TTS) such as the ones which are displayed in Figure 1-2. We shall refer to the frequency range, inside of which such TTS are observed, as the "Mossbauer Window". It is delimited, approximately, by 10fm < f(window) < 1000fm and we note that these bounds depend on the static Mossbauer parameters of the bulk material.

The effect of unequal relaxation frequencies cannot be seen at temperatures far below Tm because F+- << fm and the spectrum is insensitive to the actual values of F+ and F- and to their ratio. The effect is also not observable when T > Tb since equation (2) (which is valid at these temperatures) gives equal relaxation frequencies for all values of h. The effect is therefore observable only in the temperature range Tm <~ T <~ Tb. If A is large enough there is a region within this temperature range for which F+- >> fm and the corresponding spectra are bulk type hyperfine-patterns whose MHS's are reduced by the factor (F+ - F-)/(F+ + F-). Superferromagnetism, therefore, occurs below Tb if A is large enough and when h is non-zero. It constitutes a new mechanism for the observed reduced MHS's of small particles below their blocking temperature.

FIGURE 2-1

Relaxation frequencies for small particles as a function of kT. Equation (1) is plotted for three values of h: 0 (———), 0.1 (- - - - -), and 0.25 (.....). The curves were terminated to indicate the crossover to Equation (2). The appropriate scale for these curves is on the right-hand side, where $R = A/(2e)^{1/2}$ in Hz. The logarithm of Equation (1) is also plotted for h=0 and 0.25 (f+ only) and the corresponding scale is on the left-hand side. It exhibits a sharp transition at kT ~ Eb/10.

FIGURE 2-4

Temperature dependence of f+/f- in small particles. The ratio f+/f-, as obtained from Equation (1), is plotted as a function of kT and for different values of h: 0.01 (-..-..), 0.05 (-.-.-), 0.1 (- - -), and 0.25 (....). Important deviations from 1 can occure at temperatures corresponding to the Mossbauer window if A is sufficiently small.

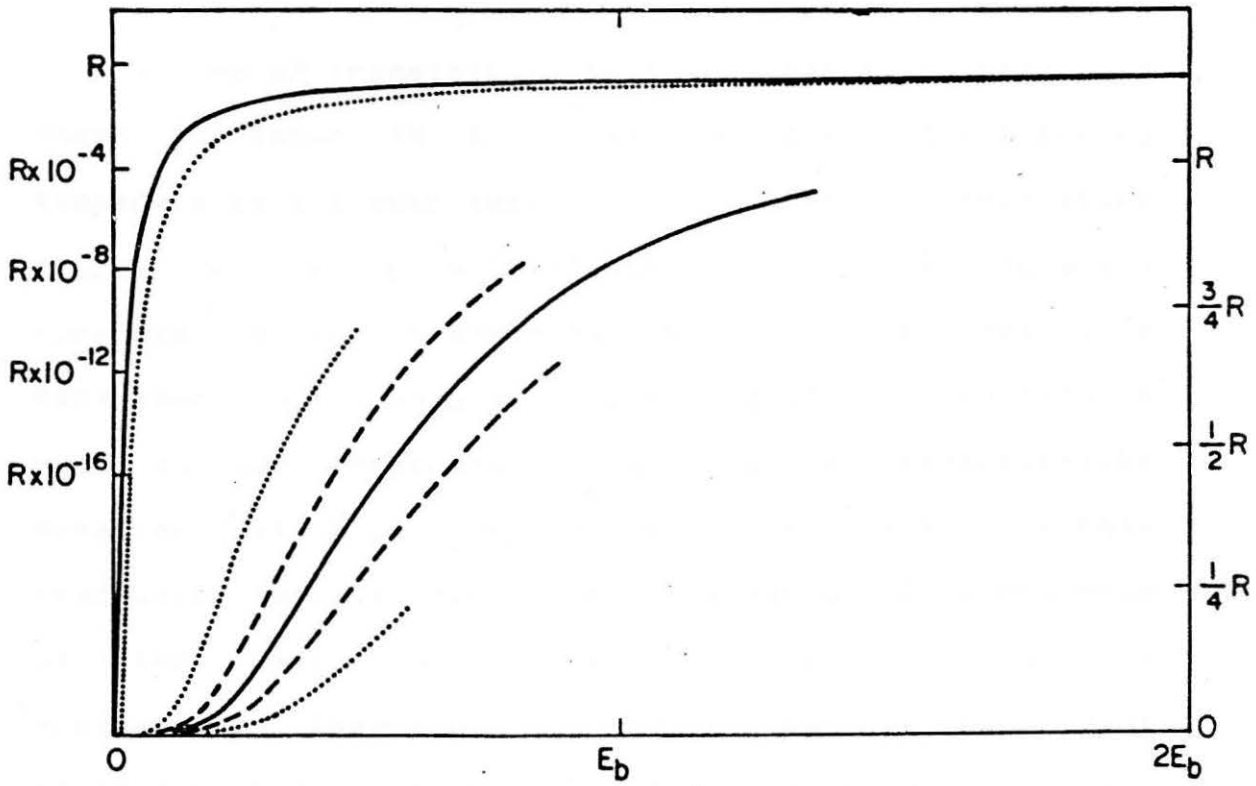
R
Rx10^-4
Rx10^-8
Rx10^-12
Rx10^-16
R
3/4 R
1/2 R
1/4 R
0
0
E_b
2E_b

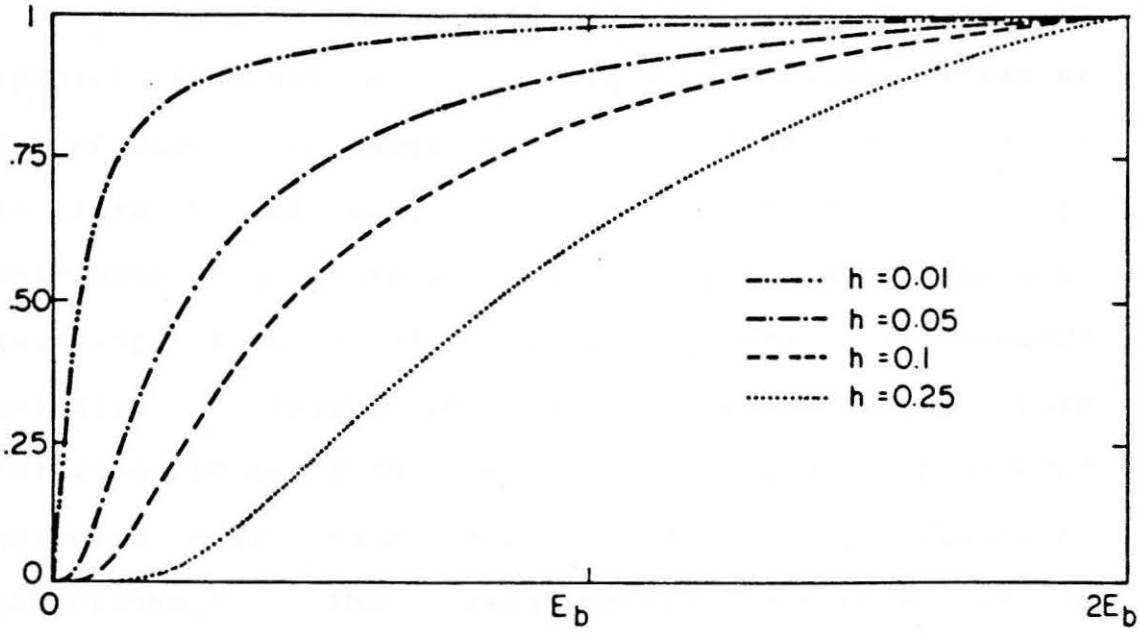
1
.75
.50
.25
0
h =0.01
h =0.05
h =0.1
h =0.25
0
E_b
2E_b

2.1.2 The superparamagnetic transition

The SP transition is the transition which is known to occur in all small particles whose blocking temperatures are much lower than the critical temperature (Curie or Néel point) of the bulk material and which consists in the transformation from the bulk-like behaviour (with only a small or negligible reduction in MHS) at low temperature to the paramagnetic-like behaviour at high temperatures. The existence of this transition is consistent with the temperature dependence of the ratio F+/F- (see Figure 2-4) and of the frequencies themselves. We expect the same characteristic dependences for "more-than-uniaxial" particles. We now describe the possible scenarios when the temperature is changed through the SP transition.

A large A, of the order of 10^{12} Hz or so, is expected from the residually small bulk magnetization of alpha-Fe2O3. This causes the change from $F+- >> fm$ to $F+- << fm$ to be very sharp, so that the TTS will contribute very little intensity to the total spectrum resulting from a distribution of small alpha-Fe2O3 particles. This is in fact the case (ref.59,22,60,64,72,73) for all the 40-1000 Å alpha-Fe2O3 particles that have been observed by Mossbauer spectroscopy; the experimental spectrum is a superposition of the paramagnetic contribution from the

particles in the sample with F+- >> fm (here h is so small that F+/F- ~ 1 in this frequency range and the MHS is effectively reduced to zero) and the bulk type contribution with only slightly (0-8%) reduced MHS's from the particles with F+- << fm. The SP transition in alpha-Fe2O3 particles with diameter, d, greater than 40 Å therefore occurs in a very narrow range around Tm and the ratio of the parmagnetic-type to the bulk-type contribution in the observed spectrum is given by the relative numbers of particles in the sample which have their Tm's above and below T. If h were large enough, a single d > 40 Å alpha-Fe2O3 particle would, as the temperature is raised, undergo a sharp transition to superferromagnetism at Tm and then a "crossover" transition to paramagnetic-type behaviour at around Tb. The second of these transitions being driven by the crossover from equation (1) to equation (2) which occurs at about Tb.

Magnetite has a bulk magnetization which is two orders of magnitude greater than that of alpha-Fe2O3; we therefore expect the value of A for magnetite to be about 10^{10} Hz or so. The Mossbauer window will therefore be positioned higher up on the curves of Figure 2-1 and will be spread over a much larger temperature range. This will correspond to a broader range of particle sizes for a distribution of particles and explains why transitional type spectra are routinely observed for superparamagnetic

Fe3O4 particles (ref.70,67). The ratio F+/F- is plotted as a function of kT and for different values of h in Figure 2-4 and it is clear from these plots that, even with an energy asymmetry as little as 5%, the ratio F+/F- can be significantly different from 1 in a large part of the temperature range that corresponds to the Mossbauer window. It is therefore important to consider the effect of unequal relaxation frequencies on the transitional type Mossbauer spectra of magnetite particles. We have in fact found (ref.25) that, for many magnetite particles that occur naturally in volcanic ash, a model that allows for unequal relaxation frequencies yields a fit that makes the most physical sense.

In general therefore, we expect a small A value to cause a very broad transition which spans from about Tm to maybe well above Tb (in order that F+ = F- >> fm). Only in this case can the Mossbauer spectrum of a distribution of SP particles show distinctive and unmistakable signs of a non-zero h. The example of d < 40 Å alpha-Fe2O3 is given in section 2.2.

In conclusion, four types of Mossbauer spectra can be observed; (1) a bulk type hyperfine pattern in which any reduction in the hyperfine splitting must be due to the more conventional mechanisms, (2) a transitional type of Mossbauer spectrum which will be most sensitive to unequal relaxation frequencies, (3) a hyperfine pattern in which an additional reduction in the

hyperfine splitting will be due to the unequal relaxation times and which corresponds to the superferromagnetic state, and (4) a quadrupole doublet pattern in which the hyperfine field has effectively been reduced to zero by the SP fluctuations. As we increase the temperature from absolute zero, not all of these spectra will necessarily be observed. The superferromagnetic state requires that F+- >> fm and that F+/F- be different from 1. Also, a broad particle size distribution can make the TTS unobservable.

FIGURE 2-2

Simulated Mossbauer spectra for three values of h, with A = 10^{10} Hz and at kT = Eb/3. The velocity scale is from -9.22 mm/s to +10.78 mm/s and the static Mossbauer parameters are those of the B site in magnetite (Fe2O4) at room temperature: L = 0.20 mm/s, C.S. = +0.78 mm/s, Z = +0.10 mm/s, g*bH = 3.13 mm/s, and η = 0.

FIGURE 2-3

Simulated Mossbauer spectra for three values of h, with A = 4 X 10^{10} Hz and kT = Eb/3. The velocity scale and static Mossbauer parameters are the same as in Figure 2-2.

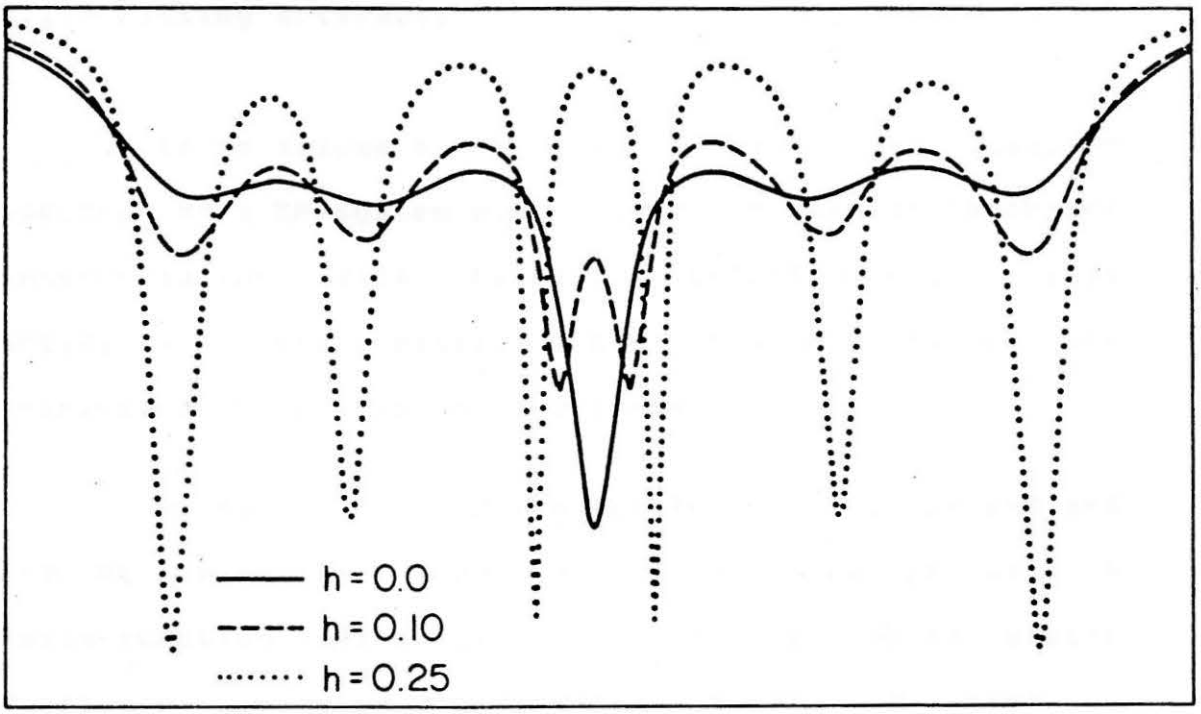
h = 0.0
h = 0.10
h = 0.25

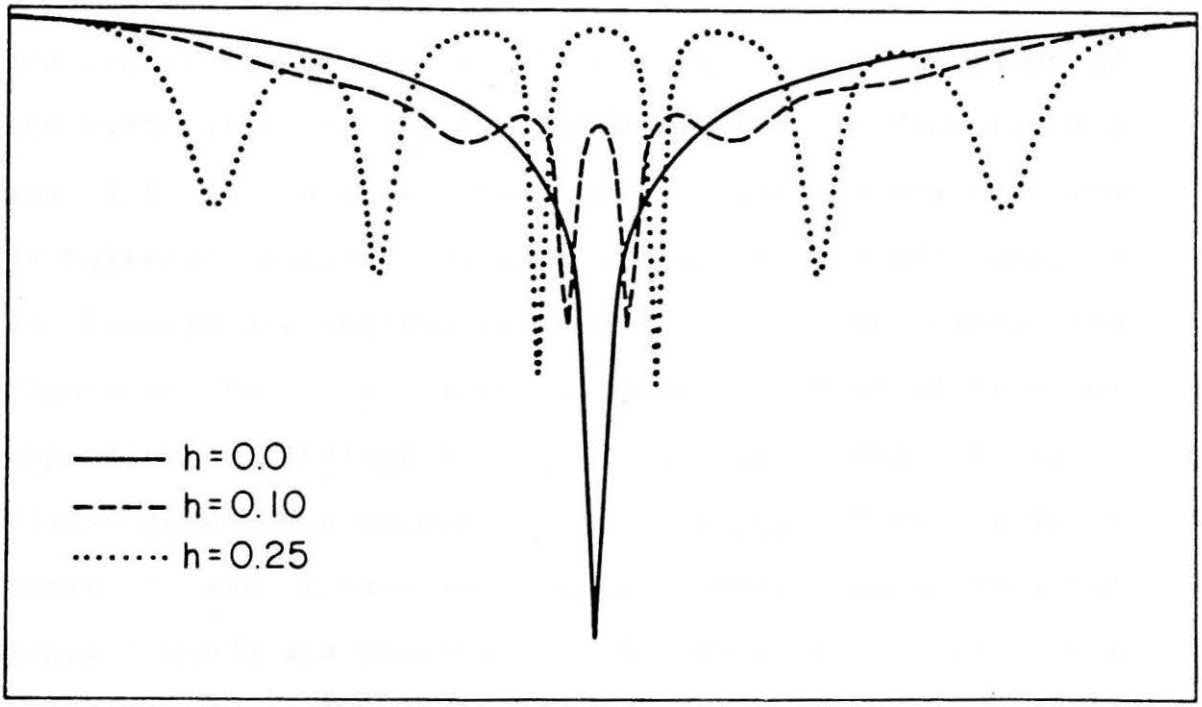
h = 0.0
h = 0.10
h = 0.25

2.1.3 Fitting artifacts

If we assume h = 0 when fitting the Mossbauer spectrum of a SP system with non-zero h then an incorrect interpretation will result. Unfortunately, this artificial interpretation has features which are intrinsically related to SP systems.

We have simulated the spectra for Figures 2-2 and 2-3 by using the Blume and Tjon lineshape with a delta-function distribution of particles whose static Mossbauer parameters are those of the "B site" in magnetite at room temperature (ref.67). We have used $A = 10^{10}$ Hz for Figure 2-2, $A = 4X10^{10}$ Hz for Figure 2-3 and kT = Eb / 3 for both figures. All the non-zero-h spectra in these figures appear to be a superposition of a quadrupole-doublet and a hyperfine-pattern whose individual lines are very broadened. Also, the shape of the outer lines in the simulated spectra of Figures 2-2 and 2-3 (h = 0.25 in both cases) suggest a distribution of hyperfine fields. We have in fact fitted the spectra of Figures 2-2 and 2-3 (with h = 0.25 in both cases) and Figure 2-2 (h = 0.1) with a gaussian distribution of hyperfine splittings (i.e. using a Voigt profile) and a simple quadrupole-doublet. In the hyperfine pattern, lines 1 and 2 have individual intensity parameters but lines 1 and 3 are constrained to have the usual area ratio of 3:1. The fits are reasonably good and show the

kind of error that is made when the more traditional lineshapes and profiles are used. The resulting parameters are listed in Table I; they represent vastly different interpretations of the spectra and not mere numerical disagreements with the true Mossbauer parameters.

TABLE I. Parameters from the fitting of the simulated spectra.

spectrum	Fig.3-2 h=.1	Fig.3-2 h=.25	Fig.3-3 h=.25	Fig.3-2 h=.1	Fig.3-2 h=.25
C.S.	0.78	0.78	0.78	0.78	0.78
Q.S.	0.10	0.10	0.10	0.10	0.10
g*bH	2.99	3.06	2.76	3.04	3.07
L/2	0.13	0.09	0.61	0.34	0.22
$s(2\ln 2)^{1/2}$	1.04	0.43	0.12	--	--
$F/10^8$	--	--	--	4.3	1.0
C.S. (q.d.)	0.68	0.68	0.67	0.68	0.68
Q.S. (q.d.)	0.57	1.01	0.98	0.63	1.01
L/2 (q.d.)	0.31	0.11	0.06	0.21	0.09
R	.144	.076	.064	.079	.057

$s(2\ln 2)^{1/2}$ is the Gaussian half-width of the distribution of hyperfine fields and "q.d." refers to the quadrupole-doublet which is required to get a good fit. F is in Hz and R is the ratio of the q.d. contribution to the total spectral area. The other parameters are in mm/s.

The spectra of Figure 2-2 (for both h = 0.1 and 0.25) can also be fitted quite well with a quadrupole doublet superposed on a relaxation profile that uses the restriction F+ = F- but the "quadrupole doublet" is suspicious, in that its lines coincide with lines 3 and 4

of the 6-line pattern. In both cases the obtained frequencies are smaller, about 2 times smaller for h = 0.1 and 12 times smaller for h = 0.25, than the true average frequencies, (F+ + F-) / 2. Also, reduced values of the hyperfine field had to be used. These parameters are also listed in Table I, and they demonstrate the trend that we have observed whenever an experimental spectrum can be fitted equally well by this profile and a relaxation profile which relaxes the condition F+ = F-.

2.2 Mossbauer characterization of d < 40 Å alpha-Fe2O3

2.2.1 Sample

The sample was prepared by L. F. Nazar using the solution phase metal atom method of L. F. Nazar et al. (ref.74). Preliminary Mossbauer results were given by Rancourt et al. (ref.78). The synthesis technique was designed to incorporate the iron within the zeolite supercages (zeolite-Y, maximum diameter of supercage is approximately 12 Å, pore size is 8-9 Å) and to avoid chemisorption onto the outer surface of the zeolite. Iron with approximatly 20% Fe-57 enrichment was used and the resulting iron loading was about 0.5-1.0%. Oxidation is probably due to residual amounts of intra-zeolitic water. The resulting alpha-Fe2O3/zeolite-Y compound is

stable in air and no special precautions were taken regarding sample environment during experimentation.

2.2.2 Microcrystal considerations

The main microcrystal contributions which increase in importance as the size of the particle decreases are: lattice expansion, defects such as vacancies and dislocations and inhomogeneities in the electric and magnetic densities. The dominant defect is the surface itself and it will largely determine the magnetostatic and dynamic (i.e., SP) behaviour of magnetic particles.

The case of alpha-Fe2O3 is complicated by the Morin transition (ref.68). This is an "anisotropy transition" (ref.23) at which the spins go from being in the c-plane with a slight canting out of the plane to being perpendicular to the c-plane as the temperature is lowered through the Morin point TM (in the bulk material TM is approximately -25 degrees Celsius). The competing anisotropies arise from the spin coupling to the lattice but, since with small particles there is a large surface contribution to the total magnetic anisotropy energy, we can easily imagine TM being enhanced or suppressed depending on how the particle's shape is correlated with the underlying crystal directions. The Morin transition in alpha-Fe2O3 has, in fact, not been seen down to 4K for

particles with d < 180 Å (ref.64). The lowering of the Morin transition in large (d > 500 Å) alpha-Fe2O3 particles has been explained in terms of the microcrystal lattice expansion (ref.84).

Bulk alpha-Fe2O3 has a single crystallographic site for iron and identical electric and magnetic enviroments for all the iron nuclei. A small particle of alpha-Fe2O3 will, on the other hand, have a distribution of inequivalent iron sites. There can, in general, exist gradients of all the Mossbauer parameters across the diameter of the particle. Iron in the surface layer of the particle or at the chemisorption interface between the particle and the supporting medium can have an anisotropic Debye-Waller factor (ref.33) which alone is enough to distinguish it from the iron in the interior of the particle. Also the microcrystal defects give a substantial spread of different electronic environments. For example, Flinn et al. (ref.33) have calculated that a missing nearest neighbour oxygen atom near an Fe+++ ion in eta-Al2O3 will cause a quadrupole splitting of approximately 1.6 mm/s. Such defects have also been proposed by Néel (ref.76) to account for the magnetic moments of ultrafine antiferromagnetic particles; the net moment being caused by a non-perfect cancellation of the two sublattices of atomic moments. This idea has received support from the experimental observations of Cohen et al. (ref.20) and it is also applicable in

understanding our observations (see section 2.2.4).

Finally, it is important to realize that every small-particle/supporting-medium preparation will contain distributions of particle sizes, shapes, and chemisorbtion centers. This spread in characteristics, together with the variations associated with a single particle, is probably the main cause for the broad line-widths reported above Tb in alpha-Fe2O3 particles.

FIGURE 2-5

T > Tb spectra for alpha-Fe2O3. Various fits of two spectra for the sample studied in section 2.2: (a) T = 296K, fitted with two independent Lorentzian lines, (b) T = 296K, fitted with two independent Gaussian lines, (c) T = 296K, fitted with two Voigt lineshapes, and (d) T = 77K, also fitted with two Voigt lineshapes. The Lorentzian fit in (a) overestimates the background whereas the Gaussian fit in (b) underestimates it - both lead to unreliable spectral areas. The Voigt fits have much lower chi squared values and fit the wings quite well. The velocity range is from -3.0 mm/s to +3.0 mm/s.

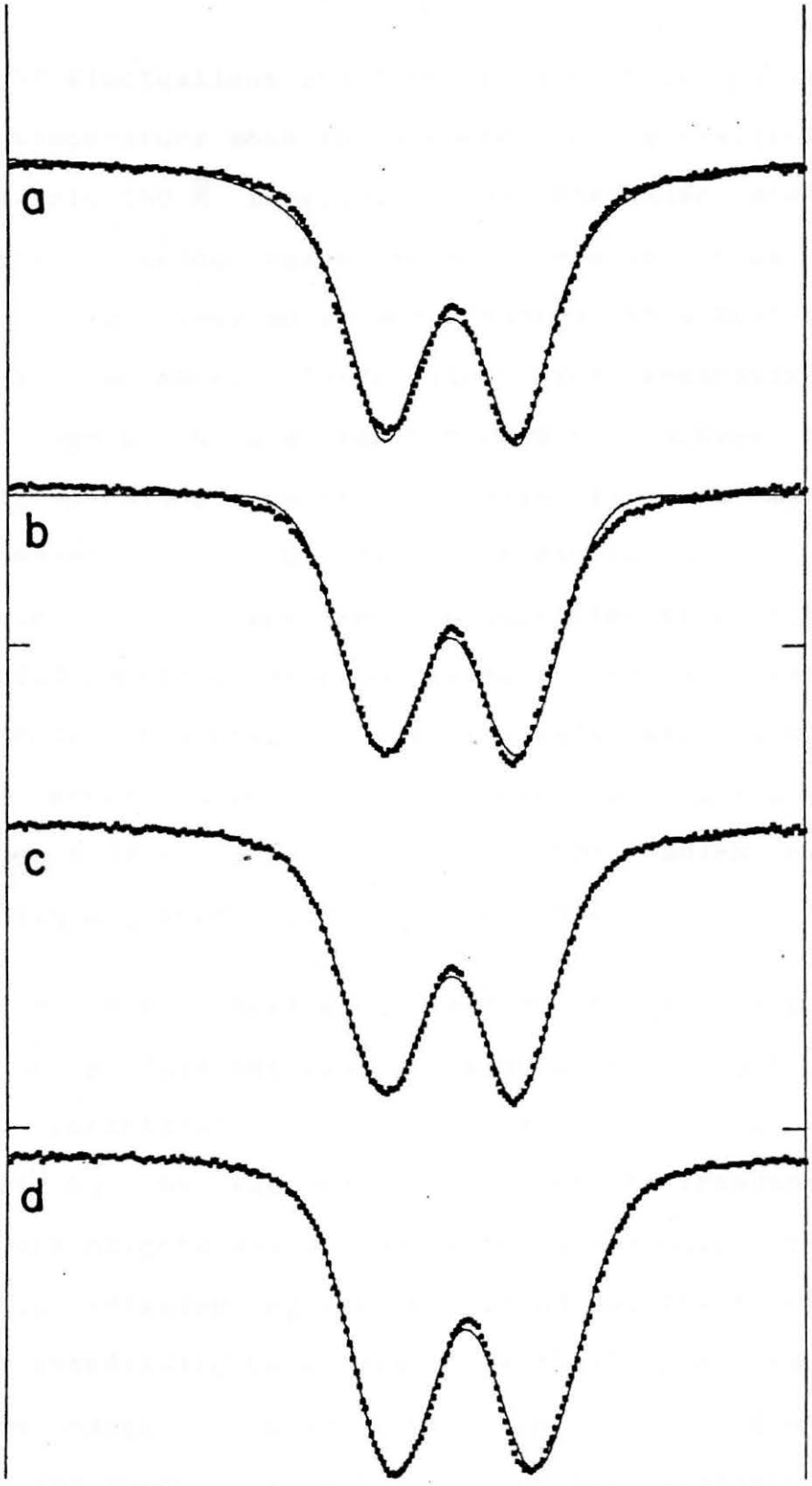
a
b
c
d

2.2.3 Above the blocking temperature

SP fluctuations are seen in alpha-Fe2O3 particles at room temperature when the diameter, d, is smaller than approximately 200 Å (ref.59). The Mossbauer spectrum above the blocking temperature is now well known. It consists of two lines which are broadened to a full-width of about 0.8 mm/s. These lines are separated by a Q.S. of roughly 1.0 mm/s (see Figure 2-5) and have their room termperature center of mass at 0.32 mm/s - corresponding to the C.S. of bulk hematite at the same temperature. This spectrum is characteristic of small alpha-Fe2O3 particles at high temperatures and can be used to rule out a possible identification with particles of some other iron oxides such as gamma-Fe2O3 (ref.36,64,5,19), or Fe3O4 (ref.70) which has a drastically different Mossbauer behaviour.

In the high frequency limit of the Blume and Tjon relaxation profile the quadrupole-doublet is constructed from two Lorentzian lines which are only negligibly broadened by the fast relaxation. As the frequency is lowered the heights and widths of the lines begin to be noticeably affected by the relaxation but the lineshape is still essentially Lorentzian. We shall refer to the frequency range in which the shape of the individual lines in the quadrupole-doublet is indistinguishable from the Lorentzian lineshape as the "high frequency domain"

(HFD). When the frequency, f, is within the HFD the two Lorentzian lines have different heights and widths but equal spectral areas (we have found this by fitting simulated spectra in the HFD with two independent Lorentzian lines). Using the static Mossbauer parameters corresponding to small alpha-Fe2O3 particles (Q.S. ~ 1.0 mm/s; hyperfine field ~ 500 kOe) and in the uniaxial case where the hyperfine field flips between the two directions parallel to the e.f.g. principal axis, we find the HFD to be given by $f > \sim 3X10^3$ fm (= $1.5X10^{11}$ Hz). As f is lowered below ~ $3X10^3$ fm the lineshapes become non-Lorentzian and the ratio of the spectral areas of the two lines diverges slowly from its high frequency value of 1. The amount of doublet asymmetry is, as pointed out by Blume (ref.8), dependent on the hyperfine field relaxation frequency, f (in this application f = F). It should therefore be possible to relate the widths (or heights) of the lines to f. We have in fact found, by an analysis of the Blume-Tjon lineshape that the convenient characterization parameter in the HFD is the difference between the Lorentzian half-width of the higher energy line (w2) and that of the lower energy line (w1). We write this parameter as δ = w2 - w1 and state our result for uniaxial relaxation:

$$\delta(par) = +-4.335\ (g*bH) \quad / 2f \quad (3)$$

$$\delta(per) = -+2.16\ (g*bH) \quad / 2f \quad (4)$$

Equation (3) refers to the case were the allowed directions of H are parallel to the e.f.g. principal axis (when the system is SP these are the easy directions of magnetization) and Equation (4) corresponds to allowed directions which are perpendicular to the principal axis of the e.f.g. The first sign is for e.f.g. > 0 and the second sign corresponds to e.f.g. < 0. In these equations f is in the same units as the natural linewidth, that is, it has units of energy (mm/s) - it is related to its value in Hz by division with Planks constant. It should be noted that $\delta_{(par)} + 2\,\delta_{(per)} = 0$, from which it can be deduced that isotropic relaxation between easy axes exhibiting cubic symmetry will not cause a noticeable δ.

Another possible cause for doublet asymmetry in the Mossbauer spectrum of iron with identical environments is the Goldanskii-Karyagin (G-K) effect (ref.39,55,37). This effect is due to anisotropies in the lattice vibrations, that is, anisotropic Debye-Waller factors which can be associated with the particle's surface layers. Unlike relaxation in the HFD, the G-K effect does cause a net difference between the spectral areas of the two lines in the quadrupole-doublet. For an axially symmetric e.f.g. and neglecting e.f.g. fluctuations (ref.94) the lineshape remains Lorentzian and only its height is scaled by the appropriate angle averaging (ref.26). The G-K effect shows a weak

temperature dependence (compared to SP fluctuations) due to the temperature dependence of the anisotropies in the lattice vibrations. It is to be noted that bulk alpha-Fe2O3 does not exhibit a G-K effect and therefore probably has isotropic lattice vibrations.

In our first series of measurements the Mossbauer spectrum remained a quadrupole-doublet down to 77K. Two examples of such spectra are shown in Figure 2-5. Attempts to fit these spectra with two Lorentzian lines with independent heights and widths resulted in unacceptable fits with reduced chi squared values typically the order of 15 (see Figure 2-5a). The Gaussian lineshape gave a much better fit (reduced chi squared ~ 8; see Figure 2-5b) and this suggests that the lineshape is dominated by a broad Gaussian distribution of line positions. When the underlying line, whose position is distributed, is a Lorentzian line the resulting lineshape is the "Voigt Profile" (ref.28). If the Lorentzian is expressed as:

$$L(n;w,l,x) = l\, w^2 \;/\; [(n - x)^2 + w^2] \quad (5)$$

where l is the height, and x is the position of its center, and the Gaussian distribution (normalized to unity) is written as:

$$G(s,x,no) = \exp[-(x - no)^2 /(2\, s^2)] \;/\; [s(2\pi)^{1/2}] \quad (6)$$

where its half-width at half maximum is given by $s[(2\ln 2)^{1/2}]$ and, no is the lineshape center, then the Voigt Profile is given by:

$$V(n;w,l,s,no) = \int_{-\infty}^{+\infty} [G(s,x,no)\ L(n;w,l,x)]\ dx \qquad (7)$$

Fitting with this lineshape typically yielded reduced chi squared values of about 2.5 and two such fits are represented by the solid lines in Figures 2-5c and 2-5d. The fits are not perfect; the remaining misfit can be attributed to a slight skewness in the actual distribution of Lorentzian line positions and to variations in the underlying Lorentzian line itself due to the spread of relaxation frequencies in the sample.

The Voigt Profile fits yield center shifts and quadrupole splittings which are listed in Table II.

TABLE II. Mossbauer parameters from high temperature Voigt Profile fits.

T(K)	% absoption	C.S.(mm/s)	Q.S.(mm/s)
77	2.32	.433	1.079
82	2.32	.430	1.075
95	2.41	.424	1.071
101	2.48	.422	1.066
108	2.56	.421	1.062
296	1.56	.323	1.011

The C.S.'s and Q.S.'s are obtained from the two Voigt line positions for each spectrum and the "% absorption" is the ratio of the spectral area (in counts) to the total number of background counts in the velocity range from -3.0 mm/s to +3.0 mm/s.

The dependence of the C.S. on the temperature is consistent with the SOD effect.

The Q.S., taken from the Voigt line positions for a doublet, is seen to increase as the temperature is lowered. This gradual increase cannot be explained in terms of the larger particles in the sample (which have a smaller Q.S. (ref.5)) being progressively "frozen out" into a hyperfine-pattern, since not even a weak trace of such a pattern is observed in these spectra nor in spectra that were run at a larger energy setting of the transducer in an effort to see the usually stronger outer lines of the hyperfine-pattern. It might be due to thermal expansion of the microcrystal but it can also be understood as follows. The smaller particles in the sample have a stronger temperature dependence of their Debye-Waller factors (i.e., the Mossbauer fraction associated with the smaller particles increases more rapidly than that associated with the larger particles as the temperature is lowered (ref.2)) and, we expect these smaller particles to have larger quadrupole splittings. The measured Q.S., which is obtained from a spectral average, will therefore be weighted more heavily towards the larger values as the temperature is decreased.

The ratio of the Voigt areas for the two lines in the doublet is independent of temperature over this range (77K-300K) and is given by $r = a2/a1 = 1.078$ where a2 and a1 are respectively the areas for the high and low energy

lines. Since the area under a Voigt Profile is proportional to the spectral area of the associated Lorentzian line, we interpret this non-unity ratio as being due to the G-K effect. This represents the first unambiguous and quantitative distinction between the G-K effect and relaxation in causing a quadrupole-doublet asymmetry in SP particles.

It then remains to convert the Lorentzian line-widths obtained from the Voigt fits into SP frequencies via an equation such as Equation 3 or 4. It turns out however, that the Lorentzian line-width is not a reliable parameter. The lineshape is largely Gaussian ($y = w/s(2)^{1/2} \approx .55 \pm .2$) but there is an important uncertainty due to Lorentzian to Gaussian line-width tradeoffs which presumably adjust in order to account for spectrum to spectrum shape variations (e.g. noise, changes in the line position distributions with temperature, etc.). This difficulty can be overcome by using the Voigt height, hv, as the frequency sensitive parameter in the HFD. hv is given by:

$$hv = V(n=no;w,1,s,no) = (\pi/2)^{1/2} \; 1 \; w \; K(0,y) / s \qquad (8)$$

where K(x,y) is a tabulated function (ref.29). We perform a linear expansion of K(0,y) about the average experimental value of y and obtain $K(0,y) \sim e - cy$ ($e = .854$, $c = .470$), from which we can show that, in the

absence of a G-K effect:

$$h\nu_1 - h\nu_2 = (\pi)^{1/2}\, c\, l\, w\, \delta / 2s \qquad (9)$$

where $h\nu_1$ and $h\nu_2$ are respectively the Voigt heights of the low and high energy lines in the quadrupole-doublet, π l w is the spectral area of the underlying Lorentzian (a quantity which is conserved in the HFD) and δ is the quantity which is directly related to the SP frequency by an equation such as Equation 3 or 4. If we define $\varepsilon = (h\nu_1 - h\nu_2) / (h\nu_1 + h\nu_2)$ then in the presence of a G-K effect we obtain:

$$\varepsilon = (1-r)/(1+r) + \delta/2[(2^{1/2})(es/c) - w] \qquad (10)$$

where $r (= a_2/a_1)$ is equal to h_2w_2/h_1w_1 in the HFD, and $w = (w_1 + w_2) / 2$. If s and w are taken to be the corresponding experimental averages (.224mm/s and .180mm/s respectively) and if ε and r are obtained directly from the spectra then a reliable value of δ can be calculated from Equation (10).

Equations 3, 4, and 10 suggest a procedure whereby the SP frequency can be obtained as a function of temperature from spectra taken at various high temperatures. From such data it is then possible to extract an estimate of the average particle volume which is independent of the magnetic anisotropy constant. This

is done in section 2.2.5 and yields a value that is consistent with what must be expected from the low temperature behaviour described in section 2.2.4.

FIGURE 2-6

Low temperature alpha-Fe2O3 spectra - below the blocking temperature. The most dramatic change in appearance occurs between the spectra at T = 22K and T = 24K. The superparamagnetic transition temperature (defined in section 2.1.2) is at T ~ 23K. The velocity range is from -11.0 mm/s to +11.0 mm/s.

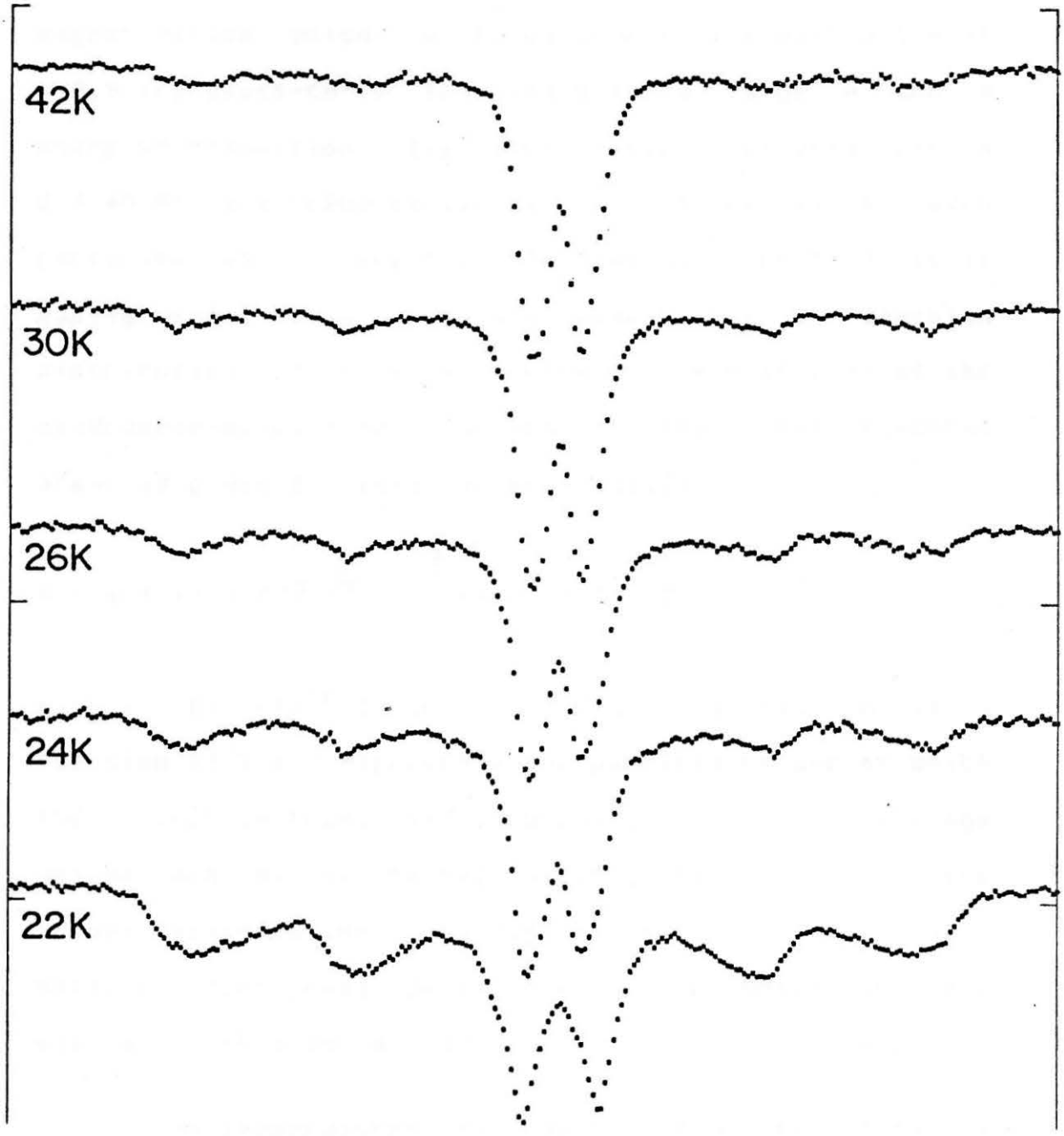
42K
30K
26K
24K
22K

2.2.4 Low temperature behaviour

Large alpha-Fe2O3 particles have a small magnetization which is comparable to the bulk value of ~ 2.5 erg/gauss-cm^3 . This leads to a large A and a sharp SP transition. TTS have, in fact, not been seen in d > 40 Å alpha-Fe2O3 particles. For a sample of such particles which have the same Mossbauer fraction, it is easily shown that when the sample has a Gaussian distribution of particle volumes, the ratio, R, of the quadrupole-doublet contribution to the total spectral area, is given by Gauss' error function:

$$R = \mathrm{erf}(x) = (2\pi)^{1/2} \int_{-\infty}^{x} [\exp(-(t^2)/2)]dt \qquad (11)$$

with $x = [(2\ln 2)^{1/2}] \cdot (vM - \langle v \rangle) / Sv$, and where vM is a function of T and represents the particle volume at which the "sharp" SP transition occurs. $\langle v \rangle$ is the average volume and Sv is the half-width at half maximum of the volume distribution. Kundig et al. (ref.5) have obtained functional dependences of R which are very similar to this for d > 40 Å alpha-Fe2O3 particles.

At temperatures below about 50K we too observe a hyperfine-pattern whose relative intensity increases as the temperature is lowered. These measurements were performed on the same alpha-Fe2O3/zeolite-Y sample and some of the spectra are shown in Figure 2-6. The

observed hyperfine-pattern is quite distinct from that of bulk alpha-Fe2O3 and from all previously measured hyperfine-patterns of d > 40 Å alpha-Fe2O3 particles. The main distinguishing features are as follows: (1) a very large line-width of ~ 2.2 mm/s - compared to 0.36 mm/s for bulk hematite under the same experimental conditions but at room temperature and to ~ 0.8 mm/s for small-particle alpha-Fe2O3 at high temperatures, (2) a line-1 to line-2 to line-3 area ratio which is far from the bulk value of 3:2:1, being typically 1:1:b where b is difficult to estimate due to the overlap of the quadrupole-doublet onto lines 3 and 4, (3) a large skewness of the lineshape - this is particularly apparent at T=22K in Figure 2-6, (4) an effective quadrupole splitting (as obtained from the average line positions of lines 1, 2, 5, and 6) which has the same sign as in the bulk material above the Morin point but whose value is more typically ~ .2 mm/s - compared to .569 mm/s [= $(e^2)qQ/2$] for bulk hematite at room temperature and to ~1.0 mm/s for small-particle alpha-Fe2O3 at high temperatures, and (5) reduced effective hyperfine field values which typically represent an 11%-16% reduction with respect to bulk hematite at the same temperature. This hyperfine-pattern is qualitatively similar to a pattern which van der Kraan (ref.2) has attributed to the surface layer in d > 40 Å alpha-Fe2O3 particles.

All the above mentioned features of the observed

hyperfine-pattern can be explained by the following picture. Firstly, it is clear that the particles are the smallest which have been studied to date by Mossbauer spectroscopy and must have d < 40 Å since at T = 42K we obtain R = .74 whereas at T = 40K van der Kraan (ref.2) has obtained R < ~.05 for d = 40 Å alpha-Fe2O3 particles. This follows from the fact that the blocking temperature is, to a good approximation, proportional to the volume of the particle.

Whereas lattice deformations have been invoked to explain the Q.S. of d > 40 Å alpha-Fe2O3 particles (ref.32), we expect that in these particles, with d < 40 Å, microcrystal defects (especially vacancies) will be the main cause of the larger-than-bulk Q.S.. In such a situation the angle between the e.f.g. principal axis and the h.f. direction will be greatly randomized over the nuclear sites within each particle. With simulated spectra where this angle is totally random and using the bulk values of line-width and h.f., we obtain a line-width which is approximately given by $(e^2)qQ/2$ (Q.S. in absence of a hyperfine splitting) and an effective quadrupole splitting of the order of .2 mm/s when $(e^2)qQ/2$ = 1.0 mm/s. This explains the observed effective quadrupole splitting but can only partially account for the unusually large observed line-width. Simulated spectra where the sign of the e.f.g. is correlated to the direction of the hyperfine field (in

such a way as to have one sign when the e.f.g. is mostly parallel to the h.f. and the opposite sign when the e.f.g. is mostly perpendicular to the h.f.) yield essentially the same features.

The remaining observed features of the hyperfine-pattern (i.e. line-width, line-skewness, line-1 to line-2 area ratio, and additional reduction of effective h.f.) can all be explained as follows. With such small particles we expect that the same vacancies which cause the Q.S. will also cause an important net imbalance in the two antiferromagnetic sublattices. The resulting magnetic moment on a particle goes as $N^{1/2}$, where N is the number of magnetic ions in the particle (this assumes that the N ions were put at random onto one or the other sublattice (ref.9)). This will correspond to a magnetization which may typically be as large as $N^{1/2}(5\mu)/(N/2)Vm \sim 10^2$ erg/gauss-cm^3 (here μ is the Bohr magneton, 5μ is the magnetic moment on an Fe+++ site in alpha-Fe2O3 (ref.31), Vm is the molecular volume of alpha-Fe2O3). Such a magnetization is more typical of magnetite than hematite and corresponds to a small A. We therefore expect to see a broadened SP transition with a large part of the spectral intensity corresponding to TTS. TTS have large line-widths (the order of 2 and 3 mm/s), skewed lineshapes, unusual line area ratios and can yield additional reductions in the effective h.f. when F+ is not equal to F-. We therefore attempted to

get quantitative agreement between the observed spectra and various TTS lineshapes by a least squares fitting procedure.

Satisfactory fits to the spectra of Figure 2-6 were first obtained by using six Voigt lines with independent parameters. The corresponding Mossbauer parameters, along with those obtained from bulk alpha-Fe2O3 at room temperature and under the same experimental conditions, are given in Table III. Here R is estimated by assuming that lines 3 and 4 in the hyperfine-pattern

TABLE III. Mossbauer parameters for low temperature spectra. Results for "six Voigt line fit" of the spectra shown in Figure 2.

T(K)	chi	q-doublet C.S. (mm/s)	Q.S. (mm/s)
22	2.7	.551	1.613
24	1.5	.481	1.221
26	1.3	.473	1.185
30	2.0	.467	1.115
42	2.2	.465	1.082
296	1.0	.356	0.980
296(bulk)			

	hyperfine-pattern C.S.	(Q.S.) eff	(g*bH) eff	R
22	.445	-.143	3.128	.35
24	.435	-.128	3.275	.61
26	.408	-.229	3.265	.64
30	.414	-.134	3.280	.69

42	.46	-.29	3.18	.74
296	---	---	---	1.00
296(bulk)	.337	-.569	3.512	.00

The center shifts (C.S.) and quadrupole splittings (Q.S.) for the quadrupole-doublet were calculated from the Voigt line positions of the two central lines in the measured spectrum. The C.S. of the hyperfine-pattern is the average Voigt line position of the four outer lines (lines 1, 2, 5, and 6) in the measured spectrum. The effective excited state Zeeman splitting, (g*bH)eff, was obtained from the seperation of the two outermost lines (lines 1 and 6). The effective quadrupole splitting, (Q.S.)eff, was obtained from the Voigt line positions (V1, V2, V5, and V6) of the four outermost lines as (Q.S.)eff = (V6-V5)-(V2-V1). The parameter R is an estimate of the fractional quadrupole-doublet contribution to the total spectral intensity.

are present under the quadrupole-doublet and have a spectral intensity equivalent to one third of the intensity for lines 1 and 6. The increase in the Q.S. of the central doublet as the temperature is lowered is consistent with the suggestion that the Q.S. increases as the size of the particle decreases.

The spectrum at T = 22K has a hyperfine-pattern which makes up a large part of the total spectral intensity and it is therefore a good spectrum on which to test various TTS fits. The chi squared values and the Mossbauer parameters for these fits are given in table IV. The fitting procedures are described in the figure caption for Table IV.

TABLE IV. Mossbauer parameters from various fits of the T = 22K spectrum.

fit	NFP	chi	C.S. (mm/s)	Q.S. (mm/s)	2w (mm/s)	g*bH (mm/s)	F+/F-	R
a	25	2.7	.551	1.613	1.0(+)	--	--	.35
			.445	-.143	2.2(+)	3.128	--	
b	12	13.6	.552	1.583	.90(+)	--		.35
			.407	0.0(++)	.90	3.240	105./105.	
c	13	11.9	.553	1.676	.78	--		.25
			.404	-.047	.97	3.127	9./9.	
d	15	6.0	.478	1.519	1.46	--		.062
			.485	-.146	.40	3.352	12.6/55.0	
e	22	2.5	.512	1.331	1.14	--		.101
			.454	-.202	.35	3.353	24.0/106.3	(.668)
			.443	-.046	.74	3.780	35.0/375.7	(.231)

NFP is the number of free parameters in a given fit, chi is the reduced chi squared for the fit, 2w is the linewidth (with the relaxation profiles, 2w refers to the underlying Lorentzian full-width which would be directly observed at very high or very low frequency) and F+ and F- are the SP relaxation frequencies in units of fm . "Fit-a" refers to the same fit which is described in Table II. "Fit-b" was obtained with the isotropic relaxation profile of Dattagupta and Blume (ref.33) for the hyperfine-pattern and two independent Lorentzian lines for the quadrupole-doublet. "Fit-c" utilises the uniaxial relaxation profile of Blume and Tjon (ref.22) with equal magnetization probabilities (F+ = F-) and in the case where the uniaxial direction is parallel to the e.f.g. principal axis. "Fit-d" and "fit-e" where obtained with the same profile as in fit-c except that we have allowed for unequal magnetization direction probabilities by letting F+ not equal F- . In fit-e we have attempted to account for distributions of the h.f., Q.S., and relaxation frequencies by using two relaxation profiles for the hyperfine-pattern - the fraction of the total spectral area which each of these represent is given in brakets at the far right of the table. (+)these numbers represent averages for more than a single linewidth. (++)this parameter was frozen at the zero value during the fitting procedure.

Fit-b was intended to check whether the paramagnetic

isotropic relaxation proposed by van der Kraan (ref.2) to occur in the surface layer of alpha-Fe203 could quantitatively explain our results. The fit is very poor and the profile is unable to give the correct line-1 to line-2 area ratio in the hyperfine-pattern. In fact, the only profile which gave satisfactory fits considering this ratio is the one used in fits "d" and "e". Anisotropic relaxation is likely the only plausible explanation for the observed line-1 to line-2 area ratio since the particles are too dispersed to align themselves magnetically and the zeolite itself is a fine randomly oriented powder. Fit-d and fit-e are therefore the two fits which make the most sense physically and they have resonably low chi squared values. It follows that the peculiarly large change in the Q.S. for the quadrupole-doublet (and in the difference between the C.S. for the quadrupole-doublet and the C.S. for the hyperfine-pattern in the same spectrum) in going from T = 24K to T = 22K in Table III is mainly due to the fitting procedure used to obtain those numbers. We can also see that the true value of R for the T = 22K spectrum is ~.1 as opposed to .35 - the other values of R from Table III for T > 24K are not noticeably affected in this way because the hyperfine-pattern is too weak for its exact functional form to be of consequence.

Finally, if we examine the C.S. in the low temperature spectra we can deduce that smaller particles

in the sample have a C.S. which is larger than that of the bigger particles by approximately .05 mm/s. The corresponding spread in the Q.S. is much larger (~.5 mm/s) and is an estimate of the fraction of the linewidth at high temperatures which is due to particle to particle Q.S. variations.

2.2.5 Average particle volume and sample anisotropy constant

The average particle volume, <v>, can be obtained in a manner that is independent of the anisotropy constant, K, as follows. First, the fractional Voigt height difference, ε, is measured directly from the high temperature spectra. The experimental values of ε at 77K and 296K are respectively +.0162+-.002 and -.0011+-.002 . Next, the corresponding differences in the Lorentzian full-width, δ, are calculated via Equation (10). This yields δ's at 77K and 296K which are respectively +.0425+-.0016 mm/s and +.0288+-.0016 mm/s. These numbers can then be used to extract SP relaxation frequencies, F, via an equation like Equation (3) or (4). Assuming that the Q.S. has a large lattice contribution which is mainly due to roughly homogeneous Fe+++ vacancies and that the ellipsoidal particles are all long and thin (i.e. needle shaped as opposed to "short and flat" or disk shaped) then, since the

magnetization is always along the shortest axis due to surface energy minimization (ref.9), most of the Fe-57 nuclei in such particles experience a negative e.f.g. whose principal axis is parallel to the long axis and the appropriate δ-F relation is given by Equation (4). The SP frequencies at 77K and 296K, as obtained from Equation (4) and using the Zeeman splitting from fit-d at T = 22K (g*bH = 3.352 mm/s), are respectively $(1.54+-.06)X10^{11}$ Hz and $(2.27+-.06)X10^{11}$ Hz. These two frequencies are then used to deduce an average magnetic moment per particle, mp, as follows. At high temperatures (i.e. above the blocking temperature) Equation (1) crosses over to Equation (2). Equation (2) immediately gives:

$$mp = Mv = (G/2\pi)\,(kT1 - kT2) / (F1 - F2) \qquad (12)$$

for any two temperatures, T1 and T2, and their associated SP relaxation frequencies, F1 and F2 respectively, in the HFD. For Fe+++ in alpha-Fe2O3 there is an almost perfect orbital quenching (ref.23) so we assume the spin only value of G [= (electron charge)/(electron mass)(speed of light)]. Using Equation (12) and the values of F at 77K and 296K we obtain $mp = (1160\ +500/-270)X10^{-21}$ erg/gauss = (24.9 +10.8/-5.7)5μ . Finally, assuming as Néel did (ref.9), that $mp = (N^{1/2})\cdot$(moment per magnetic ion) we obtain $\langle v\rangle = (N/2)Vm = 15600\ +16300/-6300\ \text{Å}^3$ and an equivalent spherical particle diameter of d = 31.0 +8.3/-5.0 Å. The

errors are the maximum errors given the experimental uncertainty in ϵ . The corresponding magnetization is 75 erg/gauss-cm^3 .

If the particles are all short and flat then the e.f.g. is positive and has its principal axis along the magnetization direction. The corresponding δ-F relation is now Equation (3) and repeating the above calculation yields: SP frequencies at 77K and 296K which are respectively (3.08 +- .11)X10^{11} Hz and (4.54 +- .11)X10^{11} Hz, mp = (581 +103/-76)X10^{-21} erg/gauss = (12.5 +2.2/-1.6)5μ, $\langle v \rangle$ = 3900 +1500/-940 Å^3, d = 19.5 +2.3/-1.7 Å, and a magnetization of 149 erg/gauss-cm^3 . Since the low temperature data (section 2.2.4) is consistent with a more or less random e.f.g. principal axis direction we conclude that the sample contains a distribution of particle shapes and that the correct δ-F relation is something between the two extreems which are represented by Equations (3) and (4). A reasonable approximation, given the "quasi-random" e.f.g. principal axis direction, is:

$$\delta = (2/3)\ (4.335)\ (g*bH)^2\ /\ 2F \qquad (13)$$

which is obtained when one third of the particles have an e.f.g. principal axis parallel to H and e.f.g. > 0 and the remaining two thirds have principal axes perpendicular to H and e.f.g. < 0 . This yields: mp =

$870X10^{-21}$ erg/gauss, $\langle v \rangle$ = 8200 $\AA^3$, d = 25 $\AA$, and M = 103 erg/gauss-cm^3 - these will be tacken to be the correct values when estimating the anisotropy constant.

The temperature at which the spectral area in the quadrupole-doublet is roughly equal to the spectral area in the hyperfine-pattern is approximately 23K. Assuming that all the particles in the sample have the same Mossbauer fraction, T = 23K is then the temperature at which the particles with $v = \langle v \rangle$ undergo their SP transition. Of the particles which contribute to the hyperfine-pattern at $T <\sim 23K$, the smaller ones have $v \sim \langle v \rangle$ and relatively high SP frequencies. They have just undergone their SP transition at $T \sim 23K$ whereas the larger particles, with $v > \langle v \rangle$, underwent their SP transition at higher temperatures and have lower SP frequencies. Therefore, the SP transition occurs at an average SP frequency, (F+ + F-)/2, which closely corresponds to the observed high frequency hyperfine-pattern (fit-e) at T = 22K and is approximately given by (35fm + 376fm) / 2 = 205fm. Using this frequency at T = 23K and with the above values of $\langle v \rangle$ and M, we solve Equation (2) for h = 0 to give an estimate of the anisotropy constant K. We obtain $K \sim 1.1X10^{6}$ erg/cm^3 which corresponds to a barrier energy ($K\langle v \rangle$) of $\sim 8.9X10^{-15}$ erg and a blocking temperature of 65K.

An estimate of the anisotropy factor, h, can be

obtained from the measured average ratio F+/F- for the sample via Equation (1). From fit-d and fit-e we have F+/F- = ~.23 which gives h = .15 and an effective applied field, Heff, of 3.2 kgauss.

FIGURE 2-7

Block diagram: Particle size characterization technique. The method for extracting the average particle volume described in section 2.2.5 is illustrated. If the distribution of line positions is very narrow it is possible to fit with a Lorentzian lineshape and obtain dw directly. When the distribution is close enough to Gaussian the procedure outlined in the text can be used. If the distribution is squewed or not gaussian then a procedure must be found whereby the underlying Lorentzian width can be deconvoluted reliably. In relating <v> to mp for ferromagnetic particles the adjusted small-particle magnetization (which takes into account vacancies, intersticial sites, and microcrystal expansion) must be used. When the particles are antiferromagnetic the adjusted small-particle molecular volume should be used although this is not a major source of error.

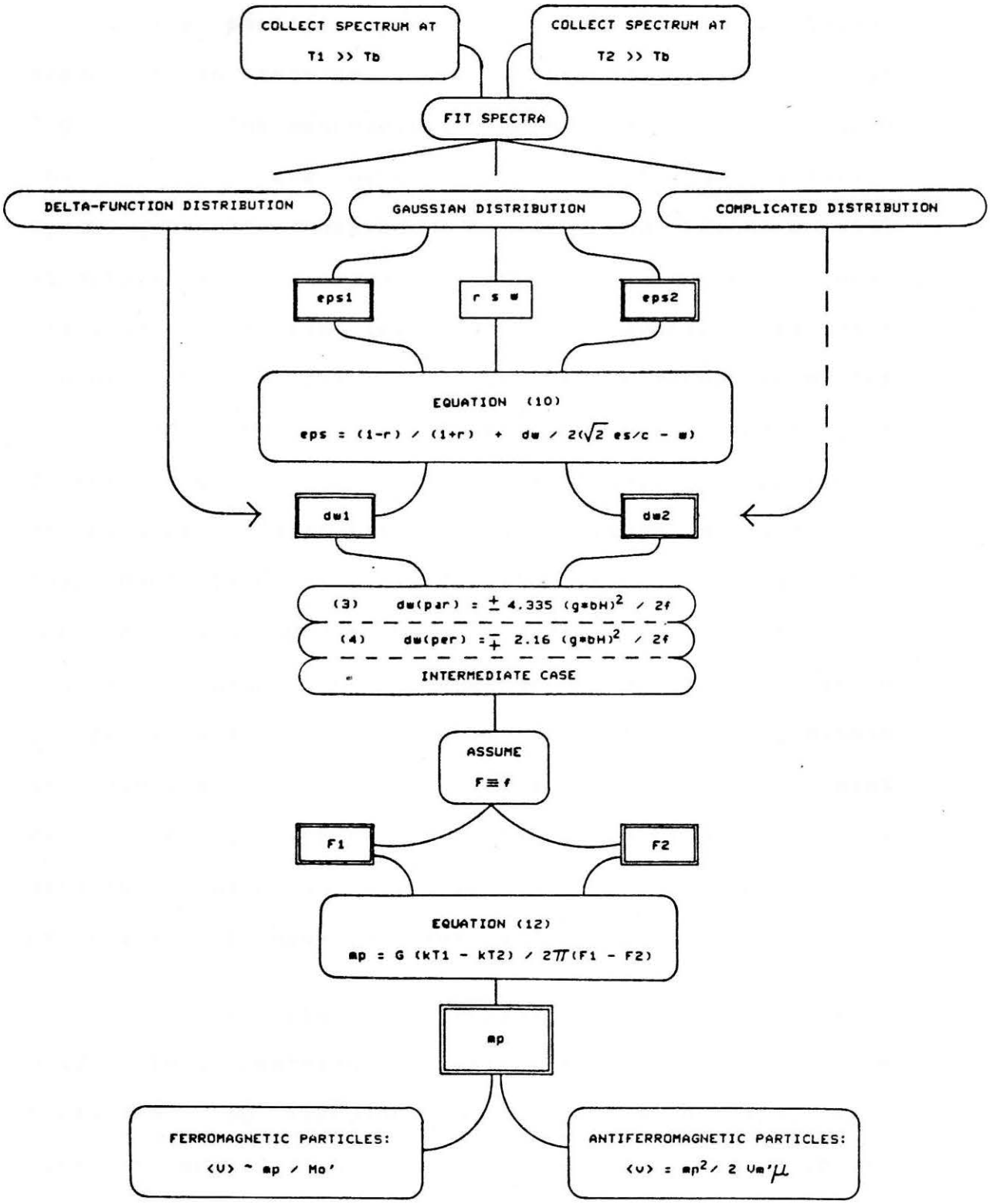
COLLECT SPECTRUM AT
T1 >> Tb
COLLECT SPECTRUM AT
T2 >> Tb
FIT SPECTRA
DELTA-FUNCTION DISTRIBUTION
GAUSSIAN DISTRIBUTION
COMPLICATED DISTRIBUTION
eps1
r s w
eps2
EQUATION (10)
eps = (1-r) / (1+r) + dw / 2(√2 es/c - w)
dw1
dw2
(3) dw(par) = ± 4.335 (g*bH)² / 2f
(4) dw(per) = ∓ 2.16 (g*bH)² / 2f
INTERMEDIATE CASE
ASSUME
F ≡ f
F1
F2
EQUATION (12)
mp = G (kT1 - kT2) / 2π(F1 - F2)
mp
FERROMAGNETIC PARTICLES:
⟨v⟩ ~ mp / Mo'
ANTIFERROMAGNETIC PARTICLES:
⟨v⟩ = mp² / 2 Um'μ

2.2.6 Conclusions regarding alpha-Fe2O3 particles.

The particle size characterization technique described in section 2.2.5 is shown diagramatically in Figure 2-7. The methodology is especially simple when the particles are very small because the SP relaxation symmetry becomes independent of the underlying crystal structure and is uniaxial for elongated and somewhat flattened particles (ref.76). The average magnetic moment per particle can then be obtained from the relaxation frequencies. Also, the high density of defects in very small antiferromagnetic particles establishes a simple relationship between mp and $\langle v \rangle$, thus permitting a reliable estimate of $\langle v \rangle$ to be made. Our sample was found to have a particle volume that is consistent with the low temperature behaviour but which is too large for most of the particles to be truly within the zeolite-Y supercages. We therefore expect that most of the particles are chemisorbed into large pores on the zeolite's outer surface and that the iron concentration decreases as we move into the zeolite.

We have obtained an anisotropy field, h, of ~ 0.15. This represents the first such measurement in SP particles. By studying various $d < 40$ Å alpha-Fe2O3 particle preparations it would be possible to establish the relationship between $\langle v \rangle$ and the average K and h - thereby elucidating the origin of K and the physical

interaction which is modelled by h.

Finally, it is important to point out that K is most likely due to the magnetocrystalline surface energy of the particles. None of the above calculations is affected and the corresponding average surface anisotropy constant, Ks, for our sample is ~ $4.6X10^{-2}$ erg/cm^2. Néel has calculated a value close to this ($1.5X10^{-2}$ erg/cm^2) for elongated ellipsoidal NiO particles (ref.76). Since the shapes and sizes vary from particle to particle in the sample we expect to have a distribution of K's, this (and the fact that different size particles have different Mossbauer fractions) makes a determination of the particle distribution practically impossible.

3. BULK FE2AS

3.1 Introduction

The intermetallic compounds in which 3d transition metals are alloyed to phosphorous, arsenic, or antimony, in a stoichiometric ratio of two to one, have a complicated electronic structure which combines the magnetism of the transition metals and the covalent character of the P, As, or Sb. As a result, they exhibit a variety of magnetic structures and constitute an interesting and almost untouched field of investigation.

A typical example of such a compound is Fe2As. Covalent bonding is indicated because the material is brittle and the structure is not close-packed. Another example is the alloy series Fe(2-X)Cr(X)As which is described in more detail in section 4.

Fe2As has the Cu2Sb-type tetragonal crystal structure with space group D 4h/7 (P4/nmm) and lattice parameters a = 3.627 Å and c = 5.973 Å. The unit cell is shown in Figure 3-1. There are two crystallographically inequivalent but equally populated sites for iron which, together with the arsenic, correspond to the following special positions of the space group:

iron site I	(0,0,0) and (1/2,1/2,0)
iron site II	(0,1/2,u) and (1/2,0,$\bar{u}$)
arsenic site	(0,1/2,u') and (1/2,0,$\bar{u}$')

where u and u' are, respectively, 0.33 and -0.265.

The compound is antiferromagnetic below its Néel temperature, TN, of approximately 350K. The spin structure of the ordered phase was worked out by Katsuraki et al. (ref.56,57,58) and has recently been confirmed by Corliss et al. (ref.24) These neutron diffraction studies have found the iron spins to be constrained to the c-plane (within the experimental accuracy of 2°-3°). Each basal plane has only one kind of iron site and all the iron moments within a plane are lined up ferromagnetically. The ferromagnetic layers are

stacked antiferromagnetically along the c-axis in the sequence I(+), II(+), II(-), I(-), II(-), II(+), I(+), ..., such that the magnetic unit cell is twice the crystallographic unit cell and contains 8 iron atoms.

The previous Mossbauer studies (ref.43,77) are in disagreement with each other and with the neutron diffraction results. Grandjean et al. (ref.43) found the site-II moments to be 60^{o} out of the c-plane but this result can be shown to depend on a perturbation theory analysis which is clearly not applicable in this case since the quadrupole parameter, $(e^{2})qQ/2$, and the excited state Zeeman splitting, g*bH, are comparable in magnitude for site-II iron at and below room temperature. The more careful work of Raj et al. (ref.77) found a site-II spin which gradually rotates out of the c-plane as the temperature is lowered so as to be 16^{o} out of the plane at 77K. The present work represents the third Mossbauer investigation of Fe2As. Our Mossbauer measurements are consistent with site-II spins which are exactly confined to the c-plane in the entire temperature range from 4K to TN. The gradual spin rotation can be shown to be an artifact of the fitting procedure whenever the e.f.g. at the Fe-57 nucleus is assumed to have axial symmetry at all temperatures. The effect of spin fluctuations (which becomes more significant as the temperature is raised from 77K) is seen in the T < TN spectra, and, at room temperature, anisotropic spin fluctuations are neccessary

to explain the lineshape.

FIGURE 3-1

Crystallographic unit cell of Fe2As.

(.) site-I iron

(o) site-II iron

(O) arsenic site.

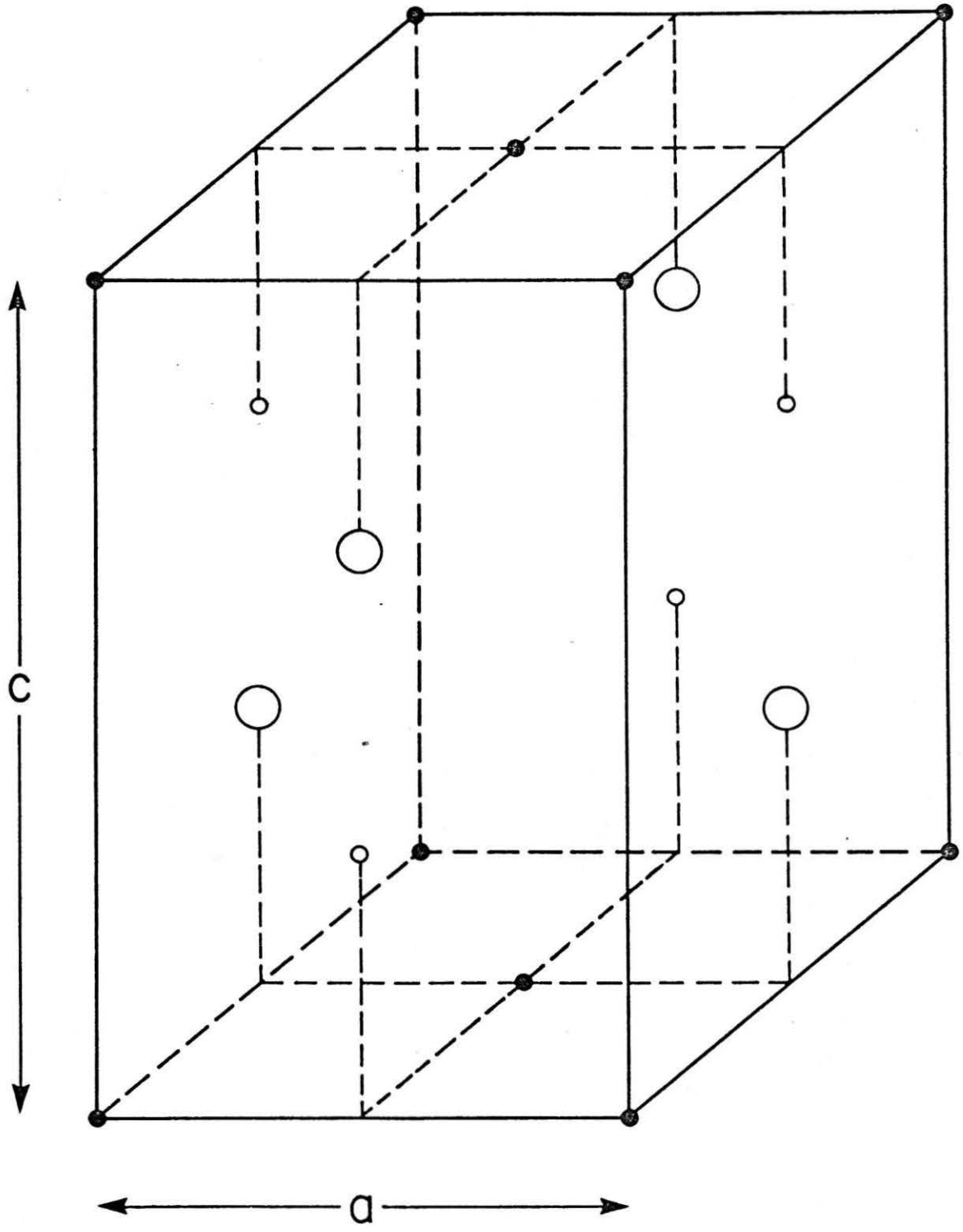
c
a

FIGURE 3-2

Fitted neutron diffraction spectrum of Fe2As at room temperature. The difference spectrum is plotted on the same scale. The data contains 650 channels which are equally spaced by 0.134° and start at 8.71°. The sample was a finely crushed powder held in a cylindrical holder which was immersed in the beam. The neutron wavelength is 1.4 Å. The data was collected by Dr. D. Khatamian at McMaster and the spectrum was fitted by Rose Morra at Chalk River. All the lattice parameters agree with the previously obtained values for an Fe2As single crystal (ref.56). The average square displacements for Fe and As were obtained to be 0.0089 $Å^2$ and 0.0038 $Å^2$ respectively - assuming isotropic Debye-Waller factors. These correspond to a Debye temperature of ~ 450K.

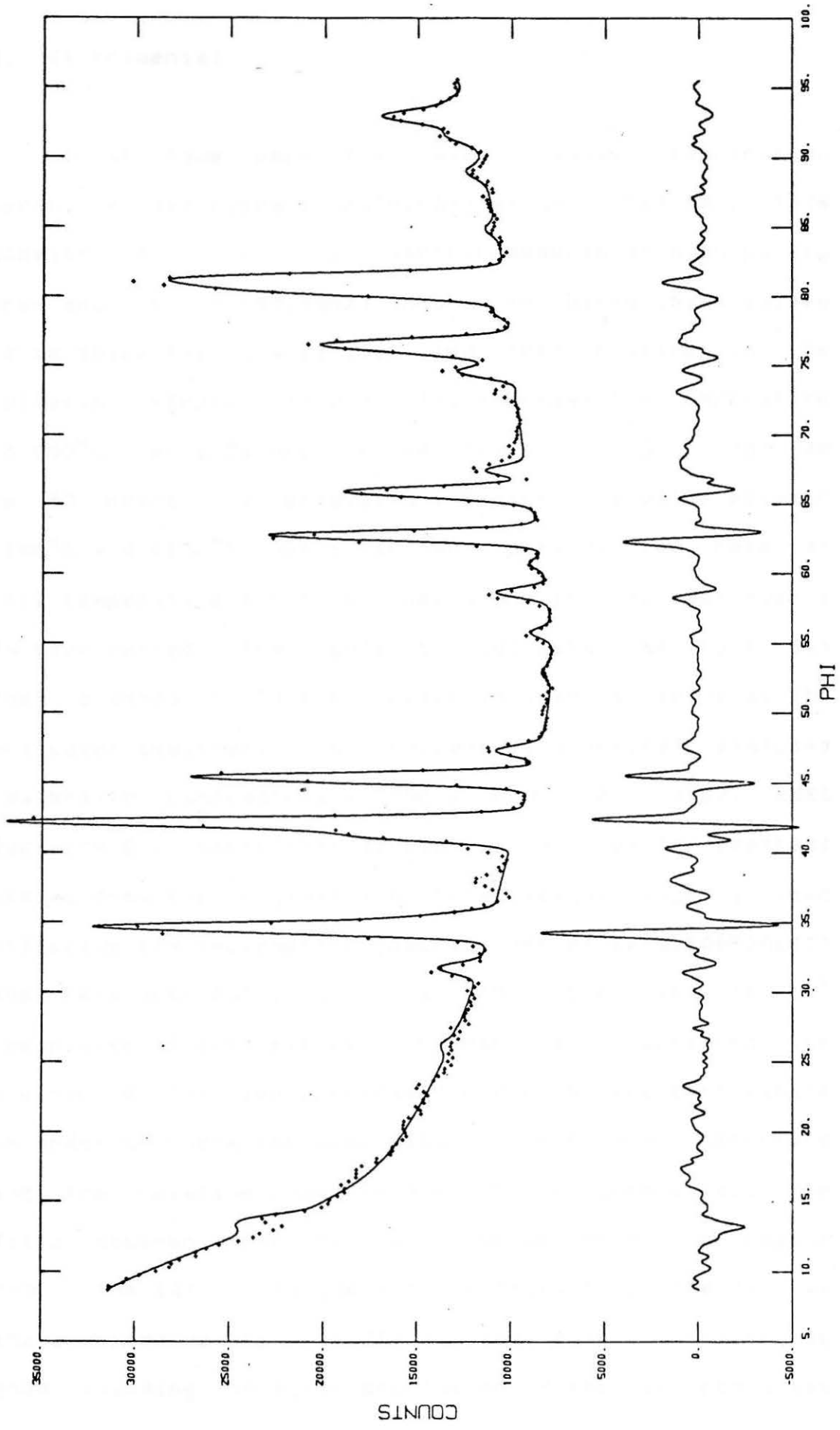
COUNTS
35000.
30000.
25000.
20000.
15000.
10000.
5000.
0.
-5000.
PHI
5.
10.
15.
20.
25.
30.
35.
40.
45.
50.
55.
60.
65.
70.
75.
80.
85.
90.
95.
100.

3.2 Experimental

We have used the same sample fabrication technique described by Katsuraki et al. (ref.56). This consists in sealing stoichiometric amounts of high purity iron and arsenic (99.999%) into an evacuated thick walled (2 mm thickness) quartz tube and then heating in the following steps: (1) gradually increase the temperature to 600°C over a 24 hour period, (2) hold at 600°C for 48 to 60 hours, (3) gradually increase to a value between 1100°C and 1150°C over a two hour period, (4) hold at this temperature for 1 to 3 hours and (5) let cool over a 24 hour period. The resulting polycrystalline ingot was then crushed to a fine powder in order to serve as the Mossbauer absorber. An independent chemical analysis (Galbraith Laboratories, Inc., P.O. Box 4187, 2323 Sycamore Dr., Knoxville, Tennessee 37921) of two seperate pieces from the original (10g total weight) ingot yielded effective stoicheiometric compositions of Fe(2.0083)As(1) and Fe(2.0087)As(1) and less than one part in 10^4 impurities in both pieces. We have also obtained the neutron diffraction spectrum for part of the same sample in order to check the integrety of the crystal structure and the relative population of the two iron sites. The fitted neutron diffraction spectrum is shown in Figure 3-2. The lattice parameters are found to be the same as the accepted values (ref.31) and the fit is reasonably good assuming an equal population of the two iron sites

and equal Debye-Waller factors for the iron in those sites. There is no evidence of an interstitial site for iron in the neutron diffraction data.

The Mossbauer absorbers contained ~ 25mg Fe_2As/cm^2 or ~ 0.33mg Fe-57/cm^2 - an amount sufficiently low to ensure the absence of saturation effects. The exposed sample area was about 1 cm^2 and the powder was sandwiched between two 0.025 mm thick pieces of ultra-pure aluminum foil so as to minimize temperature gradients across the area of the absorber. The maximum temperature variation over the duration of an experiment was typically 1/4°C for both high and low temperature measurements.

The noise/signal ratio in our spectra is typically ~ 0.020 or better whereas the previous Mossbauer measurements (ref.43,77) have had noise/signal ratios which were approximately 0.08.

FIGURE 3-3

Fe2As at three temperatures above TN (= 350K). The spectra are fitted (solid line) assuming two sites for iron in the tetragonal structure. The resulting parameters are given in Table V. The velocity range is from -4.0 mm/s to +4.0 mm/s.

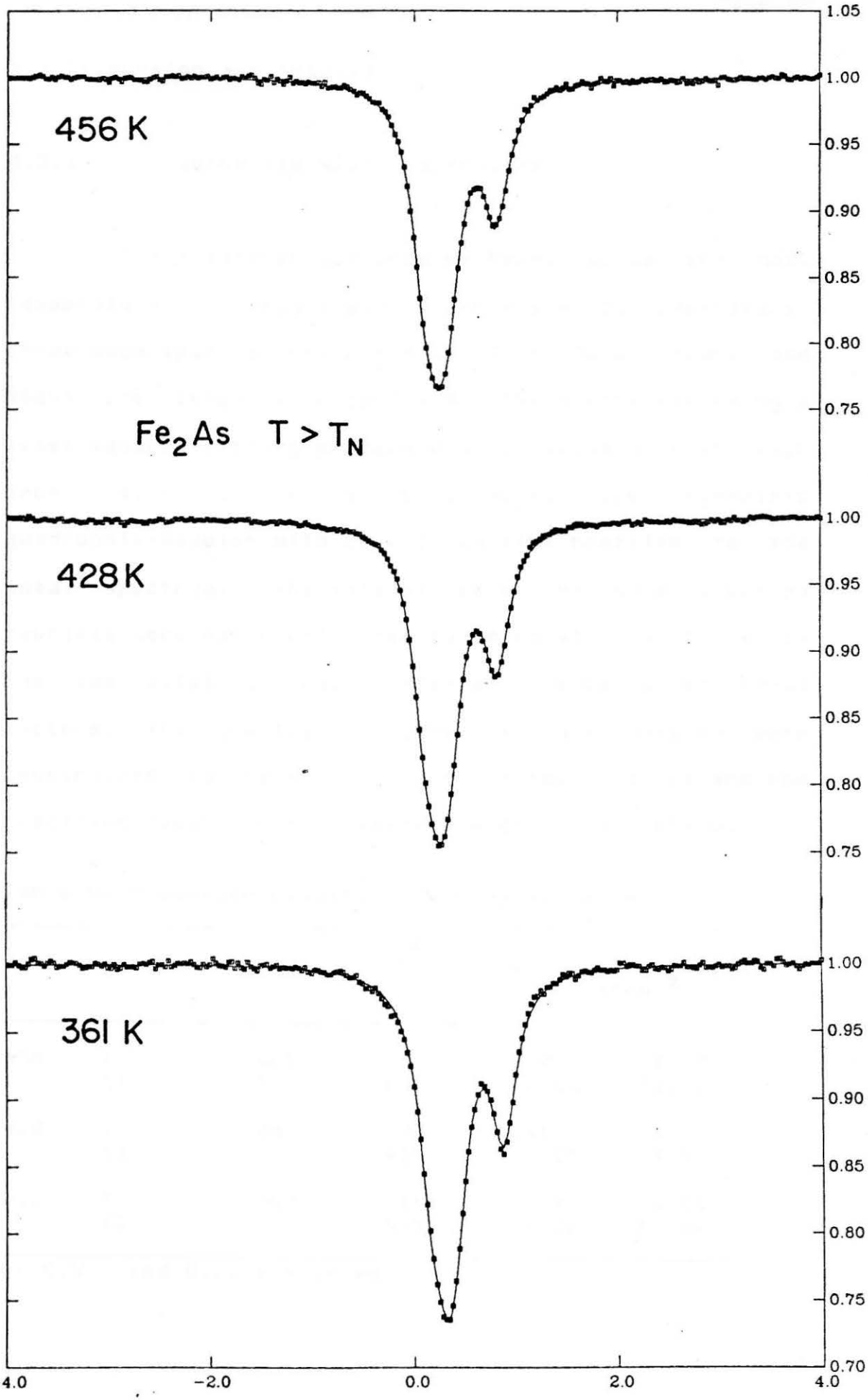
456 K
Fe2As T > TN
428 K
361 K
1.05
1.00
0.95
0.90
0.85
0.80
0.75
0.70
-4.0
-2.0
0.0
2.0
4.0

3.3 Discussion and results

3.3.1 Fe2As above its Néel temperature

The Mossbauer spectrum of Fe2As above the Néel temperature is relatively insensitive to temperature. Three such spectra (collected at T = 361K, 428K, and 456K) are shown in Figure 3-3. These were fitted by a least squares fitting procedure which assumed that each iron site in Fe2As contributes one symmetric quadrupole-doublet with Lorentzian line profiles to the total spectrum. The intensities of the two contibuting doublets were not constrained to be equal so as to allow the two sites to have different Debye-Waller (D-W) factors. The Lorentzian widths at half maximum were constrained to be the same for the two doublets and the resulting Mossbauer parameters are given in Table V.

Table V. Mossbauer results for Fe2As above TN.

T(K)	pattern	L	C.S.	Q.S.	A(I)/A(II) [chi^2]
456	I	.301	.271	.122	1.17
	II	"	.440	.7166	[1.23]
428	I	.291	.290	.117	1.14
	II	"	.457	.7128	[1.39]
361	I	.302	.341	.094	1.01
	II	"	.508	.7128	[1.04]

L, C.S., and Q.S. are in mm/s

Having the Lorentzian widths independent did not give better chi squared values and did not change the parameters significantly except for an ~3% increase in the Lorentzian width of pattern-I with an associated decrease (of ~.006 mm/s) in its Q.S.. The non-unity area ratio A(I)/A(II) does not necessarily imply a difference in D-W factors (whose effect on the ratio goes as T^3) because each quadrupole-doublet may in fact be asymmetric and this asymmetry (which would most likely be due to hyperfine field fluctuations in the manner described by Blume (ref.8)) could have the required temperature dependence.

In agreement with previous work, we assign the quadrupole-doublet with the largest Q.S. to the site with the lowest symmetry (site-II). This is supported by measurements on the Fe(2-X)Mn(X)As system in which part of the site-II iron is replaced by manganese (ref.43). The S4 symmetry at site-II requires that $\eta = 0$ and that the principal axis of the electric field gradient tensor at this site be the c-axis. The Q.S.'s given in Table V can therefore be identified with $(e^2)qQ/2$. We hasten to point out that the Weiss field, which is present at $T < TN$, breaks the 4-fold symmetry at site-II and can cause a non-zero η by its action on the distribution of 3d-electrons at that site. This idea is discussed further in section 3.3.5.

FIGURE 3-4

Fe2As at T = 296K; fit-a and relax-fit. The two fits (solid lines) are discussed in the text. The improvement when relaxation effects are allowed is clear - especially in the central part of the spectrum. The velocity range is from -4.0 mm/s to +4.0 mm/s.

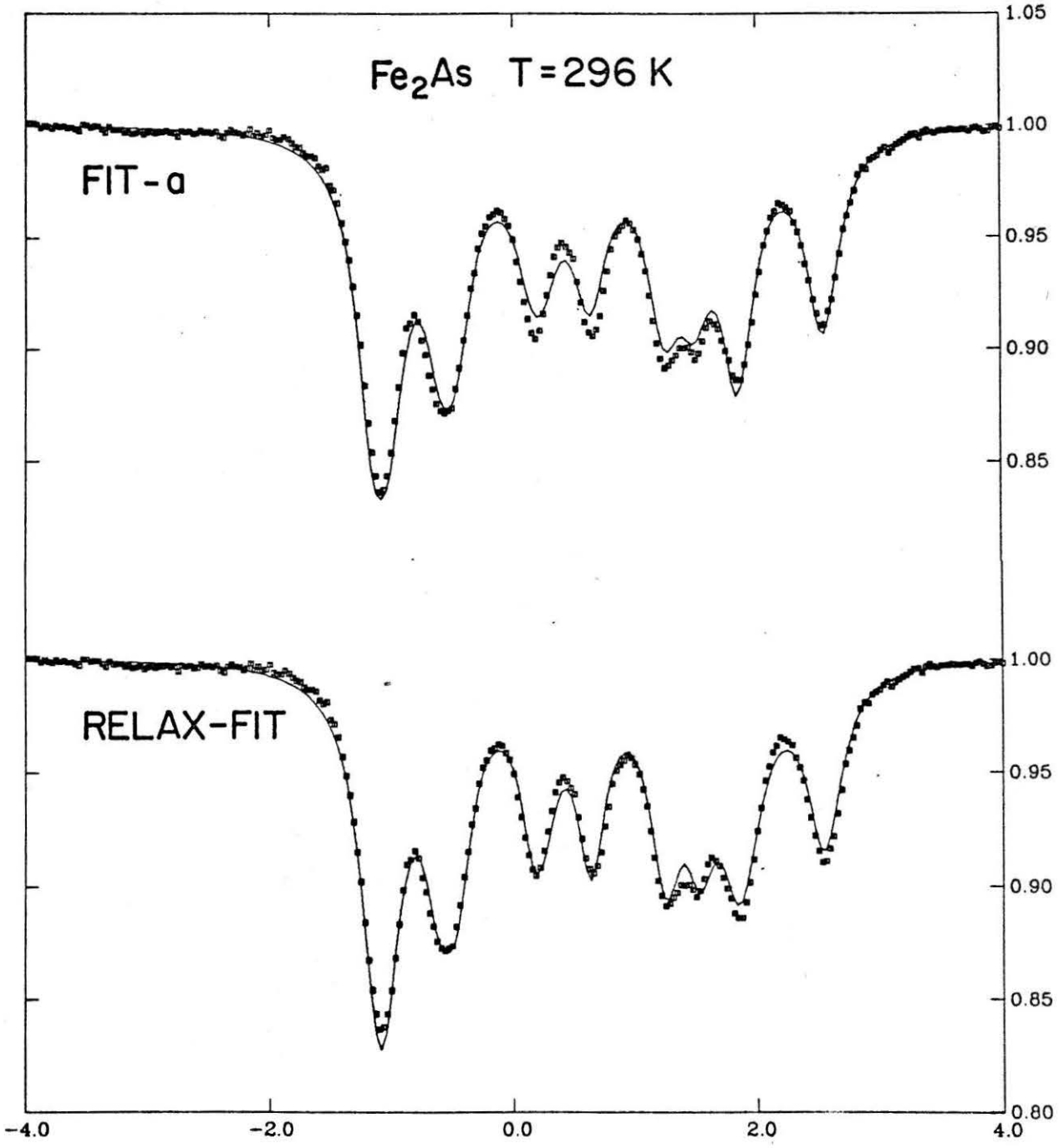
Fe2As T=296 K
FIT-a
RELAX-FIT
1.05
1.00
0.95
0.90
0.85
1.00
0.95
0.90
0.85
0.80
-4.0
-2.0
0.0
2.0
4.0

FIGURE 3-5

Fe2As at T = 90K; fit-a with seperate patterns for sites I and II. The velocity range is from -4.0 mm/s to +4.0 mm/s.

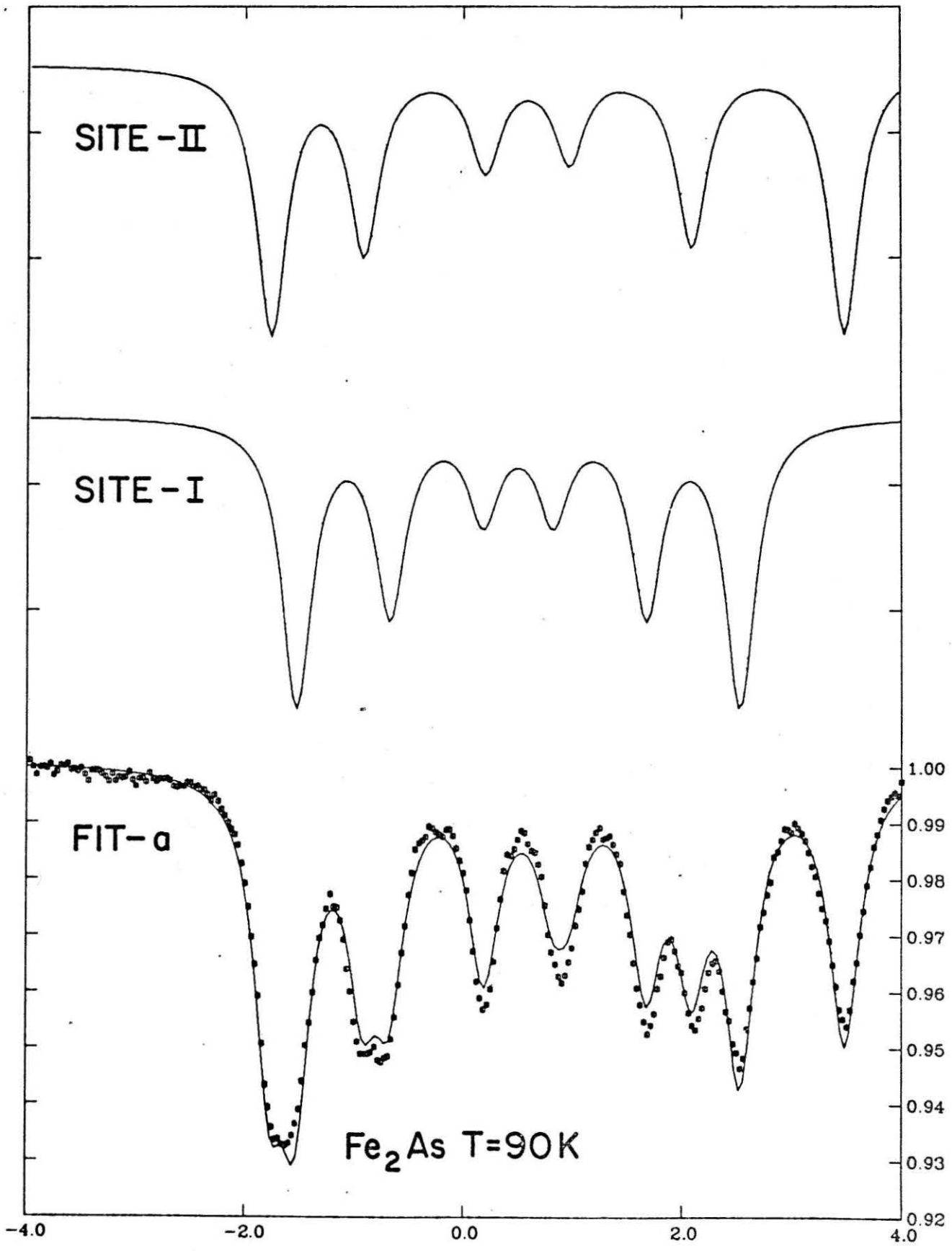
SITE-II
SITE-I
FIT-a
Fe2As T=90K
1.00
0.99
0.98
0.97
0.96
0.95
0.94
0.93
0.92
-4.0
-2.0
0.0
2.0
4.0

FIGURE 3-6

Fe2As at T = 25K; fit-a and fit-b. Here the velocity goes from -5.0 mm/s to +5.0 mm/s. Some qualitative differences between the two fits can be appreciated. The chi squared values are 5.1 for fit-a and 7.5 for fit-b. Fit-b has center shifts which are unphysical - as discussed in section 3.3.2.

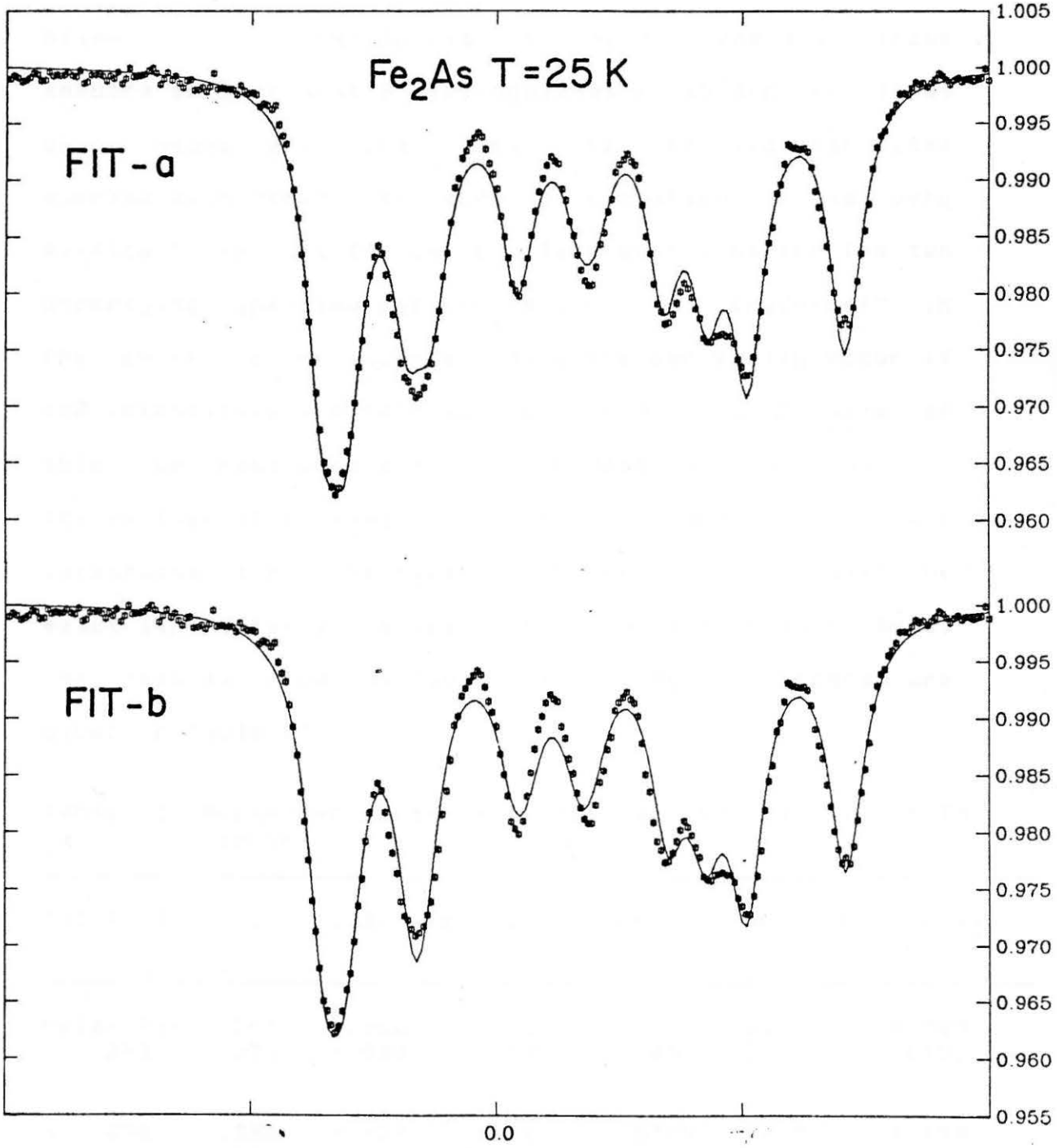
Fe2As T=25 K
FIT-a
FIT-b
1.005
1.000
0.995
0.990
0.985
0.980
0.975
0.970
0.965
0.960
1.000
0.995
0.990
0.985
0.980
0.975
0.970
0.965
0.960
0.955
0.0

3.3.2 Fe2As below its Néel temperature

The Mossbauer spectrum at three temperatures below TN is shown in Figures 3-4, 3-5, and 3-6. These spectra show at most 9 distinguishable absorption lines which means that the lines from the two iron sites overlap each other. In such a situation it is very difficult to get the correct line positions for the two underlying hyperfine patterns because a "trade-off" in the positions of overlapping lines can easily occur if the intensities are left as free parameters. In view of this, we have used a fitting program which diagonalizes the excited state Hamiltonian at each iterative step and constructs the lineshape from Lorentzian lines with the exact line intensities obtained from the Golden Rule. The results from various fits using this program are given in Table VI.

Table VI. Mossbauer parameters from various fits of T < TN spectra.

fit	T(k)	L	C.S.	$(e^2)qQ/2$	g*bH	θ	A(I)/A(II) [chi^2]
relax-fit		.261	+.366	+.027	.901	90.	1.280
	296	.271	+.582	-.631	1.148	90.	[10.1]
a	296	.326	+.326	+.212	.6300	62.5	1.154
		.326	+.593	-.764	.7182	83.5	[15.4]
b	296	.327	+.354	+.072	.6340	90.	1.194
		.327	+.594	-.707	.7245	90.	[16.6]
c	296	.329	+.387	-.043	.6127	90.	1.169
		.329	+.554	-.538	.7656	90.	[27.1]

a	90	.334	+.487	-.001	.8597	80.1	1.048
		.334	+.709	-.730	1.0848	75.3	[9.1]
b	90	.363	+.424	+.197	.8981	90.	1.110
		.363	+.775	-.805	1.0371	90.	[17.5]
c	90	.331	+.487	-.005	.8609	90.	1.067
		.331	+.709	-.550	1.0977	90.	[10.5]
a	25	.400	+.499	+.009	.8665	82.9	.997
		.400	+.735	-.707	1.1029	76.3	[5.1]
b	25	.430	+.432	+.209	.9075	90.	1.032
		.430	+.803	-.790	1.0547	90.	[7.5]
c	25	.400	+.500	+.007	.8676	90.	1.008
		.400	+.735	-.556	1.1134	90.	[5.6]

L, C.S., $(e^2)qQ/2$, and g*bH are in mm/s. A(I)/A(II) is the ratio of the spectral areas for the patterns which correspond to the two iron sites.

When η is constrained to be zero and the angle, θ, between the e.f.g. principal axis and the hyperfine field direction is frozen at a value of 90° (corresponding to site-II spins in the c-plane) we obtain two different minima in the chi squared surface. These two minima are most easily characterized by their distinct values of $(e^2)qQ/2$ for site-II. One minimum (labelled as "fit-c" in Table VI) has $(e^2)qQ/2$ (site-II) ~ -.55 mm/s and the other minimum (labelled as "fit-b" in Table VI) has $(e^2)qQ/2$ (site-II) ~ -.75 mm/s. Fit-b has the $|(e^2)qQ/2|$ at site-II which is closest to the above TN value of .713 mm/s but yields C.S.'s for both sites which do not have the correct temperature dependence (i.e. the linear temperature dependence expected from

the second order Doppler effect for all temperatures above and below TN which are much smaller than the Debye temperature). Therefore, fit-b is physically unacceptable. By contrast, when the fit-c C.S.'s for site-II are plotted as a function of temperature they fall exactly onto the straight line (with slope equal to $-7.35X10^{-4}$ mm/s per K - corresponding roughly to $-3k/2mc = -7.29X10^{-4}$ mm/s per K, where k is Boltzman's constant, m is the Fe-57 mass and c is the speed of light) which can be drawn through the T > TN site-II center shifts. However, fit-c seems to imply that there is a large change in $(e^2)qQ/2$ at site-II as the temperature is changed through the critical point. Such a change in $(e^2)qQ/2$ is usually taken to mean that the transition is a first-order one and is accompanied by a sudden change in the lattice parmeters. The continuity of the lattice parameters of Fe2As near TN has been verified by the X-ray measurements of Raj et al. and the second-order nature of the transition was established by the observed critical point behaviour (ref.24). On the assumption that the magnitude of $(e^2)qQ/2$ cannot change by more than ~ 6% (see section 3.3.5), therefore, fit-c is also physically unacceptable.

If we now free the parameter θ but keep η at zero both fit-b and fit-c go to a lower point on the chi squared surface. We have labelled this minimum "fit-a" in Table VI. It has a value of $|(e^2)qQ/2|$ for site-II

which is comparable to the T > TN value and has the expected temperature dependence of the C.S.'s. It also corresponds to site-II spins which are, for 296K, 90K, and 25K, respectively, ~ 6.5°, ~ 14.7°, and ~ 13.7° out of the c-plane. These angles are in disagreement with the neutron diffraction results which find spins which are at most 3° out of the c-plane at 296K and at 77K (ref.24).

We show (section 3.3.4) that the "true" minimum in chi squared, which is constistant with the requirements, for site-II, that $|(e^2)qQ/2|$ ~ .71 mm/s, that θ ~ 90°, and that the C.S.'s have the correct temperature dependence, occurs at a non-zero value of η. We also explain the existence of the fit-a, fit-b, and fit-c minima in a constistant way and suggest a mechanism (section 3.3.5) which can produce a non-zero η of the right magnitude at T < TN.

3.3.3 Effect of dependent Mossbauer parameters in Fe2As

In the limit that Z/2 << g*bH where Z = $(e^2)qQ/2$, (which is certainly the case for site-I iron in Fe2As) the influence of the e.f.g. on the line positions is given by a single parameter which may be written as $Z\,[1 - (1/2)\,(3 - \eta\cos(2\phi))\,\sin^2(\theta)]$ where ϕ is the angle between the axis of largest e.f.g. in the plane perpendicular to the e.f.g. principal axis and the

projection of the h.f. in that plane. To first order perturbation, the line intensities are not affected by the magnitude of the e.f.g. and are given by the usual 3:2:1 ratio for powder absorbers. In this limit, therefore, given the Mossbauer spectrum for a system whose true parameters are $Z = Z_o$, $\eta = \eta_o$, and $\theta = \theta_o = 90^\circ$ (and assuming $\phi = \phi_o = 0^\circ$; this is equivalent to assuming that the largest e.f.g. direction in the c-plane is along [100] since Ashiwa et al. (ref.1) have shown, from a magnetic anisotropy measurement, that the sublatice magnetizations are along the [100] direction), the equation:

$$Z\,[2 - (3 - \eta)\sin^2(\theta)] = Z_o\,(\eta_o - 1) \qquad (14)$$

defines the surface in the coordinate system (Z, η, θ) of the minimum in the chi squared function. The points on this surface are indistinguishable by means of a Mossbauer measurement and the spectroscopist must depend on such things as symmetry arguements, independent spin direction measurements, and the temperature dependence of the Mossbauer parameters in order to further constrain Z, η, and θ. We note that, since site-I has $Z/2g*bH \sim .08$ at 296K, the parameters Z (= $(e^2)qQ/2$) and θ for site-I given in Table VI are not reliable in that they represent only one of the many equivelant points on the line given by equation (14) when $\eta = 0$.

When the ratio Z/2g*bH is increased the line intensities begin to be affected and the points on the surface described by equation (14) become slightly non-equivelant in that some correspond to lower chi squared values than others. We shall refer to this surface of quasi-equivalent points (and to the closely related surface of strictly equivalent points given by equation (14)) as the "equisurface". We expect that, during the iterative process of least squares fitting, the points on the equisurface will "flow" towards the point (Zo, η_o, Θ_o =90°). Even for large Z, however, many of the points on the equisurface remain equivalent in that their chi squared values are only indistinguishably different. This subject has been discussed more thoroughly by van Dongen Torman et al. (ref.28).

Site-II in Fe2As has Z/2g*bH ~ .49 at 296 K but it is still possible to construct its equisurface by using the computer program described in section 3.3.2. We first simulate various site-II-like spectra (i.e. with L ~ .36 mm/s, g*bH ~ 1.10 mm/s, Z ~ -.713 mm/s, and η = 0, .5, .1, ...) and then fit these spectra with the same program. By constraining one or more of the relavent fitting parameters (Z, η, and Θ) to have values which are different from those of the original simulated spectrum we construct a surface of constrained chi squared minima. We have found that, for site-II-like

simulated spectra, the constrained-chi squared-minimum surface is very closely given by equation (14) where Zo and η_o now represent the site-II-like values used in the simulated spectra (also, $\Theta = 90^\circ$ and $\phi = \phi_o = 0^\circ$). We illustrate the slight deviation of this site-II equisurface from the behaviour described by equation (14) by the following. Assume that the spin canting out of the c-plane is small (as witnessed by fit-a in Table VI) then equation (14) becomes:

$$Z\,[2 - (3 - \eta)(1 - \Delta^2)] = Zo\,(\eta_o - 1) \qquad (15)$$

where $\Delta = (90^\circ - \Theta)\pi/180^\circ$ is the spin canting in radians. This means that, in the plane Z = Zo and for $\eta << 3$, the perturbation approach predicts $3\Delta^2 = (\eta_o - \eta)$ to be the line of minimum chi squared. By comparison the site-II simulations with Zo = -.713 mm/s and g*bH = 1.1134 mm/s yields $3.575\ \Delta^{1.88} = (\eta_o - \eta)$ and a Mossbauer spectrum which changes only indistinguishably as we move along this line.

We are now in a position to understand the various results given in Table VI and most of the inconsistencies in the previous Mossbauer studies of Fe2As. The real case of fitting the actual spectral data, however, is complicated by two further considerations: (1) there are two overlapping

subspectra, and (2) the minimum chi squared increases to the unacceptable value of ~ 15 as we raise the temperature to 296 K - a clear sign of spin relaxation since this phenomenon usually has an important temperature dependence and can have a large effect on the spectral lineshapes (section 3.3.6 for details).

FIGURE 3-7

Fe2As site-II equisurface. The surface is viewed from two different orientations and the points corresponding to fits a, b, and c are indicated. The parameter space is: Δ - the site-II spin canting out of the c-plane in radians, Z - the quadrupole parameter (whose origin is not at the intersection of the Δ and η axes), and η - the asymmetry parameter. In the text it is shown that point-d corresponds to the correct Mossbauer parameters for site-II in Fe2As; (Δ , Z, η) = (0, -.71 mm/s, .21).

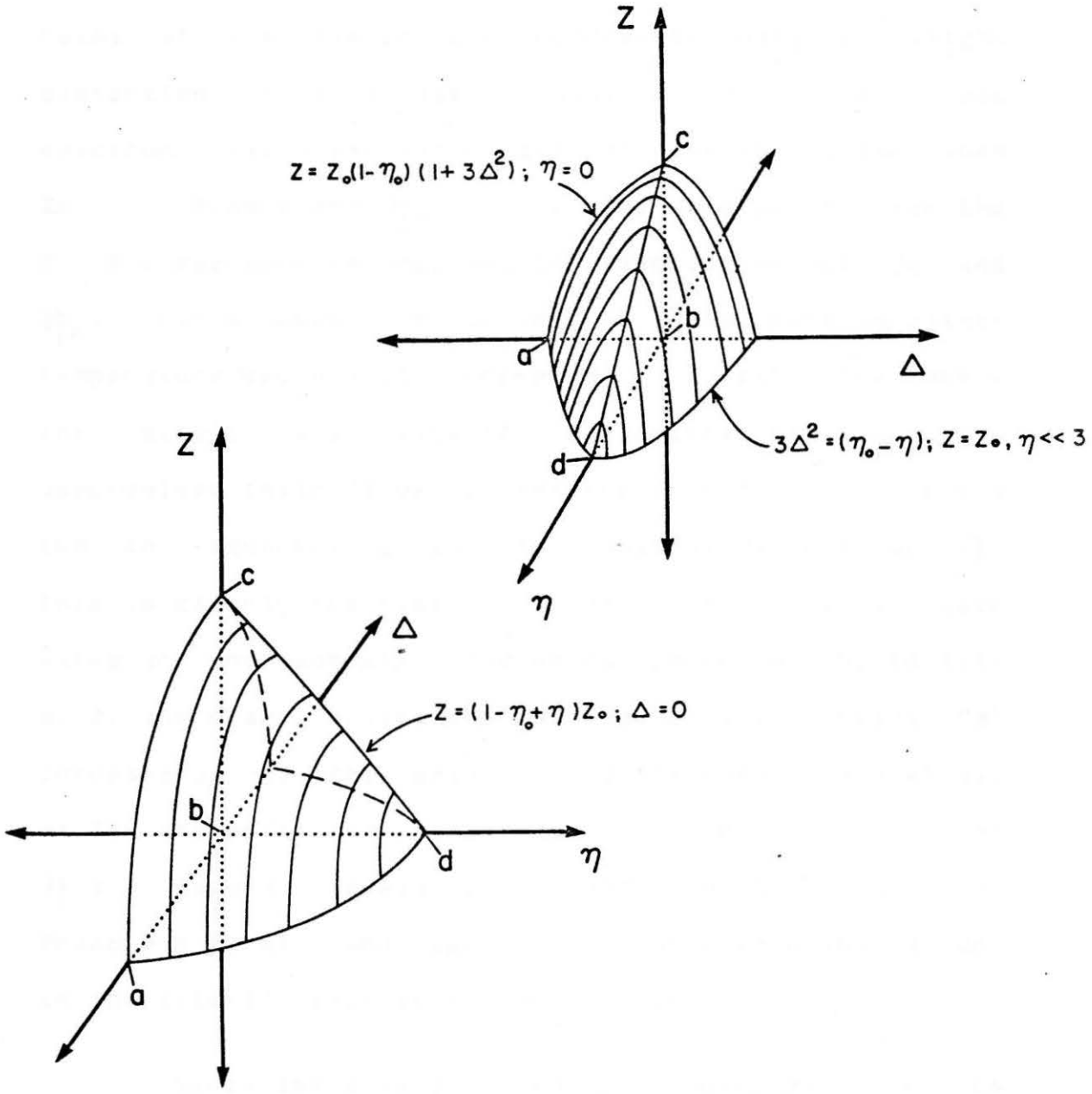
Z
c
$Z = Z_0(1-\eta_0)(1+3\Delta^2)$; $\eta = 0$
b
a
Δ
$3\Delta^2 = (\eta_0 - \eta)$; $Z = Z_0$, $\eta << 3$
d
η
Z
c
Δ
$Z = (1-\eta_0+\eta)Z_0$; $\Delta = 0$
b
d
η
a

3.3.4 Site-II equisurface

The surface given by equation (15) is shown in Figure 3-7. We know that the site-II equisurface for Fe2As at low temperature represents only a slight distortion of this basic shape. Consider the T = 25K spectrum: fit-a and fit-c fall onto the equisurface when Zo ~ -.7 mm/s and η_o ~ .21 . The same is true for the T = 90K spectrum for roughly the same values of Zo and η_o. Fit-b does not touch the equisurface at either temperature because it corresponds to a situation where the site-I and site-II subspectra have mutually compromised their "true" parameters in order to achieve a low chi squared, given the constraints on Θ and η. This is clearly the case since the fit-b C.S.'s for both sites are unreasonable. The points corresponding to fits a, b, and c are indicated in Figure 3-7. Point "a" corresponds to the spin canting observed by Raj et al. at 77K and point "c" (or some point close to c on the η = 0 curve) closely corresponds to the result of Grandjean et al. who reported a large discontinuous jump in the site-II value of $(e^2)qQ/2$ at TN.

Since there is one redundant parameter in the expression for the site-II subspectrum, the minimum chi squared lies along a line in the parameter space for that site. We are therefore at liberty to constrain one parameter on the basis of an independent measurement and,

since two separate neutron diffraction studies have found the spins to be in the c-plane, we chose to constrain Θ to be 90°. An a posteriori justification for this is that the resulting chi squared is as low as, or lower than, any other which we have obtained. We conclude that the "true" chi squared minimum for Fe2As at low temperatures occurs when the site-II parameters are $\Delta = 0 \pm 2^{\circ}$, $Z = (e^2)qQ/2 = -.71 \pm .02$ mm/s, and $\eta = .21 \pm .02$ but admit that, whereas the parameter Z is fairly certain due to the observed equisurface flow along η = constant tranjectories (such as when fit-c "flows" into fit-a with an associated 10% decrease in chi squared), the points which relate Δ and η in the Z = Zo plane are indistinguishable on the basis of the chi squared alone (i.e., on the basis of the Mossbauer measurement alone).

3.3.5 Mechanism for non-zero η

When the symmetry is strictly axial η is exactly zero. In Fe2As, below TN, there is a sublattice magnetization which is perpendicular to the e.f.g. principal axis at site-II. Even if the ion at site-II is orbitally quenched the spin-orbit coupling enables the Weiss molecular field to mix the orbital states such that the expectation value of η is non-zero.

In a simple model we think of the site-II iron as

being acted upon by the following spin Hamiltonian:

$$\mathcal{H} = (C/6)\,[Lx^4 + Ly^4 + Lz^4 - (1/5)\,L\,(L+1)\,(3L^2 + 3L - 1)] - (D/4)\,[Lz^2 - (1/3)\,L\,(L+1)] + W\,Sx + \lambda\,L.S \qquad (16)$$

Where the terms, in order of appearance are, respectively, the cubic and tetragonal crystal field terms, the magnetic interaction with the local moment and the spin-orbit coupling term. With a 3d-transition metal such as iron the orbital angular momentum is $L = 2$ (see Bleaney and Stevens for details (ref.7)). Since the site-II local moment at T = 0K is ~ 2μ (ref.56), we assume that the ion is orbitally quenched and has an effective spin $S = 1$. The ionic states are then linear combinations of the fifteen basis functions which are constructed from the five 3d-orbitals and the three $S = 1$ spinors. The relevant expectation values and thermal averages can then be taken in the manner suggested by Ingalls (ref.49).

We have performed a calculation where we assume the Weiss field [note, the W in Equation (16) is given by $W = (\text{Weiss field}) \cdot 2\mu$] to follow the $S = 1$ Brillouin magnetization curve and find that the thermally averaged η is effectively "turned on" at the critical temperature. This can be seen in Figure 3-8 where $\langle \eta \rangle$ is plotted as a function of temperature for typical values of C, Wo, and λ and various values of D. These

simulations yield η's which are of the right order and thermally averaged e.f.g.'s ($\langle q \rangle$) which have very little temperature dependence (less than 6% change in magnitude) over most of the temperature range. Also, in the above calculation, the ionic ground state has its largest contribution from the orbital wave function which is conventionally written $|x^2 - y^2\rangle$. This is consistent with the covalent bonding scheme in which each site-II iron has a bond with the four nearest neihgbour arsenic atoms.

FIGURE 3-8

Temerature dependence of the asymmetry parameter for various values of the tetragonal crystal field term, D, in wavenumber units (cm^{-1}). The temperature dependence of the molecular field which was used is also given - as obtained from the S = 1 Brillouin function. At T = 0K W = 2000 cm^{-1} which is of the same order as kT at a critical temperature of ~ 350K. The other terms in the spin Hamiltonian (Equation (16)) were taken to be C = -18000 cm^{-1} (cubic crystal field) and λ = -300 cm^{-1}. Also, L = 2 since the participating electrons are in 3d - orbitals. We have assumed that the thermal transition times between the ionic levels are much shorter than tm so that the Boltzman ensemble average could be used to calculate the temperature dependence.

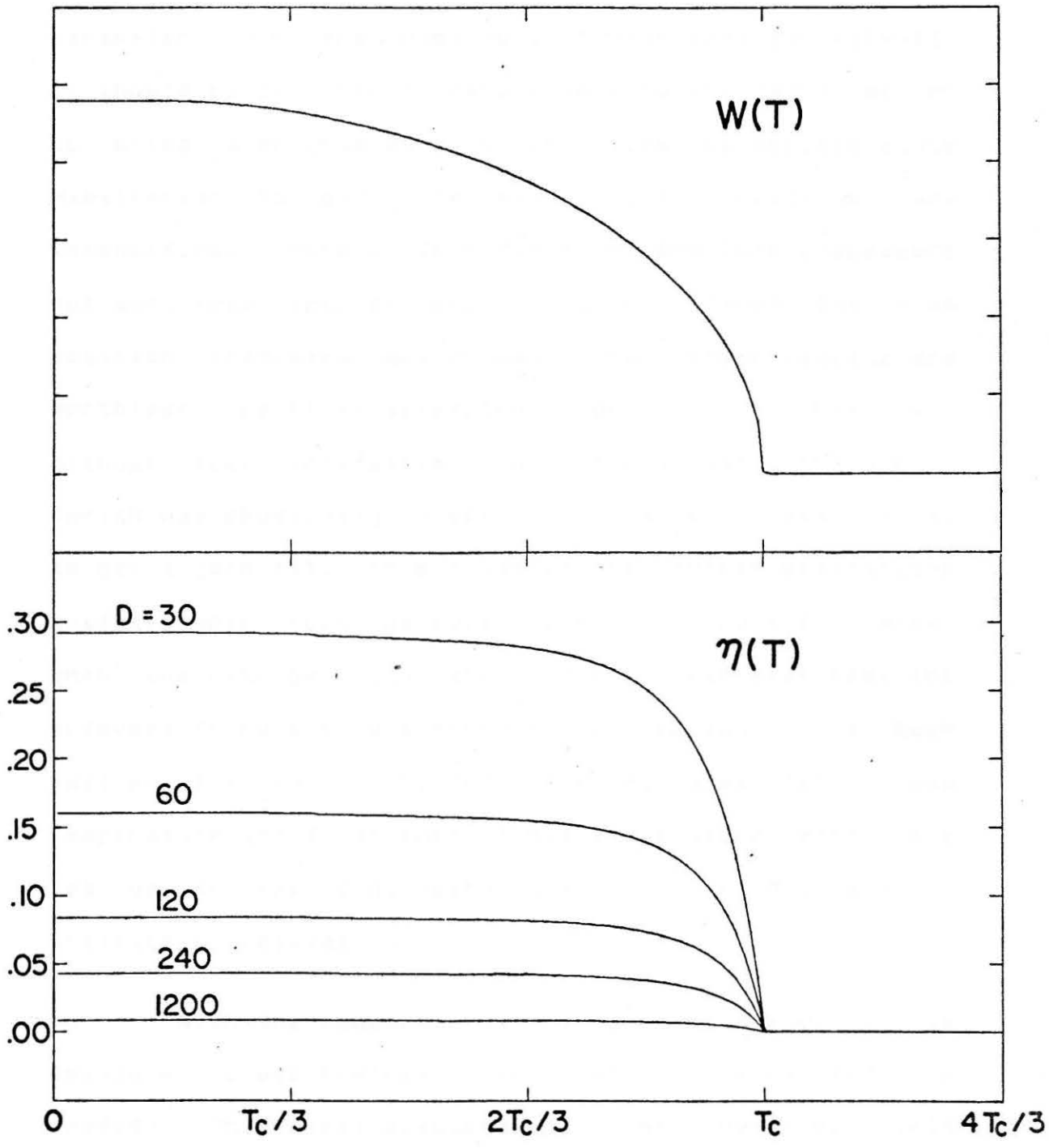
W(T)
η(T)
D = 30
60
120
240
1200
.30
.25
.20
.15
.10
.05
.00
0
Tc/3
2Tc/3
Tc
4Tc/3

3.3.6 Relaxation effects in Fe2As

Since at room temperature the e.f.g. and the parameter g*bH are comparable in magnitude for site-II, it should be possible to obtain an accurate value of θ by using a program which diagonalizes the excited state Hamiltonian to give the exact line positions and intensities. Others (ref.77) have used this proceedure but with free intensities, therefore, given the line position tradeoffs which can occur, their results are worthless. We first attempted to get θ in this way, without free intensities, but found that a third site (which had physically acceptable parameters) was needed to get a good fit. This prompted the neutron diffraction analysis which found no evidence for a third site. Also, when the nitrogen temperature spectrum was examined, the supposed third site was found to correspond to a much smaller fraction of the total spectral area (12% at room temperature and 4% at 90K). This temperature dependence led us to the conclusion that the third site is an artifact of relaxation.

With the constraints $\theta = 90^{\circ}$ and $\eta = 0$, it is possible to use the relaxation profile of Blume and Tjon (ref.9). This model assumes that the hyperfine field jumps between two parallel directions and allows the two jump frequencies to be unequal. Since the h.f. is aligned with the local atomic moment, we expect the time

spent in the direction of the sublattice magnetization (1/f-) to be different from the time spent in the opposite direction (1/f+). Taking the h.f. to be negative (as in most iron compounds) implies f+ < f- at temperatures below the Néel temperature. In such a situation, and when the frequencies are large enough compared to fm, the h.f. is reduced to an effective value given by (h.f.)eff = (h.f.)(f+ - f-)/(f+ + f-). Fitting with unequal relaxation frequencies should therefore yield the T = OK magnitude of the h.f. when the measured frequencies can be directly associated with the critical fluctuations that cause the phase transition.

In fitting Fe2As at T = 296K, we have found that, although equal relaxation frequencies do not give better fits, unequal frequencies significantly improve the chi squared. Also, the resulting h.f.'s for sites I and II are in agreement with and slightly larger than the T = 25K values. This indicates the essential correctness of the fit. The other static parameters are also reasonable and are given in Table VI under "relax-fit". The frequency parameters, in units of fm, are 56 and 310 for site-I and 220 and 980 for site-II.

We expect the frequencies for each site to become more equal as T is increased (until f+ = f- for T > TN) however, the spectra are too "crowded" to permit reliable fits at these temperatures. Also, at lower temperatures, the ratio f-/f+ is greater than ~100. From various

simulations of the Blume and Tjon lineshape (ref.9), we have found that, for these values of f-/f+, the Mossbauer spectrum does not show relaxation effects for whatever average frequency f [=(f+ + f-)/2], whether f << fm, f >> fm, or f ~ fm. We conclude that the relative absence of relaxation effects in our T < ~80K spectra is mainly due to the large ratio f-/f+ and this explains why reliable frequencies could not be obtained at low temperatures.

3.4 Conclusions regarding Fe2As

In order to interpret the Mossbauer spectrum of Fe2As we have introduced the "equisurface" which is a surface in a space of n dependent Mossbauer parameters. Points on this surface correspond to the best fit given constraints in the redundant variables and an assumed lineshape. We note that even a parameter such as the center shift (which can be uniquely determined from the 8 line positions in a single Fe-57 pattern) can become a dependent parameter when there are two or more subspectra.

We have shown that, when we allow a non-zero asymmetry parameter in the ordered state, there exists a small region on the site-II equisurface which corresponds to (1) site-II spins in the c-plane (in agreement with the neutron measurements), (2) an e.f.g. which is

consistent with the T > TN value, (3) an asymmetry parameter, η ~ .21 and, (4) center shifts for both sites which have the expected temperature dependence. We argue that this is the correct Mossbauer interpretation and suggest a mechanism which can produce an η of this size which is effectively "turned off" at and above the Néel temperature.

The presence of anisotropic spin fluctuations (f+ not equal to f-) was identified in the T = 296K Fe2As spectrum. While such fluctuations are not usually observed in Fe-57 Mossbauer spectroscopy they have been seen, for example, in the Ru-99 spectrum of Na3-Ru-04 (ref.93).

We expect anisotropic spin fluctuations to have a measurable effect on the Mossbauer spectrum of all magnetically ordered substances whose relaxation frequencies (f+ and f-) are (1) not too different from each other and (2) comparable to fm. In Fe-57 "not too different from each other" means $f-/f+ < \sim 10^2$ and "comparable to fm" means $f+ < f- < \sim(10^3)$fm. We note that these bounds depend on the static Mossbauer parameters and on the degree to which relaxation-like effects, such as distributions of static Mossbauer parameters, can be ruled out.

Slow spin-spin relaxation is commonly observed in paramagnetic substances and the associated frequency is

seen to increase with the strenth of the exchange coupling. We can effectively decrease the exchange coupling in Fe2As by replacing some of the iron with chromium. The spin relaxation time of these alloys is found to increase with chromium content (section 4.6). The work on Fe(2-X)Cr(X)As, while not yet conclusive, therefore represents further evidence for relaxation in Fe2As.

4. THE FECRAS - FE2AS ALLOY SYSTEM

4.1 Introduction

Fe(2-X)Cr(X)As with X > 0.0 has not previously been studied by Mossbauer spectroscopy or by any other means and, until fairly recently, only the crystal structures for the two extremes Cr2As (X = 2) and Fe2As (X = 0) were known. Cr2As has the same tetragonal structure as Fe2As (Figure 3-1) and comparable lattice parameters; a = 3.613 Å and c = 6.333 Å compared to a = 3.627 Å and c = 5.973 Å for Fe2As. We therefore expected the intermediate compounds (such as FeCrAs) to retain the same crystal structure throughout the entire range of composition.

The system Mn(2-X)Fe(X)As is known to have the Fe2As crystal structure for all values of X between zero

and one (ref.42). Cr, Mn, and Fe are side by side in the periodic table and Cr and Mn have the same atomic radius (1.17 Å; that of iron is 1.16 Å) but we were surprised to find that FeCrAs has a hexagonal crystal structure. The crystallography was worked out recently by R. Fruchart (ref.34) and the unit cell is shown in Figure 4-1. The new structure is not a mere distortion of the tetragonal cell. Fruchart has shown that the tetragonal and hexagonal structures mentioned above are two of the three observed structures for the compounds M-N-B with M,N = Fe, Ni, Co, Mn, and Cr, and B = As or P. That author has also made the following relevant observations: (1) the presence of directional covalent-type forces with some charge transfer is indicated, (2) in all three structures the B atom is at the center of a polyhedron whose nine corners are occupied by the metal atoms, (3) the phosphorus (or arsenic) atoms form triangular arrays of tetrahedra and square base pyramids which are alternately stacked along [010] for the hexagonal structure and along [010] for the tetragonal and orthorhombic structures, (4) the metal atoms M and N are usually ordered; one occupies the tetrahedral site (site-I in Fe2As) and the other occupies the pyramidal site (site-II in Fe2As), and (5) the intermetallic distances are typically those found in the pure metal. These points are helpful in trying to unravel the Mossbauer behaviour of these alloys and they illustrate the underlying crystallography.

We now turn more specifically to the alloys between FeCrAs and Fe2As. We verify their structure by neutron diffraction and examine the magnetism of their crystal phases by Mossbauer spectroscopy.

FIGURE 4-1

FeCrAs crystallographic unit cell. The hexagonal structure has a = 6.096 $\mathring{A}$ and c = 3.651 $\mathring{A}$. It is interesting to note that, as X is increased, the structure for Fe(2-X)Cr(X)As alternates from tetragonal to hexagonal and back to the same tetragonal structure whereas the mass density follows a more regular path from 4.72 g/cm^3 for Fe2As to 4.67 g/cm^3 for FeCrAs and finally to 4.37 g/cm^3 for Cr2As.

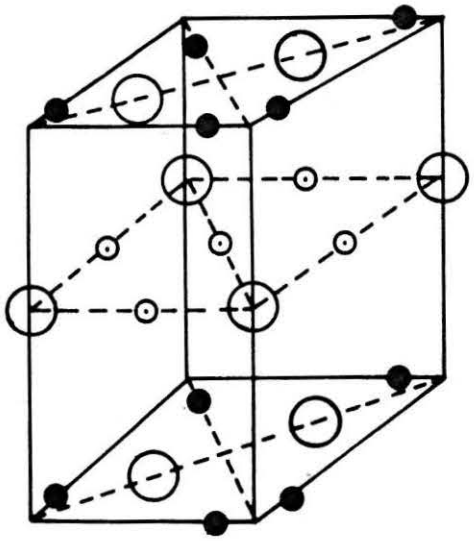

○ ARSENIC SITE

○,● METAL SITES

FIGURE 4-2

Room temperature neutron spectra for Fe(2-X)Cr(X)As. The angular range is from 5.90° to 57.32° and contains 378 channels which are equally spaced by 0.136°. The neutron wavelength is 1.4 Å. The sample was a finely divided random powder and, in most cases, was exactly the same material from which the Mossbauer absorber was made - in the remaining cases both absorbers were from the same original ingot. The predominant tetragonal peaks are labelled "T" and their identification is as follows: T1 (0 0 1/2) (magnetic reflection); T2 (0 0 1); T3 (0 1 0); T4 (1 1 0); T5 (1 1 1); T6 (1 1 3/2) (magnetic reflection; note that the magnetic reflections were not included in the fitting of Fe2As - see Figure 3-2); T7 (0 0 3); T8 (1 1 2); T9 (0 2 0); T10 (0 1 3) and (0 2 1); and T11 (0 0 4). The hexagonal peaks are labelled "H" and can be identified as: H1 (1 1 0) and (0 1 0); H2 (0 0 1); H3 (0 1 1), (1 1 1), and (1 2 0); H4 (1 2 1); H5 (0 2 1) and (2 2 1); H6 (1 3 0) and (2 3 0); H7 (0 0 2); H8 (0 3 0), (3 3 0), (2 3 1), and (1 3 1); and H9 (3 3 1) and (0 3 1). The hexagonal labelling is done with the basis a(1) = a<x>, a(2) = (a/2)<x> + $[(3)^{1/2}]$(a/2)<y>, a(3) = c<z> where <x>, <y>, and <z> are the othonormal unit vectors. (h k l) refers to the reflection from the crystal plane normal to the vector h a(1) + k a(2) + l a(3).

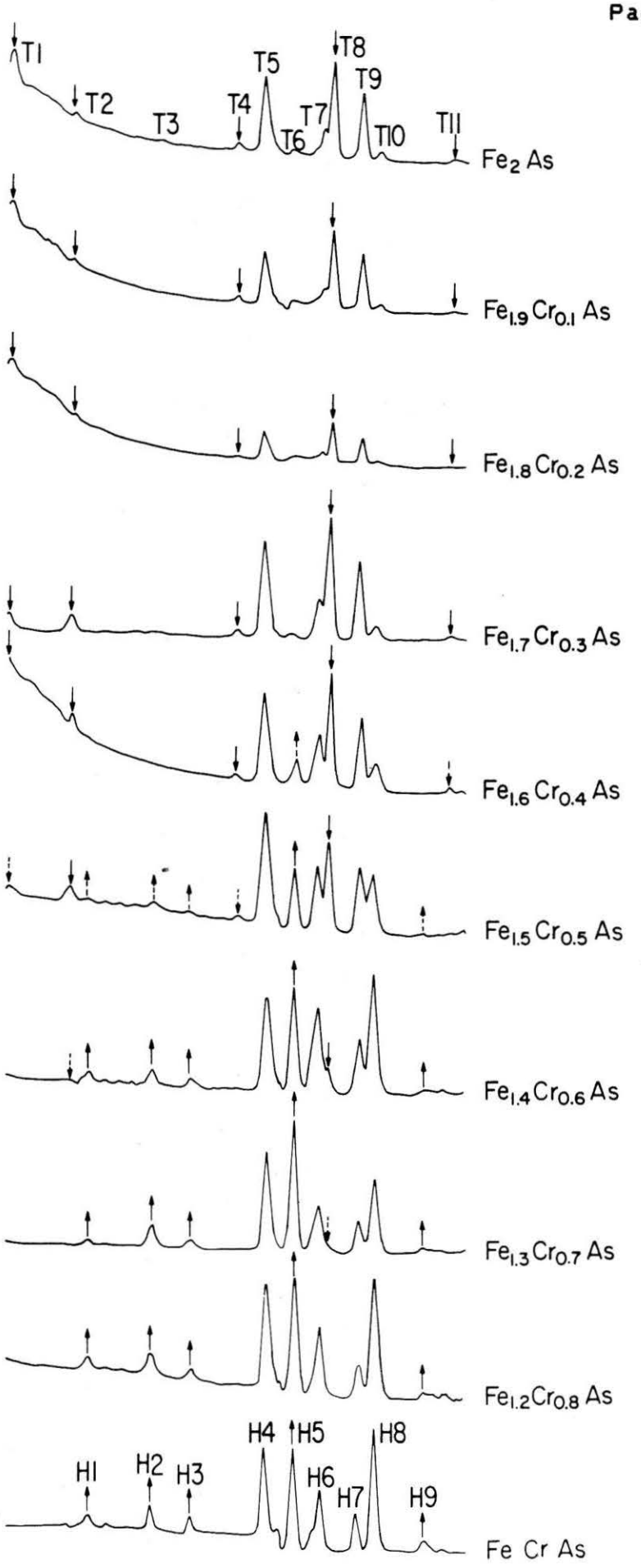
T1
T2
T3
T4
T5
T6
T7
T8
T9
T10
T11
Fe_2As
$Fe_{1.9}Cr_{0.1}As$
$Fe_{1.8}Cr_{0.2}As$
$Fe_{1.7}Cr_{0.3}As$
$Fe_{1.6}Cr_{0.4}As$
$Fe_{1.5}Cr_{0.5}As$
$Fe_{1.4}Cr_{0.6}As$
$Fe_{1.3}Cr_{0.7}As$
$Fe_{1.2}Cr_{0.8}As$
H1
H2
H3
H4
H5
H6
H7
H8
H9
Fe Cr As

FIGURE 4-3

Room temperature neutron spectra for Fe(2-X)Cr(X)As / data only. The raw data from Figure 4-2 is shown alone. There are in fact two data sets for each spectrum. These have been scaled to the same background but a small discontinuity is still present at ~ 37^{o}.

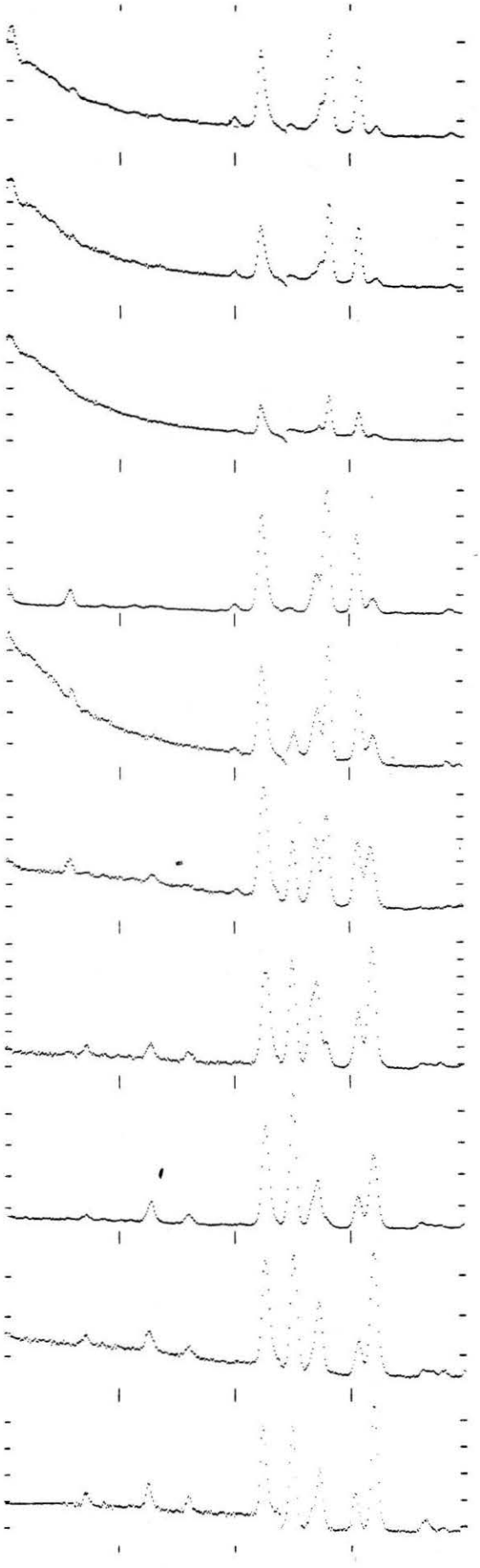

FIGURE 4-4

Percent, per weight, of tetragonal phase in the alloy Fe(2-X)Cr(X)As, as a function of X. ,The horizontal axis is the fraction of tetragonal phase. The dashed lines (- - -) give an estimate of the error. The dot-dashed line (-.-.-.) is the result of assuming that all of the available chromium goes into making FeCrAs[H].

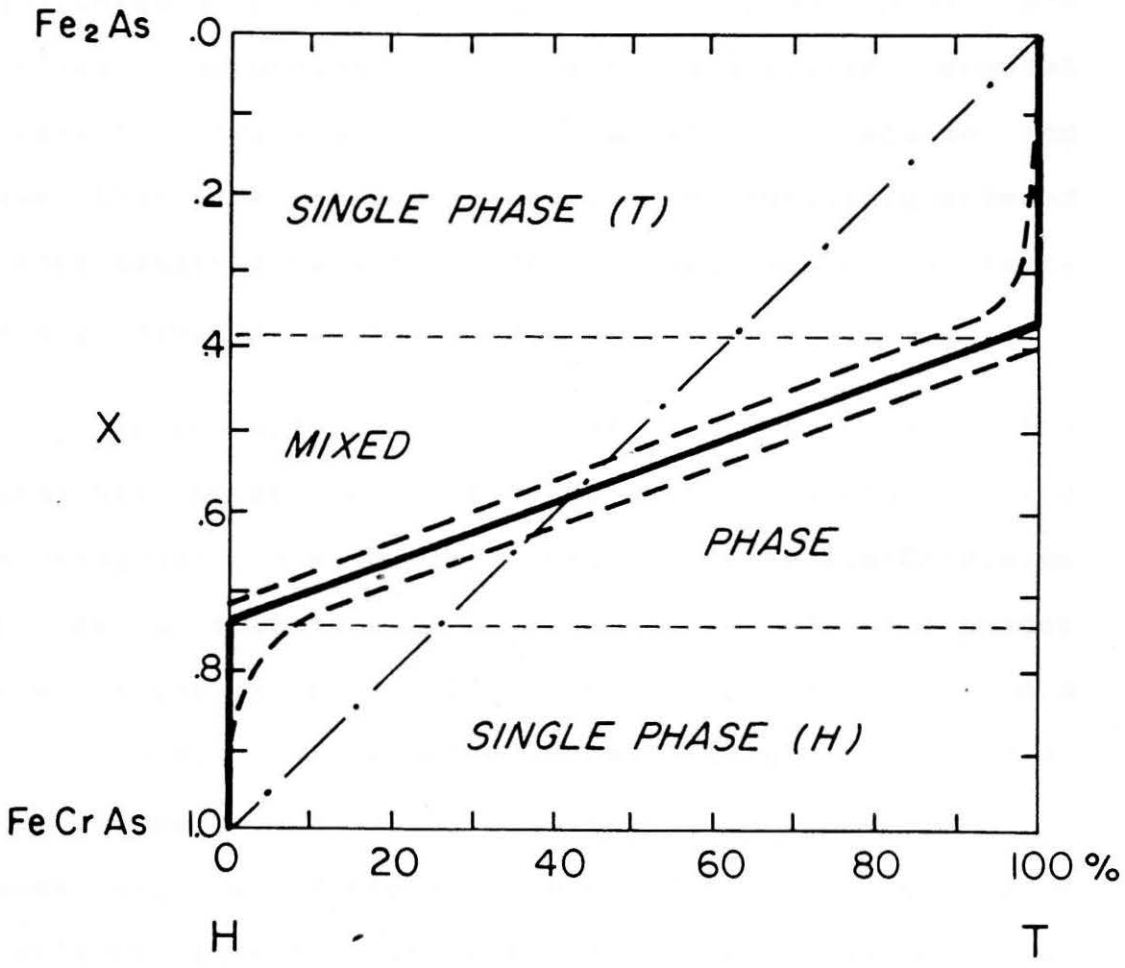
Fe2As
.0
.2
SINGLE PHASE (T)
.4
X
MIXED
.6
PHASE
.8
SINGLE PHASE (H)
FeCrAs
1.0
0
20
40
60
80
100 %
H
T

4.2 Neutron results for Fe(2-X)Cr(X)As

We have obtained neutron spectra* at room temperature for the series of samples with X = 1.0, 0.8, 0.7, 0.6, 0.5, 0.4, 0.3, 0.2, 0.1, and 0.0; these are shown in Figures 4-2 and 4-3. The main features are highlighted in Figure 4-2 and the predominant peaks are labelled according to their associated crystal structures. The peak T1 is a magnetic reflection and shows that the tetragonal phase is magnetically ordered at room temperature with a magnetic cell which is twice the crystalographic cell along the c-axis.

As indicated by the arrows in Figure 4-2, the tetragonal phase persists down to Fe(1.3)Cr(0.7)As and the hexagonal phase is still present at Fe(1.6)Cr(0.4)As when we move up the series from FeCrAs. The two phases therefore coexist over the composition range from X ~ 0.4 to X ~ 0.7. This is shown schematically in figure 4-4. Since the neutron data was not fitted and since the two phases may have different D-W factors, there is a large uncertainty in the relative amount of each phase - as indicated by the dashed lines.

In a given alloy, which is a mixture of the two phases, we expect the tetragonal phase to be iron-rich and the hexagonal phase to have comparable amounts of Fe and Cr. In fact, if we assume that all the available chromium goes into making the hexagonal compound FeCrAs

---

* The data was collected by Dr. D. Khatamian, see page 3.

and that the remaining iron crystallizes into tetragonal Fe2As, then we obtain the dot-dashed line (.-.-) shown in Figure 4-4. The deviations from this line should be interpreted in the following way: (1) for small X (< ~0.4) there is an abundance of iron and most of the chromium crystallizes into the iron-rich tetragonal compound Fe(2-e)Cr(e)As[T] (where the "T" denotes "tetragonal"), and (2) for large X (> ~0.7) the iron is exclusively taken up by hexagonal compounds such as FeCrAs[H], Fe(1-e)Cr(1+e)As[H], and Fe(1+e)Cr(1-e)As[H] which have comparable amounts of iron and chromium. Also, since more iron than chromium is available when 1.0 > X > ~0.7, the compound Fe(1+e)Cr(1-e)As[H] is more abundant than Fe(1-e)Cr(1-e)As[H].

The alloy series is, on the basis of the above discussion, divided into three regions: a single phase region where the compounds are Fe(2-X)Cr(X)As[T] with 0 < X < ~.35; a two phase region where there is a mixture of [T] and [H] for ~.35 < X < ~.7; and another single phase region with the compounds Fe(2-X)Cr(X)As[H] where ~0.7 < X < ~1.0.

FIGURE 4-5

Room temperature Mossbauer spectra of Fe(2-X)Cr(X)As. The spectra typically contained eight million counts per channel after folding. All of the changes are gradual and there is no sign of a sudden crystallographic transformation. The velocity range is from -4.0 mm/s to +4.0 mm/s.

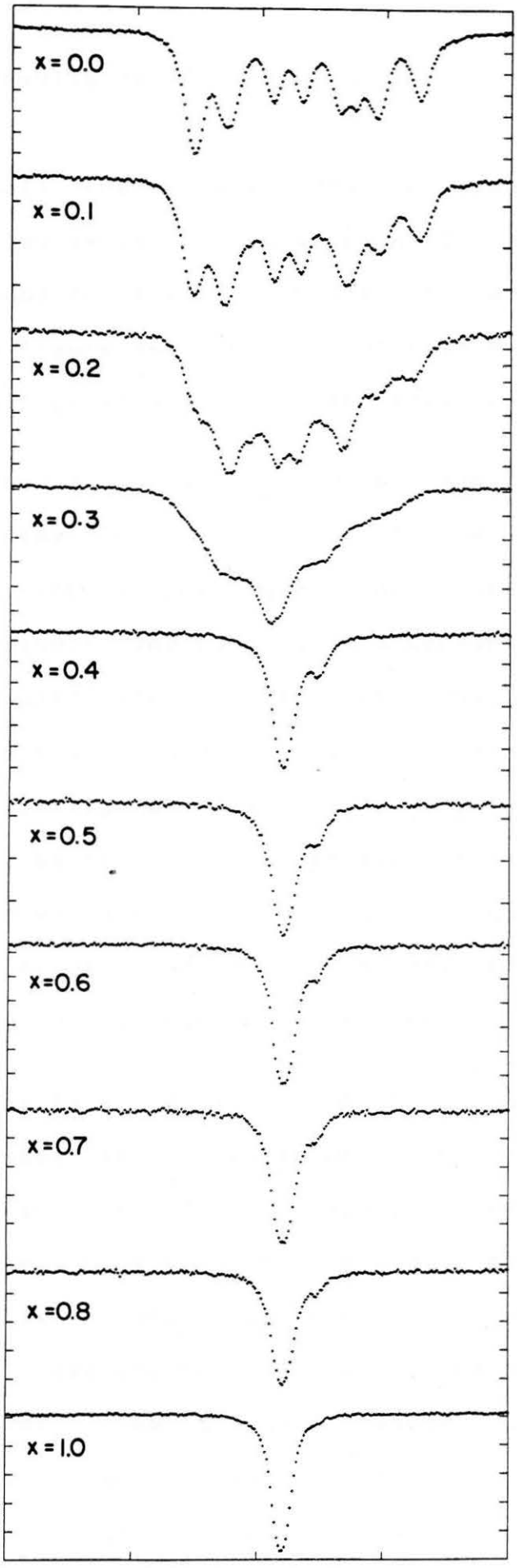
x = 0.0
x = 0.1
x = 0.2
x = 0.3
x = 0.4
x = 0.5
x = 0.6
x = 0.7
x = 0.8
x = 1.0

4.3 Mossbauer results for Fe(2-X)Cr(X)As

Given all the crystallographic changes which occur in the alloy series, it is surprising that the room temperature Mossbauer spectra change so continuously. This is seen in Figure 4-5. On a first examination there is no sign of a crystallographic transformation.

The behaviour for $X > 0.35$ and at room temperature seems normal in that the number of distinguishable lines is preserved. The line positions change only slightly and roughly in accordance with the second order Doppler effect. The continuous change in the intensity of the weaker line at ~ 0.9 mm/s suggests that this line corresponds to a single crystallographic site which is being gradually depleted of iron as X is increased. This was our first idea in analysing these spectra - the analysis led to many inconsistencies which prompted the neutron diffraction experiments.

The hyperfine splitting which is present at $X < 0.35$ decreases in a manner which is analoguous to what happpens near a second-order magnetic transition as T approaches the critical temperature. The behaviour sugggests a single magnetically ordered crystal phase whose critical temperature decreases gradually with chromium content; being just above 296K for Fe(1.7)Cr(0.3)As and just below 296K for Fe(1.6)Cr(0.4)As. It is a coincidence that the critical

temperature of the supposed single-phase system is about equal to room temperature at the composition which corresponds to the edge of the two-phase region. We might expect that Mossbauer spectra taken at a lower temperature would exhibit a sudden qualitative change at the onset of the mixed-phase region. Such a change is in fact seen at $X \sim .35$ in the T = 90K spectra which are shown in Figure 4-6.

The continuity of the hyperfine pattern for X = 0, .1, .2, and .3, at T = 90K, reaffirms the neutron diffraction result that the system is essentially single-phase at these concentrations. It should be noted that the hyperfine splitting is essentially the same (within five percent or so) for all the alloys in this single-phase region. This is because, at low temperatures, the magnitude of the effective hyperfine field is not affected by thermal averaging and is determined by the net local spin on the iron (which is not expected to be sensitive to low concentrations of chromium).

We now consider the compounds with $X \leq 0.3$ in more detail. This is a natural choice since these alloys include Fe2As which is now well understood, contain a single crystal phase whose structure is known, can at most give rise to two subspectra in the Mossbauer data (corresponding to each of the iron sites in the tetragonal unit cell), and have Néel temperatures which

are easily attainable experimentally - thereby giving access to a rich temperature dependent behaviour.

FIGURE 4-6

Some T = 90K Mossbauer spectra of Fe(2-X)Cr(X)As. At this temperature there is a sudden qualitative jump at X ~ .35 which corresponds to the boundary between the iron-rich tetragonal phase and the mixed phase region (see Figure 4-4). The velocity range is from -4.0 mm/s to +4.0 mm/s.

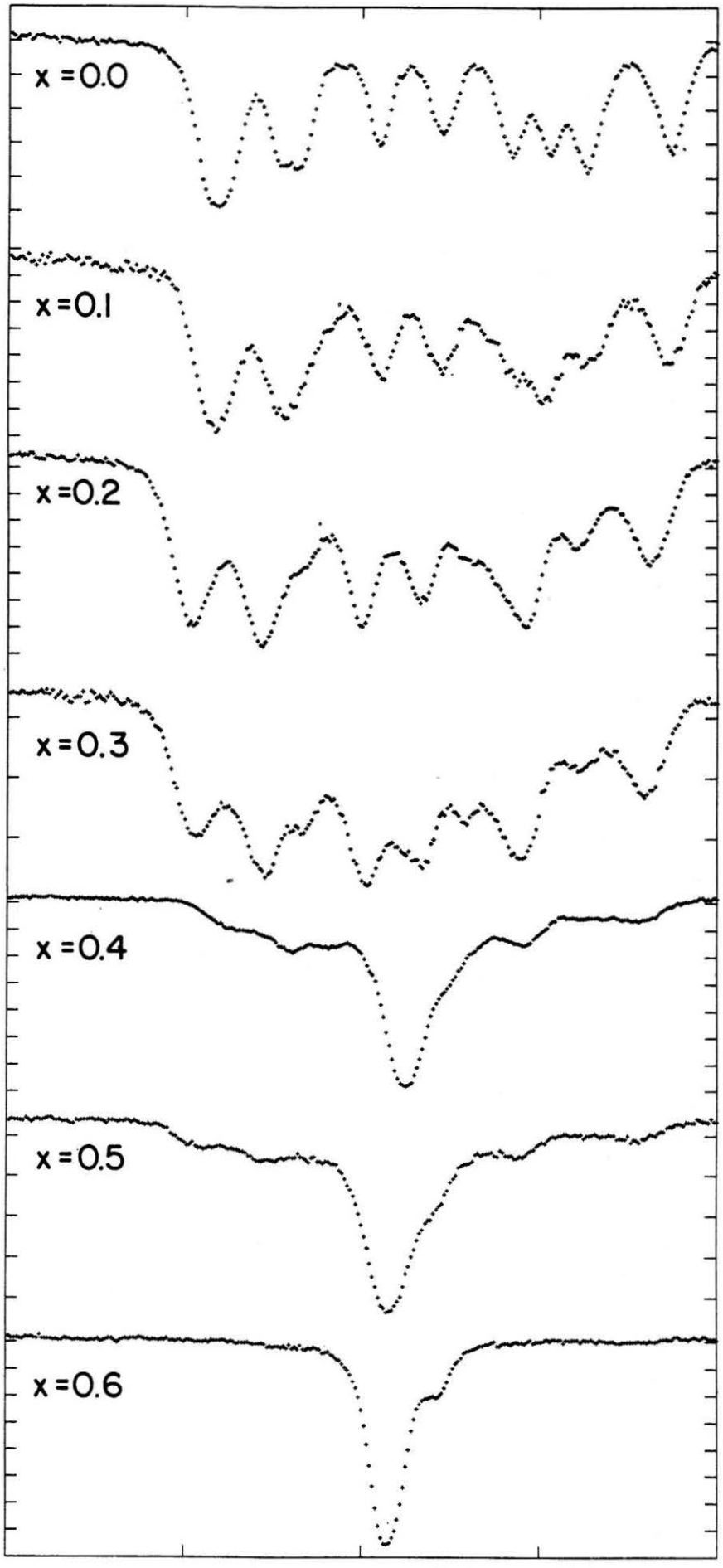
x = 0.0
x = 0.1
x = 0.2
x = 0.3
x = 0.4
x = 0.5
x = 0.6

FIGURE 4-7

Mossbauer spectra for Fe(1.7)Cr(0.3)As at four temperatures near TN. These spectra illustrate how to obtain an estimate of the Neel Temperature. As we cool the sample past ~ 42°C the lines begin to broaden dramatically. The velocity range is from -4.0 mm/s to +4.0 mm/s.

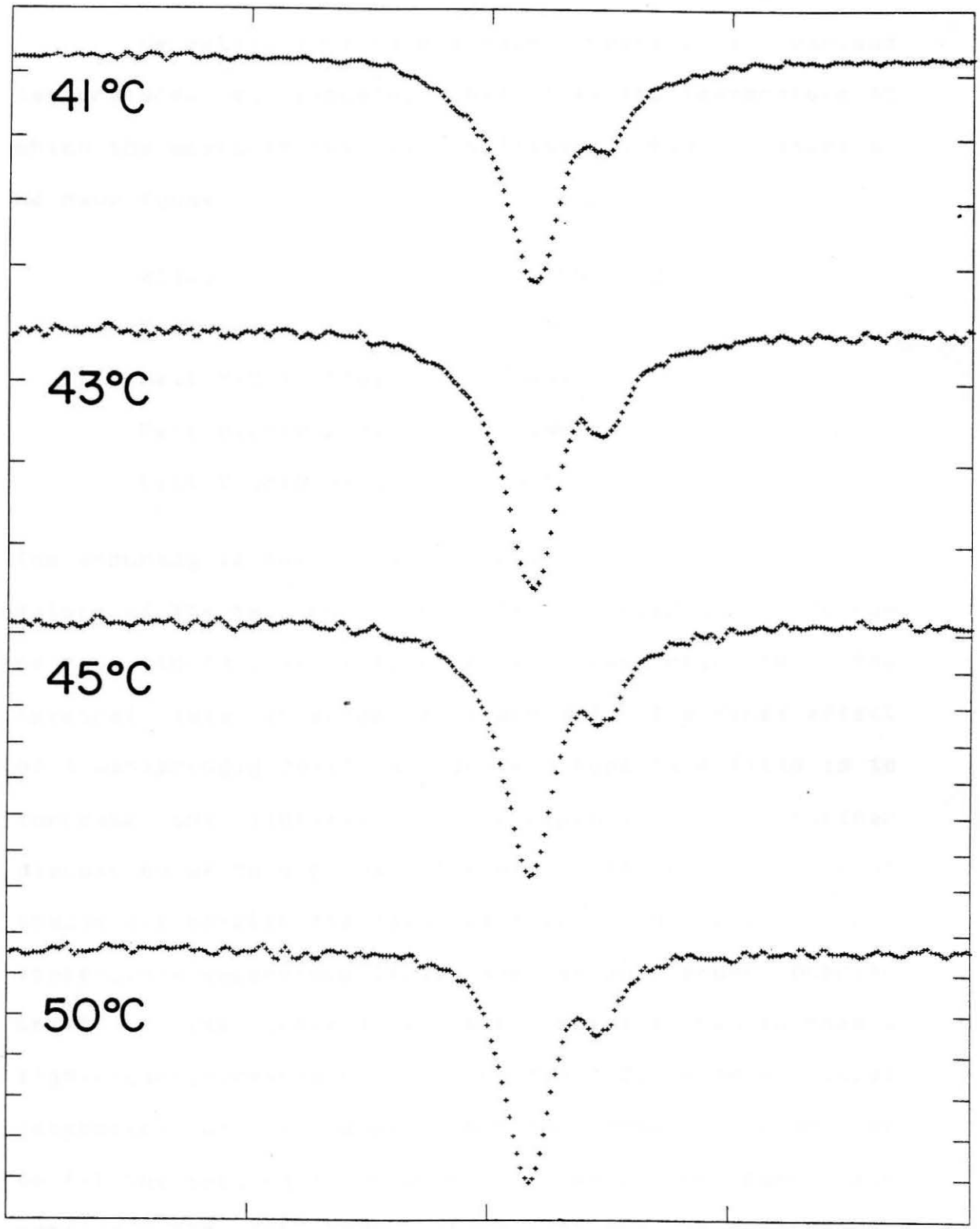
41°C
43°C
45°C
50°C

4.4 Néel temperature in Fe(2-X)Cr(X)As[T]; X < 0.35

We obtain TN from Mossbauer spectra at various temperatures by assuming that it is the temperature at which the measured hyperfine splitting (MHS) dissapears. We have found:

alloy	T (MHS = 0)
Fe(2)As	350K
Fe(1.9)Cr(0.1)As	345K
Fe(1.8)Cr(0.2)As	334K
Fe(1.7)Cr(0.3)As	315K

The accuracy is one or two degrees. To illustrate the nature of the measurement consider the Mossbauer spectrum of Fe(1.7)Cr(0.3)As at four temperatures near TN. The spectral data is shown in Figure 4-7. The first effect of a vanishingly small but non-zero hyperfine field is to increase the linewidth - see Appendix A for a further discussion of this point. Therefore, the critical point should lie between the last spectrum to show only a minor temperature dependence (from the second order Doppler shift of its center) and the first spectrum to show a significant line-broadening. We conclude, from a visual inspection of Figure 4-7, that TN ~ 315K (X = 0.3). If we fit the spectra in Figure 4-7 with the same line profile used for Fe2As above its Néel temperature we obtain the numbers given in Table VII.

Table VII. Mossbauer parameters for Fe(1.7)Cr(0.3)As near its Néel temperature

T (K)	pattern	L	C.S.	Z	A(I)/A(II)	chi^2
318	I	.64	.29	.00	3.15	1.25
	II	.29	.68	.60		
316	I	.67	.29	.00	3.37	1.45
	II	.29	.68	.60		
314	I	.77	.29	.00	4.28	2.58
	II	.28	.68	.61		

L, C.S., and Z (= $(e^2)qQ/2$) are in mm/s

This table confirms the result that there is a sudden change in the spectrum at T ~ 315K. The full width of pattern-I changes by 0.10 mm/s (by comparison, the natural linewidth of Fe-57 is 0.097 mm/s) and the ratio of the spectral areas for the two patterns jumps from ~ 3 to ~ 4. Also, the chi squared almost doubles in going from T = 316K to T = 314K - a sure sign that the lineshape is no longer Lorentzian at T = 314K.

The above procedure for finding a critical point with Mossbauer spectroscpy assumes that the critical fluctuations in the h.f. are very fast compared to fm ($f > \sim(10^4)fm$) and will, in most circumstances, overestimate the transition temperature if this is not the case. This is due to the "residual hyperfine field" which is discussed in Appendix A.

The dependence of TN on X implies that the spin-spin coupling decreases with chromium content, and

this is consistent with the observation (section 4.6) that the spin-spin relaxation time increases with X.

4.5 Above the Néel temperature in Fe(2-X)Cr(X)As[T]; X < 0.35

Above the Néel temperature the spectra are like those of Figure 3-3 for Fe2As. They can all be fitted quite well with two symmetric quadrupole-doublets - examples of some resulting Mossbauer parameters can be found in Tables V and VII.

Assuming that each quadrupole doublet can be assigned to one of the two metal atom sites in the tetragonal structure leads to abnormal spectral area ratios for X > 0.0. Spectral areas usually reflect site populations and, if this were the case here, the parameter A(I)/A(II) should fall between (1-X)/1 and 1/(1-X), corresponding to all of the chromium going respectively into sites I and II. A(I)/A(II) does not fall within these bounds for X > 0.0 but is much greater than 1/(1-X) - being typically 1.4, 1.7, and 3.0, respectively, for X = 0.1, 0.2, and 0.3. Also, the ratio has a temperature dependence; it is somewhat larger at higher temperatures.

Some tentative explanations for the anomaly in A(I)/A(II) follow. (1) The structure has many more Fe

vacancies in site-II than in site-I. The iron which would thereby be made available must then go into an interstitial site which has Mossbauer parameters comparable to those of site-I or which cannot be seen by our Mossbauer measurement for some other reason (i.e. lower D-W factor, relaxation time comparable to tm, etc.). (2) Site-II has a lower Debye-Waller factor than site-I. While this could produce a temperature dependence in A(I)/A(II), it would be unusual for the difference to be large enough to explain the deviation from 1/(1-X). (3) The contributing quadrupole-doublets are asymmetric due to the G-K effect. A G-K effect of the required magnitude has never been reported for iron compounds. And finally, (4) the quadrupole-doublets are asymmetric due to relaxation effects, that is, due to hyperfine field fluctuations.

We have been unable to quantitatively determine the extent to which each of the above explanations contributes to the anomaly in A(I)/A(II) at T > TN. The low temperature behaviour does, however, put us on the right track.

FIGURE 4-8

Mossbauer spectra for Fe(2-X)Cr(X)As, at T = 4.2K, with X = 0.1, 0.2, 0.5, 0.8, and 1.0. The velocity scale, for the spectra with X = 0.1 and 0.2, is from -9.0 mm/s to +9.0 mm/s while, for the spectra with X = 0.5, 0.8, and 1.0, it is from -4.0 mm/s to +4.0 mm/s.

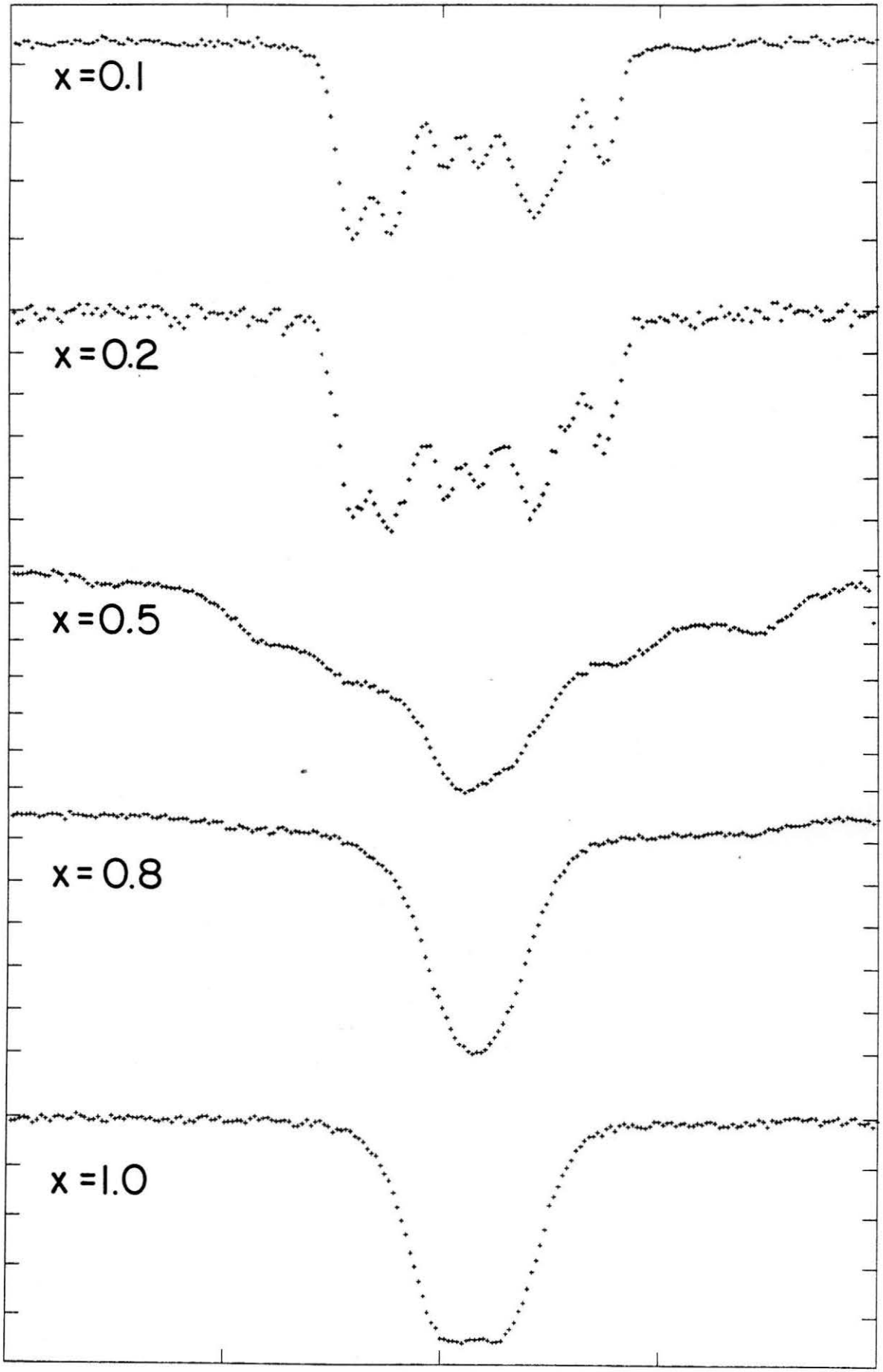
x = 0.1
x = 0.2
x = 0.5
x = 0.8
x = 1.0

FIGURE 4-9

The fitted Mossbauer spectrum of Fe(1.9)Cr(0.1)As at T = 90K. The solid lines correspond to the fit, given in Table VIII, which has the lowest chi squared. Patterns I and II correspond very closely to those shown in Figure 3-5 for Fe2As. The difference lies essentially in the positions of line-1 for the two patterns. This visual discrepancy disappears when the other fit, given in Table VIII, is shown instead. The velocity range is from -4.0 mm/s to +4.0 mm/s.

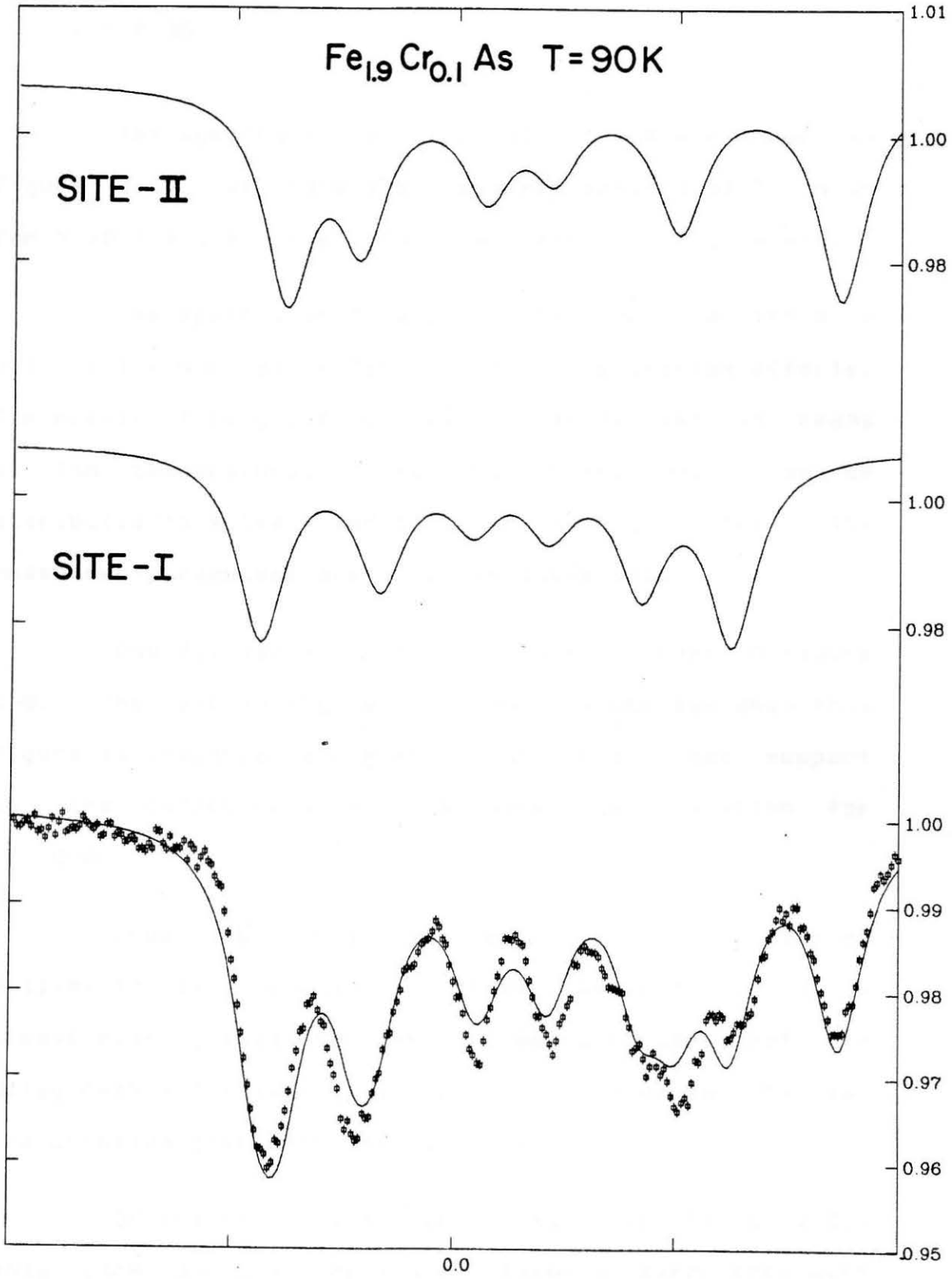
Fe1.9 Cr0.1 As T=90K
SITE-II
SITE-I
1.01
1.00
0.98
1.00
0.98
1.00
0.99
0.98
0.97
0.96
0.95
0.0

4.6 Below the Néel temperature in Fe(2-x)Cr(X)As[T]; X < 0.35

The spectra for X < 0.35 at T ~ 90K are shown in Figure 4-6. We have also obtained spectra at T = 4.2K for X =0.1 and X = 0.2 - these are shown in Figure 4-8.

The spectra at T =4.2K and the spectrum with X = 0.1 at T = 90K can be fitted without relaxation effects. The result closely corresponds to what is seen in Fe2As at low temperatures - two subspectra which can be attributed to sites I and II in the tetragonal cell. The Mossbauer parameters are given in Table VIII.

One fit for X = 0.1 at T = 90K is shown in Figure 4-9. The similarity with Fe2As is obvious when this figure is compared to Figure 3-5 and this lends support to the correctness of the site identification for X > 0.0.

From Table VIII we see that the parameter A(I)/A(II) is "normal" at these temperatures and is almost exactly equal to (1-X)/1. We conclude that the alloy Fe(2-X)Cr(X)As[T] with X < 0.3 is ordered, that is, the chromium goes only into site-I.

Of the other parameters listed in Table VIII, only g*bH and L are reliable. Based on experience with Fe2As it cannot be assumed that η = 0. The four parameters η, θ, Z, and C.S. for site-I and the same

parameters for site-II form a set of eight dependent Mossbauer parameters. The corresponding equisurface is an (8-1)-dimensional manifold and each of the fits in Table VIII corresponds to only one point on this manifold. The unreliability is therefore easily understood and is illustrated when different starting points are used in the fitting procedure - only A(I)/A(II), g*bH, and L come out the same.

Table VIII. Mossbauer parameters for various fits of Fe(2-X)Cr(X)As[T]; X < 0.35, low T

T (K) X	L	C.S.	Z	g*bH	Θ	A(I)/A(II) [chi^2] (1-X)
90K(*)	.53	.41	+.60	.872	66.	.88
X=0.1	.53	.75	-1.09	1.002	78.	[11.8] .90
90K(*)	.53	.47	+.05	.850	69.	.83
X=0.1	.53	.70	-1.17	1.027	71.	[12.2] .90
4.2K	.60	.49	-.02	.839	80.	.89
X=0.1	.60	.75	-1.04	1.076	70.	[8.2] .90
4.2K(+)	.67	.47	-.44	.741	62.	.77
X=0.2	.67	.69	-1.58	.972	69.	[3.1] .80
4.2K(+)	.67	.48	+.28	.751	47.	.77
X=0.2	.67	.70	-1.61	.967	69.	[3.1] .80

L, C.S., Z, and g*bH are in mm/s
(+),(*) These are two different fits for the same data. They illustrate the relative reliability of the Mossbauer parameters.

In examining the spectra at T = 90K (Figure 4-6), it seems to us that relaxation effects become progressively more important as chromium is added to the

lattice. What happens to the subspectra as X is increased is analogous to moving up the middle column of Figure 1-2 from $10^4/2X10^4$ towards 200/400. The depth of lines 2 and 5 increases with respect to lines 1 and 6 and the central part of the spectrum is lowered considerably. These are the main features which cause a misfit at large X when a non-relaxation profile is used. The X-dependent relaxation would also explain the A(I)/A(II) anomaly at high T since this anomaly has the same X-dependence (i.e., [A(I)/A(II) - (1-X)] increases dramatically with X at T > TN). We have, in fact, found that the area anomaly can be resolved by using relaxation-type asymmetric quadrupole-doublets with frequencies between ~ 50 fm and ~ 5000 fm but the work, at this stage, is non-conclusive due to the difficulties in fitting the low temperature spectra.

We turn now again to a more general discussion of the Fe(2-X)Cr(X)As alloy series.

4.7 Conclusions regarding Fe(2-X)Cr(X)As; $0.0 \leq X \leq 1.0$

Apart from relaxation, the most troublesome factor in understanding the behaviour of Fe(2-X)Cr(X)As is the similarity between the Mossbauer parameters of the hexagonal phase and those of the tetragonal phase above its Néel temperature. The similarity can be shown

quantitatively by fitting a series of spectra, at the same temperature, with the same line profile. Results for X > 0.35, at room temperature, and with two symmetric quadrupole doublets are given in Table IX.

Table IX. Mossbauer parameters for Fe(2-X)Cr(X)As; X > 0.35, T = 296K

X [%T]	L	C.S.	Q.S.	A(I)/A(II)
0.4	.42	.39	.10	3.13
[95%]	.26	.61	.68	
0.5	.40	.40	.13	3.57
[65%]	.28	.60	.66	
0.6	.30	.40	.20	4.55
[35%]	.24	.65	.54	
0.7	.32	.41	.15	5.88
[10%]	.22	.59	.66	
0.8	.32	.41	.14	7.69
[0%]	.20	.60	.68	
1.0	.28	.38	.15	one pattern
[0%]	--	--	--	only

L, C.S., and Q.S. are in mm/s

Fe(1.4)Cr(0.6)As is slightly anomalous but the numbers nevertheless confirm the structural observation of Fruchart that the local enviroments at the metal atom sites are virtually the same for the two crystal structures.

A series of spectra for Fe(1.6)Cr(0.4)As at various low temperatures are shown in Figures 4-10 and 4-11. These have not been fitted. The broad hyperfine

pattern is believed to be due to the fraction of the tetragonal phase which is magnetic at these temperatures. It exhibits a relaxation type profile whose temperature dependence is not obvious since it is composed of two subspectra.

FeCrAs is the simplest alloy in the series because it is ordered and therefore leads to a single Mossbauer pattern. The single Lorentzian line which is present at room temperature is considerably broadened at T = 4K (see Figure 4-8). We have simulated spectra which are very similar to this with a lineshape which assumes isotropic paramagnetic spin relaxation (lineshape of S. Dattagupta and M. Blume (ref.27)) and an e.f.g. of zero. Although this preliminary result is not conclusive we strongly suspect that such paramagnetic spin fluctuations are present in FeCrAs at 4.2K.

FIGURE 4-10

Mossbauer spectrum of Fe(1.6)Cr(0.4)As at five low temperatures. If there is no interstitial iron, then each spectrum is composed of four subspectra - two for each of the crystal phases which coexist at this composition. The velocity scale is from -4.0 mm/s to +4.0 mm/s.

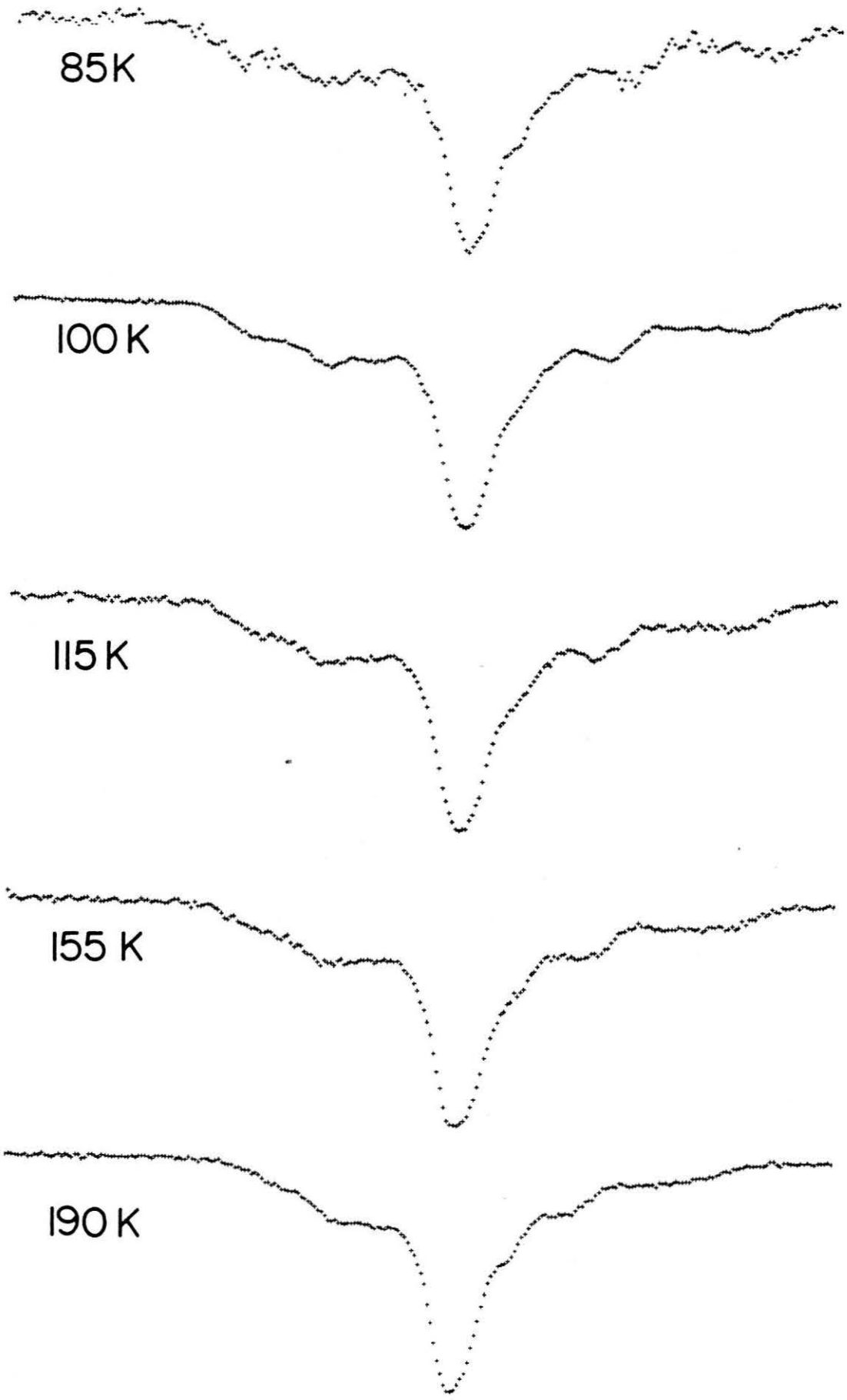
85K
100 K
115 K
155 K
190 K

FIGURE 4-11

Mossbauer spectrum of Fe(1.6)Cr(0.4)As at T = 100K and 190K. These are two spectra from Figure 4-10 - plotted together and with a different vertical scale in order to emphasize the hyperfine patterns. The velocity range is from -4.0 mm/s to +4.0 mm/s.

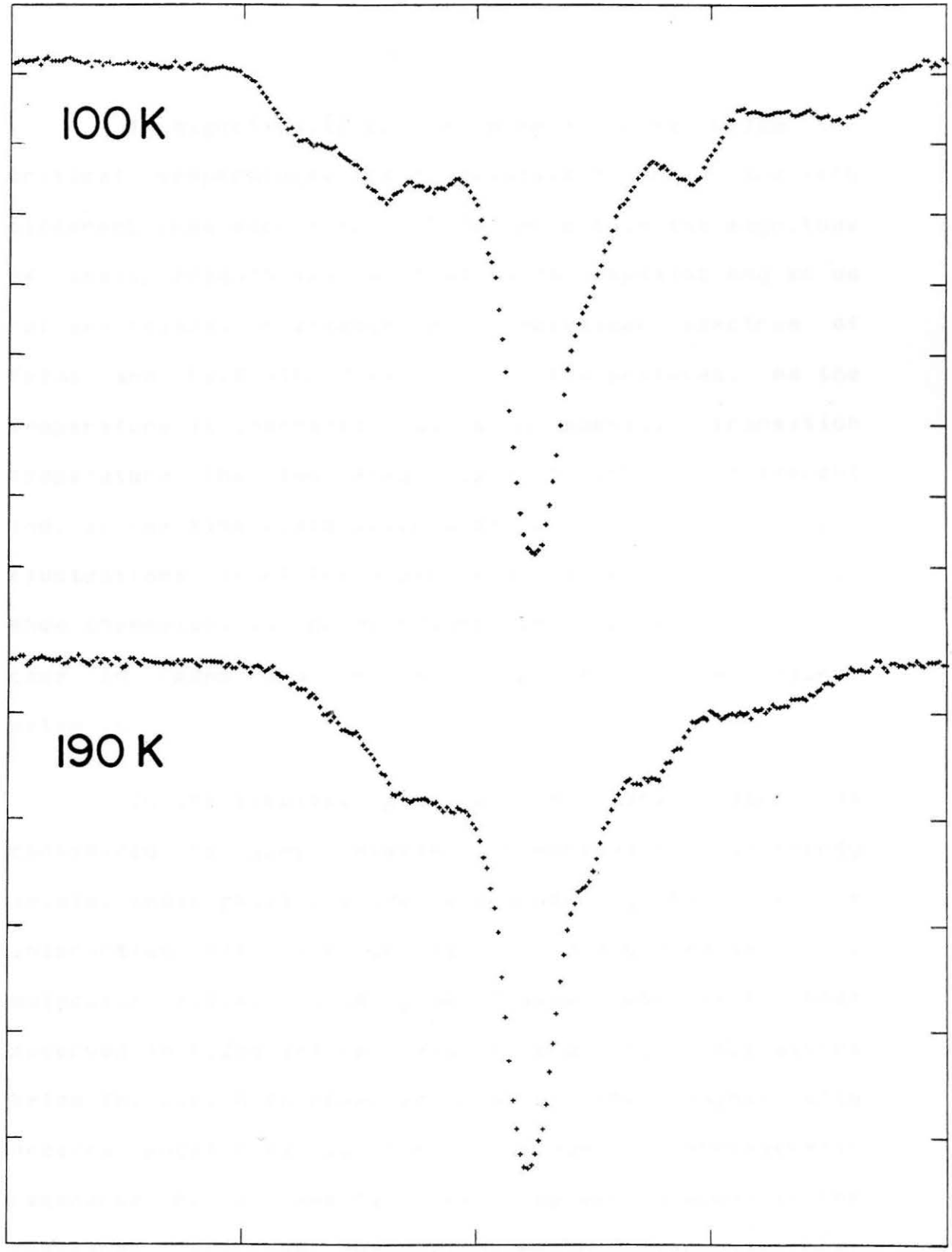
100 K
190 K

5. CONCLUSION

In magnetically ordered materials, far below the critical temperature, the frequencies f+ and f- are very different from each other. This, more than the magnitude of these frequencies relative to fm, explains why we do not see relaxation effects in the Mossbauer spectrum of Fe2As and Fe(2-X)Cr(X)As at low temperatures. As the temperature is increased towards the magnetic transition temperature the two frequencies become less different and, if the time scale associated with individual spin fluctuations is of the order of 1/fm, relaxation effects show themselves in the Mossbauer spectrum. This is the case in Fe2As and Fe(2-X)Cr(X)As at high temperatures below TN.

In the simplest picture, the local moment is considered to jump between its various (ionic) energy levels, whose positions are determined by the moment's interaction with the crystal field and with the Weiss molecular field. Slow jump frequencies, like those observed in Fe2As and Fe(2-X)Cr(X)As at high temperatures below TN, have been observed in many other magnetically ordered substances by the technique of ferromagnetic resonance (ref.95) and have been proposed to occur in the Mossbauer spectrum of alpha-FeOOH near its Néel temperature of 393K (ref.98) - an antiferromagnet whose

Néel temperature is comparable to that of Fe2As ... The Néel temperature and the spin fluctuation frequency both decrease with decreasing strength of the exchange coupling between spins. This is consistent with the observed behaviour of Fe(2-X)Cr(X)As, with X < 0.35, and may also explain the spectral area anomaly seen in this material above its Néel temperature.

We anticipate that many other antiferromagnets with iron should exhibit slow spin relaxation near their Néel temperatures; especially for Néel temperatures of the order of and below room temperature. The difficulties in observing the critical behaviour of a magnetic material, by Mossbauer spectoscopy, when slow spin fluctuations are present, are discussed in Appendix A. As a counter example, the critical behaviour of the bulk antiferromagnet hematite has been studied successfully (ref.51) - the Néel temperature of hematite is ~950K and that study was able to neglect fluctuations altogether.

The bulk antiferromagnets which we have studied have a sublattice magnetisation in the plane perpendicular to the electric field gradient principal axis and can therefore exhibit a non-zero asymetry parameter, η, even if the crystal symmetry requires η to be zero in the magnetically disordered state. We have established this by a crystal field calculation and have measured an η of 0.21 in the ordered state of Fe2As. We

expect all magnetic materials who have a component of magnetisation in the XY-plane of the e.f.g. to have a non-zero η. The presence of such an η will not be obvious in most cases since η, θ, ϕ, and Z are dependent Mossbauer parameters and reasonable fits can often be achieved even when even only one of these parameters is free. However, many Mossbauer studies, which assume zero η's on the basis of the crystal symmetry, report various e.f.g. "anomalies" and "spin rotations" above and below the magnetic transition temperature.

Very small particles of alpha-Fe203 are very illusive. Their magnetisation curves are difficult to interpret. They have an X-ray line broadening which rules out characterization by that technique. They are always supported (or absorbed into) some substrate - thereby making electron micrography practically impossible and not representative of the particle distribution.

With most techniques, including chemical characterization, the support material can be a serious inhibitor.We have shown the usefulness of a technique which is only sensitive to iron - Fe-57 Mossbauer spectorcopy. We have extended its traditional usefulness by developping a Mossbauer size determination technique and by demonstrating the importance of unequal superparamagnetic relaxation frequencies. A measure of

these frequencies leads to information about the particle's shape and about the particle's interaction with its support.

The biggest single complication with small particles is the particle distribution of shapes, sizes, and chemisorption centers. A natural extension to this work would be to synthesize a small-particle preparation with a narrow (or at least well known) particle distribution. It was hoped that the zeolite confinment work (ref.74) would lead to a delta-function distribution given by the intra-zeolitic dimensions. Maybe a laser induced synthesis on a clean single crystal face is the answer? One where each laser pulse produces exactly the same microcrystal - chemisorbed in exactly the same way. Also,the magnetic material FeCl3 has successfully been intercolated into graphite and the Mossbauer spectrum shows relaxation (ref.66) - this avenue seems promising.

A P P E N D I X A

Residual Hyperfine Fields and the Random Walk

In a Mossbauer measurement the hyperfine field is averaged over a time 1/fm . In a paramagnetic material, when the paramagnetic spin fluctuation frequency is much larger than fm, the average is zero. If f is large, but not much larger than fm, fluctuations in the average of the h.f. will become large enough to be observable in the Mossbauer spectrum. The Mossbauer measurement is an ensemble average of the Fe-57 nuclei in the sample and, if the spectrum shape is conserved under sign reversal of the hyperfine field, then the fluctuations in the average will lead to a small effective h.f. in the Mossbauer spectrum - the "residual hyperfine field", Hres.

We can estimate Hres by solving a random walk problem. We take the total number of steps to be N = f/fm and the net displacement after N steps to be H, then:

$$Hres = \int_0^{+\infty} P(N,H)\, H\, dH$$

where we integrate only from zero to plus infinity because of the sign reversal invariance. The result is:

$$Hres \sim (2fm / f)^{1/2} Ho$$

where the magnitude, Ho, of the true h.f. on the nucleus has entered the calculation, via P(N,H), from the normalization of the step size.

One situation where the Mossbauer spectrum is sensitive to such a small h.f. is when there is a large quadrupole splitting. By treating Hres as a perturbation on the quadrupole parameter, Z, we have found that the effect of Hres is to induce a height (or width) difference between the two Lorentzian lines in the doublet. Our result is:

$$(I1 - I2) = (\langle I \rangle / L)(L2 - L1) \sim \langle I \rangle (g*bHres / L)^2$$

where L is the underlying Lorentzian width and <I> is the average Lorentzian height [= (I1 +I2)/2].

If we use the random walk result we obtain:

$$\delta = L2 - L1 \sim 1/L \; 2fm/f \; (g*bHo)^2$$

This result should be compared to Equations (3) and (4), from section 2.2.3, read as

$$\delta = \text{constant} \; (g*bHo)^2 / 2f$$

where f is in units of Γ and the constant is of the

order of 1. The comparison leads to constant $\sim 4\Gamma / L \sim 2$.

We can therefore understand the relaxation profile of Blume and Tjon in the HFD as simply being equivalent to the presence of a residual hyperfine field.

The extension to the non-paramagnetic case where the frequencies are slightly different (to model a magnetic material near its critical temperature) is immediate.

The above discussion shows that, near critical temperatures and if the spin fluctuations are not large enough, the small h.f. will have an indistinguishable contribution from Hres.

11:29 PM, 19.07.1984. TOR Denis Gabriel Rancourt

REFERENCES:

/1/ achiwa,n., yano,s., yuzuri,m., takaki,h.,
magnetic anisotropy in the c-plane of fe2as
j. phys. soc. japan, 22, 156, 1967.

/2/ aharoni,a.,
effect of a magnetic field on the superparamagnetic
relaxation time
phys. rev., 177(2), 793, 1969.

/3/ armstrong,b.h.,
spectrum line profiles: the voigt function
j. quant. spectrosc. radiat. transfer., 7, 61, 1967.

/4/ austin,a.e., adelson,e., cloud,w.h.,
magnetic structures of chromium-modified mn2sb
phys. rev., 131, 1511, 1963.

/5/ biasi(de),r.s., portella,p.d.,
magnetic-resonance study of the transformation
gamma--alpha-fe2o3
phys. rev. b, 22(1), 304, 1980.

/6/ blaauw,c., mackay,g.r., leiper,w.,
mossbauer investigation of mn2sb doped with fe and cr
j. of magnetism and magnetic materials, 8, 240, 1978.

/7/ bleaney,b.,stevens,k.w.h.,
paramagnetic resonance
reports on progress in physics, 16, 108, 1953.

/8/ blume,m.,
magnetic relaxation and asymmetric quadrupole doublets in
the mossbauer effect
phys. rev. lett., 14(4), 96, 1965.

/9/ blume,m., tjon,j.a.,
mossbauer spectra in a fluctuating environment
phys. rev., 165, 446, 1968.

/10/ bowers,k.d., owen,j.,
paramagnetic resonance ii
reports on progress in physics, 18,304, 1955.

/11/ brown,w.f.,
micromagnetics,
interscience publishers (new york,1963)

/12/ brown,jr.,w.f.,
the fundamental theorem of fine-ferromagnetic-particle
theory

j. appl. phys., 39(2), 993, 1968.

/13/ brown,jr.,w.f.,
thermal fluctuations of a single domaine particle
phys. rev., 130, 1677, 1963.

/14/ brown,jr.,w.f.,
time constants of superparamagnetic particles
physica, 86-88b, 1423, 1977.

/15/ carlson,b., golin,m., rundqvist,s.,
determination of the homogeneity range and refinement of the crystal structure of fe2p
j. of solid state chemistry, 8, 57, 1973.

/16/ catalano,a., arnot,r.j., wold,a.,
magnetic and crystallographic properties of the system fe2p1-xasx
j. of solid state chemistry, 7, 262, 1973.

/17/ clauser,m.j., blume,m.,
stochastic theory of lineshape: off-diagonal effects in fine and hyperfine structure
phys. rev. b, 3(3), 583, 1971.

/18/ cloud,w.h.,
four magnetic structures of arsenic-modified mn2sb
phys. rev., 168, 637, 1968.

/19/ coey,j.m.d., khalafalla,d.,
superparamagnetic gamma-fe2o3
phys. stat. sol., (a)11, 229, 1972.

/20/ cohen,j., creer,k.m., pauthenet,r., srivastava,k.,
proprietes magnetiques des substances antiferromagnetiques en grains fins
j. phys. soc. japan, 17, suppl. b-1, 685, 1962.

/21/ collins,d.w., dehn,j.t., mulay,l.n.,
superparamagnetism and mossbauer spectroscopy: a review and new results on iron dispersion
mossbauer effect methodology, vol. 3, ed. i. j. gruverman, plenum press, new york, 1967.

/22/ constabaris,g., lindquist,r.h., kundig,w.,
the mossbauer effect for finely divided iron oxide porous eta-alumina, silica, and silica-alumina
appl. phys. letters, 7(3), 59, 1965.

/23/ corliss,l.m., hastings,j.m., goldman,j.e.,
neutron diffraction study of the anisotropy transition in alpha-fe2o3
phys. rev., 93(2), 893, 1954.

/24/ corliss,l.m., hastings,j.m., kunnmann,w.,

begum,r.j., collins,m.f., gurewitz,e., mukamel,d.,
magnetic phase diagram and critical behaviour of fe2as
phys. rev. b, 25, 245, 1982.

/25/ daniels,j.m., lam,h.y., rancourt,d.g.,
westgate,j., york,d.,
the discrimination of pyroclastic deposits on the basis of
the mossbauer spectra of their magnetites
submitted: earth and planetary science letters

/26/ darnel,f.j., cloud,w.h., jarrett,h.s.,
x-ray and magnetization studies of cr-modified mn2sb
phys. rev., 130, 647, 1963.

/27/ dattagupta,s., blume,m.,
stochastic theory of line shape. i.nonsecular effects in
the strong-collision model
phys. rev. b, 10(11), 4540, 1974.

/28/ dongen torman(van),j., jagannathan,r.,
trooster,j.m.,
analysis of fe-57 mossbauer hyperfine spectra
hyp. int., 1, 135, 1975.

/29/ dormann,j.l.,
le phenomene de superparamagnetisme
revue phys. appl., 16, 275, 1981.

/30/ eibschutz,m., shtrikman,s.,
restoration of motionally narrowed hyperfine splitting in
superparamagnetic particles by magnetic field
j. appl. phys., 39(2), 997, 1968.

/31/ elander,m., hagg,g., westgren,a.,
x-ray work: crystal structure of fe2as
ark. kemi mineral. geol., 12b(1), , 1935.

/32/ finn,g.d., mugglestone,d.,
"voigt function tabulation"
mon. not. r. astr. soc., 129, 221, 1965.

/33/ flinn,p.a., ruby,s.l., kehl,w.l.,
mossbauer effect for surface atoms: iron-57 at the surface
of neta-al2o3
science, 143, 1434, 1964.

/34/ fruchart,r.,
effects d'electronegativite et interaction metalliques
dans les phosphures et arsenures ternaires des elements
de transitions 3d,4d,5d de type metallique
ann. chim. fr., 7, 563, 1982.

/35/ fruchart,r., roger,a., senateur,j.p./j. b.
goodenough (chairman),
crystallographic and magnetic properties of solid

solutions of the phosphides m2p, m=cr, mn, fe, co, and ni/transition metal compounds
j. of applied physics, 40, 1250, 1969.

/36/ galembeck,f., leite,n.f., miranda,l.c.m., rechenberg,h.r., vargas,h.,
an epr and mossbauer study of ultrafine iron (iii) oxide particles in polytetrafluorethylene (ptfe) matrix
phys. stat. sol., (a)60, 63, 1980.

/37/ goldanskii,v.i.,
the mossbauer effect: its application to chemistry, page 23, 1966.

/38/ goldanskii,v.i., makarov,e.f., khapov,v.v.,
on the difference in peak heights from quadrupole splitting of mossbauer spectra
j. exptl. theoret. phys., 44, 752, 1963.

/39/ goldanskii,v.i., gorodinskii,g.m., karyagin,s.v., korytko,l.a., krizhanskii,l.m., makarov,e.f., suzdalev,i.p., khrapov,v.v.,
the mossbauer effect in tin compounds
doklady akademii nauk sssr, 147(1), 127, 1962.

/40/ gonser,u., wiedersich,h., grant,r.w.,
mossbauer studies on the superparamagnetic behaviour of magnesioferrite precipitates
j. appl. phys., 39(2), 1004, 1968.

/41/ goto,m., tange,h., tokunaga,t., fujii,h., okamoto,t.,
magnetic properties of the (fe1-xmx)3p compounds
japanese j. of applied physics, 16, 2175, 1977.

/42/ grandjean,f., gerard,a.,
study by mossbauer spectroscopy of arsenides fe2-xmnxas
j. of magnetism and magnetic materials, 1, 64, 1975.

/43/ grandjean,f., gerard,a., sobry,r.,
study by mossbauer spectroscopy of the antiferro-para-magnetic transition of fe2as
int. j. magnetism, 4, 1, 1972.

/44/ gressier,j.c., levesque,g., patin,h., varret,f.,
polymer-supported transition-metal complexes ....
macromolecules, 16, 1577, 1983.

/45/ griffiths,c.h., o'horo,m.p., smith,t.w.,
the structure, magnetic characterization, and oxidation of colloidal iron dispersions
j. appl. phys., 50(11), 7108, 1979.

/46/ gunsser,w., adolph,j., schmidt,f.,
a magnetic and mossbauer-spectroscopic study on the

reduction of iron(ii)-a-zeolites
j. magn. magn. mater., 15-18, 1115, 1980.

/47/ hellner,e., heger,g., mullen,d., treutmann,w.,
on the crystal structures of the intermetallic system cr1+dsb-fe1+dsb: a combined single crystal x-ray and neutron diffraction study
mat. res. bull., 10, 91, 1975.

/48/ humlicek,j.,
an efficient method for evaluation of the complex probability function: the voigt function and its derivatives
j. quant. spectrosc. radiat. transfer., 21, 309, 1979.

/49/ ingalls,r.,
electric-field gradient tensor in ferrous compounds
physical review, 133(3a), a787, 1964.

/50/ ingalls,r., ono,k., chandler,l.,
quadrupolar hyperfine anisotropy in fe(nh4so4)2.6h2o and its comparison with the magnetic susceptibility
physical review, 172(2), 295, 1968.

/51/ irshinskii,a.l., cherepanov,v.m.,
mossbauer study of the critical behaviour of hematite
sov. phys. jetp 51(3), 644, 1980.

/52/ ishizawa,y., hirahara,e.,
magnetic properties of single crystal mn2as
j. phys. soc. japan, 21, 189, 1964.

/53/ kagan,yu.,
on the anisotropy of the mossbauer effect
sov. phys.-doklady, 6(10), 881, 1962.

/54/ kanomata,t., goto,t., ido,h.,
crystal structures and magnetic properties of intermetallic compounds with cu2sb-type structures in the fe-mn-as system (not translated from the japanese)
japan institute of metals, sendai journal, 42, 480, 1978.

/55/ karyagin,s.v.,
a possible cause of doublet component asymmetry in mossbauer absorption spectra of certain powder like tin-compounds
dokl. akad. nauk sssr, 148(5), 1102, 1963.

/56/ katsuraki,h.,
neutron diffraction study of fe2as single crystal
j. phys. soc. japan, 19, 1988, 1964.

/57/ katsuraki,h., ashiwa,n.,
the magnetic structure of fe2as
j. phys. soc. japan, 21, 2238, 1966.

/58/ katsuraki,h., suzuki,k.,
magnetic structure of fe2as
j. of applied physics, 36, 1094, 1965.

/59/ kraan(van der),a.m.,
mossbauer effect studies of surface ions of ultrafine alpha-fe2o3 particles
phys. stat. sol. a, 18, 215, 1973.

/60/ kraan(van der),a.m.,
superparamagnetism of small alpha-fe2o3 crystallites studied by means of the mossbauer effect
j. phys., 32, c1-1034, 1971.

/61/ kraan(van der),a.m., loef(van),j.j.,
superparamagnetism in submicroscopic alpha-feooh particles observed by the mossbauer effect
phys. lett., 20(6), 614, 1966.

/62/ krupyanskii,yu.f., suzdalev,i.p.,
magnetic properties of ultrafine iron oxide particles
sov. phys.-jetp, 38(4), 859, 1974.

/63/ kundig,w., ando,k.j., lindquist,r.h., constabaris,g.,
mossbauer studies of ultrafine particles of nio and alpha-fe2o3
czech. j. phys., b17, 467, 1967.

/64/ kundig,w., bommel,h., constabaris,g., lindquist,r.h.,
some properties of supported small alpha-fe2o3 particles determined with the mossbauer effect
phys. rev., 142(2), 327, 1966.

/65/ lindquist,r.h., constabaris,g., kundig,w., portis,a.m.,
mossbauer spectra of fe-57 in superparamagnetic nickel
j. appl. phys., 39(2), 1001, 1968.

/66/ milman,s.e., corson,m.r., hoy,g.r.,
phys. rev. b, 25, 6595, 1982.

/67/ mcnab,t.k., fox,r.a., boyle,a.j.f.,
some magnetic properties of magnetite (fe3o4) microcrystals
j. appl. phys., 39(12), 5703, 1968.

/68/ morin,f.j.,
magnetic susceptibility of alpha-fe2o3 and alpha-fe2o3 with added titanium
phys. rev., 78, 819, 1950.

/69/ morrish,a.h., haneda,k.,
magnetic structure of small nife2o4 particles

j. appl. phys., 52(3), 2496, 1981.

/70/ morup,s., topsoe,h., lipka,j.,
modified theory for mossbauer spectra of superparamagnetic particles: application to fe3o4
j. de phys., 37, c6-287, 1976.

/71/ morup,s., topsoe,h.,
mossbauer studies of thermal excitations in magnetically ordered microcrystals
appl. phys., 11, 63, 1976.

/72/ muench,g.j., arajs,s., matijevic,e.,
magnetic properties of monodispersed submicromic alpha-fe2o3 particles
j. appl. phys., 52(3), 2493, 1981.

/73/ nakamura,t., shinjo,t., endoh,y., yamamoto,n., shiga,m., nakamura,y.,
fe-57 mossbauer effect in ultra fine particles of alpha-fe2o3
physics letters, 12(3), 178, 1964.

/74/ nazar,l.f., ozin,g.a., hugues,f., godber,j., rancourt,d.g.,
metal atoms in solution: versayile ....
j. mol. catal., 21, 313, 1983.

/75/ néel,m.l.,
theorie du trainage des ferromagnetiques en grains fins avec application aux terres cuites
annales de geophysiques, 5, 99, 1949.

/76/ néel,l.,
proprietes magnetiques des grains fins antiferromagnetiques: superparama-gnetisme et superantiferromagnetisme
j. phys. soc. japan, 17, suppl. b-1, 676, 1962.

/77/ raj,p., kulshreshtha,s.k.,
mossbauer studies of fe2as
physica scripta., 14, 125, 1976.

/78/ rancourt,d.g., daniels,j.m., nazar,l.f., ozin,g.a.,
the superparamagnetism of very small particles supported by zeolite-y
hyp. int., 15/16, 653, 1983.

/79/ rancourt,d.g., daniels,j.m.,
influence of unequal magnetization direction probabilities on the mossbauer spectra of superparamagnetic particles
phys. rev. b, 29(5), 2410, 1984.

/80/ rancourt,d.g., julian,s.r., daniels,j.m.,

mossbauer characterization of very small superparamagnetic particles; application to intra-zeolitic alpha-fe2o3 particles
submitted: j. magn. magn. matter.

/81/ rancourt,d.g., daniels,j.m.,
iron-57 mossbauer study of fe2as; anisotropic spin fluctuation near the critival temperature and a magnetically induced electric field gradient asymmetry
submitted: j. magn. magn. matter.

/82/ rosenberg,r.m., cloud,w.h., darnell,f.j., flippen,r.b.,
first order magnetic transitions in the fe-mn-as system
physics letters, 25a, 723, 1967.

/83/ sato,k., adachi,k., ando,e.,
mossbauer effect of fe2p
j. phys. soc. japan, 26, 855, 1969.

/84/ schroeer,d.,
the mossbauer effect in microcrystals
mossbauer effect methodology, vol. 5, ed. i. j. gruverman,plenum press, new york, 1970.

/85/ schroeer,d.,
the quadrupole interaction in alpha-fe2o3 microcrystals
phys. lett., 27a(8), 507, 1968.

/86/ shinjo,t.,
mossbauer effect in antiferromagnetic fine particles
j. phys. soc. japan, 21(5), 917, 1966.

/87/ shirakawa,k., ido,h.,
magnetic transition of the mn2sb-mn2as system
j. phys. soc. japan, 40, 666, 1976.

/88/ shull,c.g., strauser,w.a., wollan,e.o.,
neutron diffraction by paramagnetic and antiferromagnetic substances
phys. rev., 83(2), 333, 1951.

/89/ sirota,n.n., ryshkovskii,v.m.,
neutronographic investigation of magnetic transformations of the mn2as-mn2sb system
soviet physics - doklady, 17, 370, 1972.

/90/ smart,j.s.,
effective field theories of magnetism,
w.b. saunders company (philadelphia,1966)

/91/ sparks,m.,
ferromagnetic-relaxation theory,
mcgraw-hill book company (new york, 1964)

/92/ suzdalev,i.p., krupyanskii,yu.f.,
a mossbauer study of the formation and growth of iron oxide particles during topochemical decomposition of ferric oxalate
kinetika i kataliz, 10(6), 1254, 1969.

/93/ gibb,t.c., greatrex,r., greenwood,n.n.,
a novel case of magnetic relaxation in the ru-99 mossbauer spectrum of na3ruo4
j. sol. state chem., 31, 153, 1980.

/94/ tjon,j.a., blume,m.,
randomly varying electric field gradients
phys. rev., 165(2), 456, 1968.

/95/ vonsovskii,s.v.,
ferromagnetic resonance,
israel program for scientific translations
(jerusalem,1964)

/96/ watanabe,h., nakagawa,y., sato,k.,
on the neutron diffraction study of cr2as
j. phys. soc. japan, 20, 2244, 1965.

/97/ wautelet,m., gerard,a., grandjean,f.,
mossbauer study of the magnetic properties of fe(2-x)m(x)p(1-y)as(y) type compounds, m=cr,mn,fe,co,ni
le journal de physique, 38, 29, 1977.

/98/ woude,van der,f., dekker,a.j.,
phys. stat. sol. 13, 181, 1966.

/99/ yoshii,s., katsuraki,h.,
neutron diffraction study of femnas
j. phys. soc. japan, 22, 674, 1967.

/100/ yoshii,s., katsuraki,h.,
crystal structure and magnetic property of femnas
j. phys. soc. japan, 21, 205, 1966.

/101/ shiga,m., nakamura,y.,
a contribution to the invar problem by hyperfine field distribution analysis
j. magn. magn. matter., 40, 319, 1984.

/102/ lam,h.-y.,
ph.d. thesis, university of toronto, toronto, canada.